

DEPARTMENT OF PHYSICS
UNIVERSITY OF JYVÄSKYLÄ
RESEARCH REPORT No. 9/2007

**STUDIES OF EXOTIC DECAY MODES
IN FISSION OF HEAVY ELEMENTS**

**BY
SERGEY YAMALETDINOV**

Academic Dissertation
for the Degree of
Doctor of Philosophy

*To be presented, by permission of the
Faculty of Mathematics and Natural Sciences
of the University of Jyväskylä,
for public examination in Auditorium FYS-1 of the
University of Jyväskylä on December 19, 2007
at 12 o'clock noon*



Jyväskylä, Finland
December 2007

When you have eliminated the impossible, whatever remains, however improbable, must be the truth.

Sir Arthur Conan Doyle
“*Sherlock Holmes*”

Preface

The work in this thesis has been carried out at the Department of Physics of the University of Jyväskylä, Finland, and at the Flerov Laboratory of Nuclear Reactions of the Joint Institute for Nuclear Research, Dubna, Russia during the years of 2000-2007.

First of all I wish to express my hearty thanks to Dr. Wlodek Trzaska for supervising and helping me. His guidance and support in the course of my work has been truly invaluable.

My special gratitude for time-proof and fruitful collaboration is going to Professor Yuri Pyatkov and to Dr. Manfred Mutterer. The cooperation with these scientists had allowed me not only to accumulate valuable experience and obtain professional skills but also have formed my scientific ideology.

Experiments are not carried out by one person alone. Therefore I would like to thank all my colleagues from Dubna and JYFL for sharing their knowledge and experience: D. Kamanin, A. Alexandrov and I. Alexanrdova, V. Tischenko, A. Tykavkin, S. Mitrofanov, V. Lyapin, Yu. Kopatch, M. Sillanpää, S. Khlebnikov, G. Tyurin and many others who are not in this list just due to forgetfulness of author.

I would also like to thank the staff of the Physics Department and especially Soili, Marjut and Anna-Liisa for all their help with administrative matters. The financial support from the Department of Physics of the University of Jyväskylä is gratefully acknowledged.

I am grateful to the referees Eryk Piasecki and Alexey Ogloblin for their careful manuscript reading and for useful suggestions that improved the thesis.

My heartfelt gratitude is addressed to the people who were all these years for me not only the colleagues, but the real friends, namely Mariana Bondila and Volodya Lyapin. I will keep the remembrance about our friendship as a pattern of faithful one.

Of no less importance are the people outside the work environment. It is a pleasure to thank all my friends: Igor, Andrey, Misha, Daniil, Zhenya, Sasha, Andrey and Alena, Luci, Natasha, Galya and many others. They shared the time with me and made living in Jyväskylä a lot nicer.

Last but not least I wish to thank my dear family, the persons are the closest to me: my dear wife Lyuda and daughter Anna, who always encouraged and stood by me. A sincere “spasibo” to my mama, papa and sister Masha, who gave me the important knowledge I need to have, supported me and were ready to help me all those years.

Contents

Introduction	1
--------------------	---

PART 1 SEARCHING FOR UNUSUAL MULTI-BODY DECAYS IN FISSION OF ACTINIDES

7

1	Experimental and theoretical studies of ternary fission	9
1.1	Motivation	9
1.2	Terminology	10
1.3	Tripartition in spontaneous and low energy fission	11
1.4	Intermediate excitation energies	16
1.5	Polar emission in fission	17
1.6	Cluster radioactivity and cold fission	19
1.7	Indications for collinear tripartition of different nuclear systems	22
1.8	Theoretical studies of multi-body decays	23
1.9	Conclusions	26
2	Experiment at modified FOBOS setup	27
2.1	Original FOBOS setup	27
2.2	Modified FOBOS spectrometer	28
2.3	FOBOS detector module	31
2.3.1	Position-sensitive avalanche counters	31
2.3.2	Axial ionization chambers	32
2.4	Calibration procedures	34
2.4.1	Checking the stability	34
2.4.2	Coordinate calibration of the PSACs	35
2.4.3	Time calibration of the PSACs	35
2.4.4	Energy calibration of the BICs	38
2.5	Reconstruction of the fragment mass	39
2.6	Results	42
2.7	Conclusions	46
3	Off-beam experiments at JYFL and at JINR	47
3.1	Experimental details	47
3.2	Calibration procedures	50
3.3	Results	51
3.4	Discussion of the results	57
3.5	Conclusions	59
4	In-beam experiment at JYFL	61
4.1	Experimental setup	61
4.2	Stability of data parameters	63
4.2.1	Checking stability by mean value and dispersion of critical spectra	64
4.2.2	Checking stability by two Gaussians fit	64
4.3	Calibration of T-channels	65
4.3.1	Procedure for determination T ₀	65
4.3.2	Modified procedure for determination of T ₀	66
4.3.3	Determination of velocity in the multi-body decay	69
4.4	Energy calibration and reconstruction of the FF masses	70
4.4.1	Pulse-height defect	70
4.4.2	Calibration of E-channels	71
4.4.3	Reconstruction of FF masses	72
4.5	Experimental results	76
4.5.1	Possible sources of false events	76
4.5.2	Analysis of ternary events	78

4.6	Conclusions to in-beam experiment	85
	Summary to Part 1	87
	Conclusions to Part 1.....	90
	PART 2 ENERGY DISTRIBUTION OF TERNARY ALPHA PARTICLES....	91
5	Measurement of the full energy distribution of ternary α-particles in $^{252}\text{Cf(sf)}$.....	93
5.1	Motivation	93
5.2	Experimental details	96
5.3	Simulation of detector efficiency	98
5.4	Data analysis.....	102
5.5	Results of the experiment	105
	Summary and conclusions to Part 2.....	111
	References	113

Introduction

Nuclear fission has become known in the late thirties of the last century as a process where a heavy nucleus such as Uranium or Thorium decays into two fragments of about the same mass. Sometimes instead of the standard "binary fission" a ternary process with three charged particles in the outgoing channel is observed, but with the third particle being very light compared to the main fission fragments. Fission of heavy nuclei into three fragments of comparable masses, the so-called "true ternary fission", has also been intensively investigated soon after the discovery of fission. Swatecki had shown in the frame of the liquid drop model [Swi58] that fission into 3 heavy fragments is energetically more favorable than binary fission for all nuclei with fission parameter $30.5 < Z^2/A < 43.3$. In 1963 Strutinsky had studied equilibrium forms of the nucleus in the same theoretical model and showed [Str63] that along with the ordinary configuration with one neck there is possible the existence of more complicated configurations with two and even three necks. On the experimental side there were multiple attempts to find in low energy fission the true ternary fission by means of counting and radiochemical studies. It became immediately clear that ternary fission is a very rare phenomenon. The schemes of these experiments were based on the assumption of comparable angles between all three flying fragments. However, using the frame of the liquid drop model, Diehl and Greiner [Die73, Die74] had shown a preference for prolate over oblate saddle-point shape for the fission of a nucleus into three equal fragments. Therefore, from the theoretical point of view searching for the collinear tripartition of low excited nuclear systems is more promising. In cluster radioactivity, which is a binary process, the magic number (the magicity) of at least one of the decay partners plays a key role in the process of fission. Immediately the question regarding the decay of heavy nucleus into magic constituents (clusters by definition) arises. Thus, searching for collinear multi-body decays of low excited heavy nuclei with creation of massive particles, which could be magic nuclei, is an interesting and actual scientific problem. To study this problem we carried out four experiments with spontaneous fissioning of ^{252}Cf at different setups and one beam experiment with the reaction $^{238}\text{U} + ^4\text{He}$ (40MeV). The processing and analysis of the data obtained in these experiments constitute the first part of the present work.

The second part of this work is devoted to the measurement of the full energy distribution of ternary α -particles originated in ^{252}Cf (sf). Since the discovery of ternary fission there have been numerous experiments to measure energy spectra of ternary particles. Nevertheless, surprisingly little is known about the low-energy part of these distributions. This is true also for ternary α -particles from the most often studied spontaneous fissioning ^{252}Cf . The main reasons for this situation are twofold. First the intense background from the alpha decay of ^{252}Cf that has forced many researchers to use protection foils on the detectors cutting α -particle spectra at and below 6 MeV. The second reason is the preference of ΔE -E method to identify ternary particles. As a result, experimental studies at low energy are still scarce and the data of these studies are not consistent. We have carried out a new experiment to re-measure the energy spectrum of ternary α -particle in ^{252}Cf spontaneous fission employing an array of unshielded silicon detectors and unambiguously discriminating α -particles from neighbouring isotopes by time-of-flight techniques using fission

fragments as the start. Details, data analysis and results of this experiment are presented in the second part of the work.

The thesis is organized in two parts and consists of five chapters:

- The first part devoted to the searching for collinear multi-body decays consists of four chapters.
 - Chapter 1 gives a review of the existing theoretical and experimental results in the field of study of ternary fission. The scientific works which contributed to the formulation of the task for the present work are considered here in details.
 - The experiment aimed at the investigation of the collinear cluster tripartition in spontaneous fission of ^{252}Cf at modified FOBOS spectrometer is described in Chapter 2. More attention is devoted to techniques and methods of calibration of FOBOS gas filled detectors and to mass reconstruction procedures. The most important results of this experiment are reported.
 - The results obtained at modified FOBOS spectrometer initiated a set of three experiments for searching the collinear cluster tripartition in spontaneous fission of ^{252}Cf at independent setups. Chapter 3 presents the description and results of these three different experiments.
 - The in-beam experiment intended for searching the collinear multicluster decay of heavy nuclei in reaction $^{238}\text{U} + ^4\text{He}$ (40 MeV) is described in Chapter 4. Data processing procedures are explained in great detail. Special attention was paid to an original procedure of energy calibration and mass reconstruction which was developed for handling data from p-i-n diodes. The analysis of possible sources of false events, which can be treated as events of collinear multi-body decay, is also presented in this Chapter. Some possible decay schemes for one group of ternary events are introduced as well.
- The second part consists of Chapter 5 and describes the experiment aimed at measuring the full energy distribution of ternary α -particles in $^{252}\text{Cf}(\text{sf})$. This chapter contains a review of available experimental results from studies of energy of ternary α 's originated from spontaneous fission of ^{252}Cf , a detailed description of the experimental setup, the procedure and results of simulation of the detector efficiency and analysis of ^4He and ^6He spectra, including the attempt to explain the observed asymmetry of these spectra.

The author has actively participated in all experiments described in the present work. His activity covered both the planning and the implementation of the experiments, as well as the main data processing for experiments reported in chapters 2-4 and the modeling for the experiment described in chapter 5. The results of the present work have been reported at different conferences and have also been published in several scientific papers. The studies devoted to the searching for collinear multi-body decay are presented (in chronological order) in the papers 1-21, while the papers 22-25 report the results concerning the measurement of the full energy distribution of ternary α -particles in $^{252}\text{Cf}(\text{sf})$.

1. Yu.V. Pyatkov, D.V. Kamanin, E.A. Sokol, A.A. Alexandrov, I.A. Alexandrova, S.V. Khlebnikov, S.V. Mitrofanov, Yu.E. Penionzhkevich, Yu.V. Ryabov, V.G. Tishchenko, S.R. Yamaletdinov
Search for collinear tripartition of the ^{252}Cf nucleus
 Scientific Report 1999-2000, Flerov Laboratory of Nuclear Reactions, Joint Institute for Nuclear Research, JINR E7-2001-173 (Ed. by A.G. Popeko), p. 77.
2. Yu.V. Pyatkov, D.V. Kamanin, E.A. Sokol, A.A. Alexandrov, I.A. Alexandrova, S.V. Khlebnikov, S.V. Mitrofanov, Yu.E. Penionzhkevich, Yu.V. Ryabov, V.G. Tishchenko, S.R. Yamaletdinov
Search for collinear tripartition of the ^{252}Cf nucleus at the modified FOBOS spectrometer.
 5-th International Conference on Dynamical Aspects of Nuclear Fission, October 23-27, 2001, Casta-Papiernicka, Slovak Republic. Conference proceedings, Editors J.Kliman, M.G.Itkis, and S.Gmuca. Published by World Scientific Publishing Co. Pte. Ltd., 2002. p. 229-233.
3. Yu.V. Pyatkov, D.V. Kamanin, E.A. Sokol, A.A. Alexandrov, I.A. Alexandrova, S.V. Khlebnikov, S.V. Mitrofanov, Yu.E. Penionzhkevich, Yu.V. Ryabov, V.G. Tishchenko, S.R. Yamaletdinov
Search for collinear tripartition of the ^{252}Cf nucleus at the modified FOBOS spectrometer.
 International Symposium on Exotic Nuclei, Lake Baikal, Russia, July 24-28, 2001. Conference proceedings, Editors: Yu.E. Penionzhkevich, and E.A. Cherepanov. Published by World Scientific Publishing Co. Pte. Ltd., 2002, p.181-185.
4. D.V. Kamanin, Yu.V. Pyatkov, E.A. Sokol, S.V. Mitrofanov, S.R. Yamaletdinov, V.G. Tishchenko, A.N. Tyukavkin, B.V. Florko, E.A. Kuznetsova, O.Yu. Gapienko
Neutron belt of the FOBOS spectrometer
 Proceedings of 10th Int. Seminar on Interaction of Neutrons with Nuclei: "Neutron Spectroscopy, Nuclear Structure, Related Topics". Dubna, May 22-25, 2002. Dubna 2003, p. 455-462.
5. D.V. Kamanin, Yu.V. Pyatkov, E.A. Sokol, A.A. Alexandrov, I.A. Alexandrova, S.V. Khlebnikov, S.V. Mitrofanov, Yu.E. Penionzhkevich, Yu.V. Ryabov, V.G. Tishchenko, A.N. Tjukavkin, S.R. Yamaletdinov
New step in searching for collinear tripartition in $^{252}\text{Cf}(\text{sf})$ at the FOBOS setup
 Proceedings of 10th Int. Seminar on Interaction of Neutrons with Nuclei: "Neutron Spectroscopy, Nuclear Structure, Related Topics". Dubna, May 22-25, 2002. Dubna 2003, p. 447-454.
6. Yu.V. Pyatkov, A.N. Tyukavkin, D.V. Kamanin, E.A. Sokol, E.A. Kuznetsova, S.R. Yamaletdinov
Mathematical model of the neutron registration channel of the modified FOBOS spectrometer
 Heavy Ion Physics, FLNR JINR Scient. Rep. 2001-2002, Dubna (2003) 229-230.

7. *S.R. Yamaletdinov, W.H. Trzaska, Yu.V. Pyatkov, D.V. Kamanin*
TOF-E calibration procedure for thick foils
 Proceedings of the XXXVII annual conference of the Finish Physical Society, March 20-22, 2003 Helsinki, Finland, Report Series in Physics HU-P-265, p. 109.

8. *D. V. Kamanin, Yu.V.Pyatkov, E. A. Sokol, S.V.Mitrofanov, S. R. Yamaletdinov, V. G. Tishchenko, A. N. Tyukavkin, B. V. Florko, E.A.Kuznetsova, and O. Yu. Gapienko*
Neutron Channel of the FOBOS Spectrometer for the Study of Spontaneous Fission
 Physics of Atomic Nuclei, Vol. 66, No. 9, 2003, pp. 1655–1658. From Yadernaya Fizika, Vol. 66, No. 9, 2003, pp. 1703–1706.

9. *Yu. V. Pyatkov, D. V. Kamanin, A.A.Alexandrov, I. A. Alexandrova, S.V.Khlebnikov, S. V. Mitrofanov, V. V. Pashkevich, Yu. E. Penionzhkevich, Yu.V.Ryabov, E. A. Sokol, V. G. Tishchenko, A. N. Tjukavkin, A. V. Unzhakova, and S. R. Yamaletdinov*
New Indications of Collinear Tripartition in $^{252}\text{Cf}(\text{sf})$ Studied at the Modified FOBOS Setup
 Physics of Atomic Nuclei, Vol. 66, No. 9, 2003, pp. 1631–1635. From Yadernaya Fizika, Vol. 66, No. 9, 2003, pp. 1679–1683.

10. *W.H. Trzaska, Yu.V. Pyatkov, D.V. Kamanin, S.R. Yamaletdinov*
Collinear cluster tripartition preliminary confirmed
 Proceedings of the XXXVIII annual conference of the Finish Physical Society, March 18-20, 2004 Oulu, Finland, Report Series in Physical Science, Report No. 25, p. 71.

11. *Yu.V. Pyatkov, D.V. Kamanin, A.A. Alexandrov, I.A. Alexandrova, S.V. Khlebnikov, E.A. Kuznetsova, V.G. Lyapin, S.V. Mitrofanov, Yu.E. Penionzhkevich, Yu.V. Ryabov, E.A. Sokol, V.G. Tishchenko, W. Trzaska, A.N. Tjukavkin, S.R. Yamaletdinov, B.V. Florko*
Experimental confirmation of the collinear cluster tripartition of the ^{252}Cf nucleus
 International Symposium on Exotic Nuclei, Peterhof, Russia, 5-12 July 2004. Conference proceedings, Editors: Yu.E.Penionzhkevich, and E.A.Cherepanov. Published by World Scientific Publishing Co. Pte. Ltd., 2005, p. 351-356.

12. *Yu.V. Pyatkov, D.V. Kamanin, W. Trzaska, S.R. Yamaletdinov, E.A. Sokol, A.N. Tjukavkin, A.A. Aleksandrov, I.A. Aleksandrova, S.V. Denisov, V.P. Krajnov, S.V. Khlebnikov, T.E. Kuzmina, E.A. Kuznetsova, S.V. Mitrofanov, Yu.E. Penionzhkevich, Yu.V. Ryabov, V.G. Tishchenko, B.V.Florko*
New results in studying of the collinear cluster tripartition of the ^{252}Cf nucleus
 Preprint JINR Dubna E15-2004-65, Dubna 2004.

13. *W.H. Trzaska, Yu.V. Pyatkov, D.V. Kamanin, S.R. Yamaletdinov, E.A. Sokol, A.A. Alexandrov, I.A. Alexandrova, E.A. Kuznetsova, S.V. Mitrofanov, Yu.E. Penionzhkevich, V.G. Tishchenko, A.N. Tjukavkin, B.V. Florko*

Evidence for collinear cluster tripartition

Seminar on Fission Pont d'Oye V, 16-19 September 2003, World Scientific 2004, ISBN 981-238-792-7, page 102 – 109.

14. *Yu.V. Pyatkov, D.V. Kamanin, W. H. Trzaska, W. von Oertzen, S.R. Yamaletdinov, V.G. Tishchenko, A.N. Tjukavkin, V.G. Lyapin, Yu.E. Peinionzhkevich, A.A. Alexandrov, S.V. Khlebnikov*
Island of the high yields of ^{252}Cf (sf) collinear tripartition in the fragment mass space
 Preprint JINR Dubna E15-2005-99, Dubna 2005.

15. *Yu.V. Pyatkov, D.V. Kamanin, W. H. Trzaska, W. von Oertzen, S.R. Yamaletdinov, V.G. Tishchenko, A.N. Tjukavkin, V.G. Lyapin, Yu.E. Penionzhkevich, A.A. Alexandrov, S.V. Khlebnikov.*
Recent results in studying of collinear tripartition of the ^{252}Cf nucleus. Programm of the study of collinear tripartition at the neutron beams
 Presented at the 13th International Seminar on Interaction of Neutrons with Nuclei, Dubna, Russia, 25-28 May 2005.

16. *S.Yamaletdinov, W.Trzaska, V.Lyapin, M.Sillanpää, Yu.Pyatkov, V. Tishchenko, Yu.Kopach, M. Mutterer, S. Khlebnikov, G. Tyurin*
Search for collinear tripartition in reaction $^{238}\text{U}+^4\text{He}$ (40 MeV)
 Proceedings of the XL annual conference of the Finish Physical Society, March 9-11, 2006, Tampere, Finland, p. 240.

17. *Yu.V.Pyatkov, D.V.Kamanin, W.H.Trzaska, S.R.Yamaletdinov, A.A.Alexandrov, I.A.Alexandrova, S.V.Khlebnikov, E.A.Kuznetsova, V.G.Lyapin, S.V.Mitrofanov, Yu.E.Penionzhkevich, Yu.V.Ryabov, E.A.Sokol, V.G.Tishchenko, A.N.Tyukavkin, B.V.Florko, V.E.Zhuchko*
New experimental data on collinear cluster tripartition of the ^{252}Cf nucleus
 Heavy Ion Physics, FLNR JINR Scientific Report 2003 - 2004, Dubna, Russia, 2006, p. 94-95.

18. *Yu.Pyatkov, W.Trzaska, M.Mutterer, S.Yamaletdinov, A.Tjukavkin, D.Bolgov, D.Kamanin, S.Khlebnikov, Yu.Kopach, E.Kuznetsova, Yu.Lavrova, V.Lyapin, M.Sillanpää, V.Tishchenko, G.Tyurin*
Peculiarities of data processing in experiment aimed at searching for rare decays of Pu* isotopes
 Proceedings of 14th International Seminar on Interaction of Neutrons with Nuclei: "Neutron Spectroscopy, Nuclear Structure, Related Topics". Dubna, May 24-27, 2006. Dubna 2007, p. 134-143.

19. *Yu. Pyatkov, W. Trzaska, M. Mutterer, S. Yamaletdinov, D. Bolgov, D. Kamanin, S. Khlebnikov, Yu. Kopach, E. Kuznetsova, J.Lavrova, V. Lyapin, M. Sillanpää, V. Tishchenko, A. Tjukavkin, G. Tyurin*
Searching for Rare Decay Modes in the Reaction $^{238}\text{U}+^4\text{He}$ (40 MeV)
 Proceedings of the International Symposium on Exotic Nuclei "EXON2006", Khanty-Mansiysk, Russia, 17-22 July 2006, AIP Conference Proceedings, Volume 912, Melville, New York, 2007, pp. 144-152.

20. *Yu. Pyatkov for HENDES and FOBOS collaborations*
Exotic decay modes of $^{242}\text{Pu}^*$ from the reaction $^{238}\text{U}+^4\text{He}$ (40 MeV)
 Presented at the 6th International Conference on Dynamical aspects of nuclear fission "DANF2006", Smolenice Castle, Slovak Republic, 2 - 6 October 2006. Proceedings will be published by World Scientific, Singapore. (in press).
21. *Yu.V. Pyatkov, D.V. Kamanin, W.H. Trzaska, w. Von Oertzen, S.R. Yamaletdinov, A.N. Tjukavkin, V.G. Tishchenko, V.G. Lyapin, Yu.E. Peinionzhkevich, A.A. Alexandrov, S.V. Khlebnikov*
Island of the high yields of $^{252}\text{Cf}(\text{sf})$ collinear tripartition in the fragment mass space
 Romanian reports in Physics, **59** (2007) 388.
22. *M. Mutterer, Yu.N. Kopatch, S.R. Yamaletdinov, V.G. Lyapin, J. von Kalben, S.V. Khlebnikov, M. Sillanpää, G.P. Tjurin, W.H. Trzaska*
Energy Distribution of Ternary α -Particles in $^{252}\text{Cf}(\text{sf})$
 6th International Conference on Dynamical Aspects of Nuclear Fission "DANF2006", Smolenice Castle, Slovak Republic, 2 - 6 October 2006. Proceedings will be published by World Scientific, Singapore. (in press).
23. *M. Mutterer, Yu.N. Kopatch, S. Yamaletdinov, V. Lyapin, J. von Kalben, S. Khlebnikov, G. Tjurin, W.H. Trzaska*
Precise Measurement of the Energy Distribution of Ternary α Particles Emitted in $^{252}\text{Cf}(\text{sf})$
 Proceedings of 14th International Seminar on Interaction of Neutrons with Nuclei: "Neutron Spectroscopy, Nuclear Structure, Related Topics". Dubna, May 24-27, 2006. Dubna 2007, p. 120-127.
24. *S. Yamaletdinov, M. Mutterer, Yu. Kopatch, V. Lyapin, J. von Kalben, S. Khlebnikov, M. Sillanpää, G. Tyurin and W. H. Trzaska*
Precise measurement of energy distribution of ternary α -particles from $^{252}\text{Cf}(\text{sf})$
 Proceedings of the XLI annual conference of the Finish Physical Society, March 15-17, 2007, Tallinn, Estonia, Report Series in Physics HU-P-267, p. 326.
25. *M. Mutterer, Yu.N. Kopatch, S.R. Yamaletdinov, V.G. Lyapin, J. Von Kalben, S.V. Khlebnikov, M. Sillanpää, G.P. Tyurin, W.H. Trzaska*
On the ternary α spectrum in $^{252}\text{Cf}(\text{sf})$
 "Seminar on Fission", Corsendonk Priory, Belgium, Sept. 18-21, 2007. Proceedings will be published by World Scientific. (in press).

Part 1

Searching for unusual multi-body decays in fission of actinides

1 Experimental and theoretical studies of ternary fission

1.1 Motivation

Very soon after the discovery of nuclear fission in 1939 the idea of possibility for nucleus to be divided into three fragments appeared. Already in 1941 *Present* had pointed out that the fission of heavy nucleus into three fragments with approximately equal masses is not only energetically permitted, but even more preferable than binary fission [Pre41]. According to estimations one might expect the maximum of the energy released in ternary fission to be with 10-20 MeV greater than that for binary fission. In 1958 *Swatecki* [Swi58] in the frame of the liquid drop model had calculated the amount of released energy at fission of nucleus into n fragments.

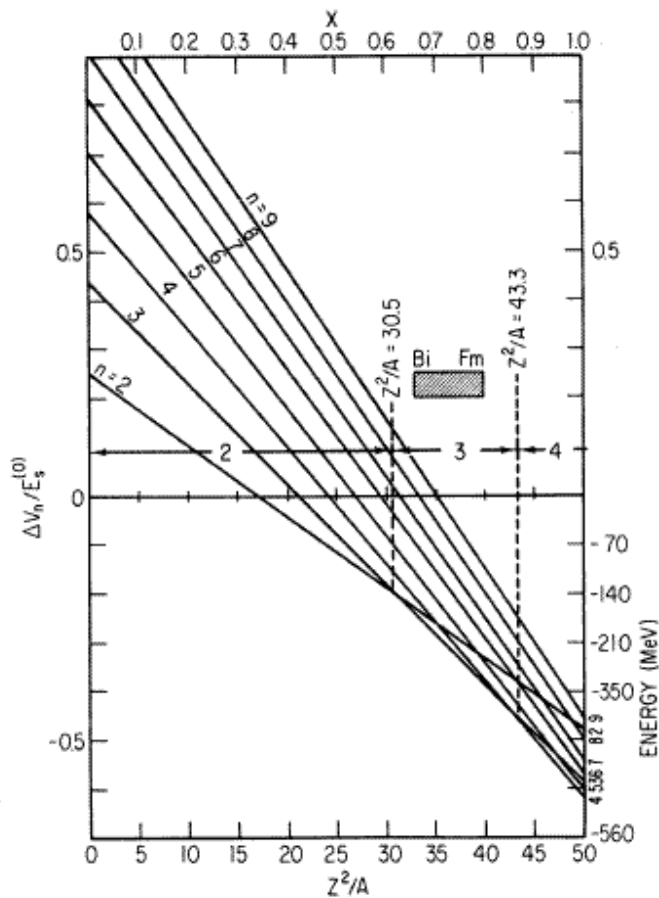


Figure 1.1 Energy released at splitting of ideal liquid drop into n equal parts as function of fission parameter Z^2/A . Figure from [Swi58]

Based on the results of his calculations, which is shown on Figure 1.1, it is possible to conclude that:

- fission into 3 heavy fragments is energetically more favorable than binary fission for all nuclei with fission parameter $30.5 < Z^2/A < 43.3$. These nuclei are nuclei from Bi to Fm;
- for the purposes of experimental detection of ternary fission one needs to choose nuclei with maximum available value of fission parameter Z^2/A .

These encouraging results had initiated intensive explorations of ternary fission in spontaneous and low energy fission of actinides. The main trends in this field cover:

- ✓ Fission of low-excited heavy nuclei into three fragments of comparable masses, the so-called “true ternary fission”. It has not been reported so far despite multiple attempts to find such a decay channel.
- ✓ The emission of charged particles moving almost along the fission axis. It was observed by *Piasecki* [Pia70] and called “polar emission”.
- ✓ The search for collinear tripartition of nuclear systems. *Diehl* and *Greiner* [Die73, Die74] showed in the frame of the liquid drop model a preference for prolate over oblate saddle-point shapes for fissioning systems. This fact can be treated as theoretical base for collinear tripartition.

Cluster radioactivity is a binary process. Nevertheless it is mentioned here due to the following reason. Considering that the magicity of one of the decay partners plays a key role in the process, the question whether multicuster decays occur arises naturally. In other words, a decay of heavy nucleus into magic constituents (clusters by definition) should be searched for.

Due to the fact that studying collinear multi-body decays into fragments of comparable masses, where participants could be magic nuclei, is overlapping with all variants of ternary fission mentioned above and with cluster radioactivity these points will be considered below in more details.

1.2 Terminology

Before dealing in detail with ternary fission, we want to define the terminology used. Besides definitions given above we will apply the next designations in this work. Normally, fission is a *binary* process, in which two primary fission fragments are formed when the fissioning nucleus splits. These primary fragments effectively attain their full energy of motion within a time scale of 10^{-18} s, having separated by about $2 \cdot 10^{-11}$ m. Much less frequently, more than two particles are formed within 10^{-18} s of the instant of scission. If precisely three particles appear within this time interval, the fission event is classified as *ternary* event. This definition covers the whole spectrum of three-particle fission events: from one extreme mode in which a scission neutron accompanies two primary fragments to the other extreme mode in which three primary fragments with approximately equal masses are emitted (“*true ternary fission*”). When the light charged particle (usually alpha particle) is formed along with the heavy fragments, the process is named “light charged particle accompanied fission (*LCP-fission*)”. In the common case of disintegration of nucleus into three fragments, when the fragment mass ratio and other parameters of fission are not essential for us, we call such process as “*tripartition*”. The term “*cluster radioactivity*” is applied for spontaneous emission of light fragments heavier than α -particle ($A = 4$) and lighter than fission fragments ($A \approx 60$) in the decays of heavy nuclei. In our experiment at the

modified FOBOS spectrometer (discussed in section 2) a specific group of events were revealed. The total mass of two registered fragments which fly apart almost collinearly was significantly less than the mass of the initial nucleus of ^{252}Cf . The mass of at least one of the detected fragments corresponded to the mass of the known magic nucleus. We called the phenomenon observed “*Collinear Cluster Tripartition (CCT)*”.

1.3 Tripartition in spontaneous and low energy fission

Experimental evidence for triple fission into two heavy particles and one light particle was first published in the literature by *San-Tsiang et al.* [Tsi47] in 1947. They irradiated ^{235}U by thermal neutrons and searched for the tracks of three fission fragments in photoemulsion. In 1950 *Rosen and Hudson* tried to find ternary fission in an ionization chamber used for detection of tripartition of ^{235}U nuclei under thermal neutron bombardment [Ros50]. A schematic view of the triple ionization chamber is shown in Figure 1.2. Each of three discriminators in the triple coincidence circuit was adjusted such that its channel would respond to a pulse size, from the appropriate section of the chamber, corresponding to a heavy fission particle of initial energy of approximately 40 MeV or higher. The coincidence circuit had an effective resolving time of approximately 1 μs , which is determined by charge collecting time in the ionization chamber, hence the main source for the background events were accidental coincidences produced by two or more binary fission events. The method for rejection these events was based on the analysis of energies of fragments in the ionization chamber.

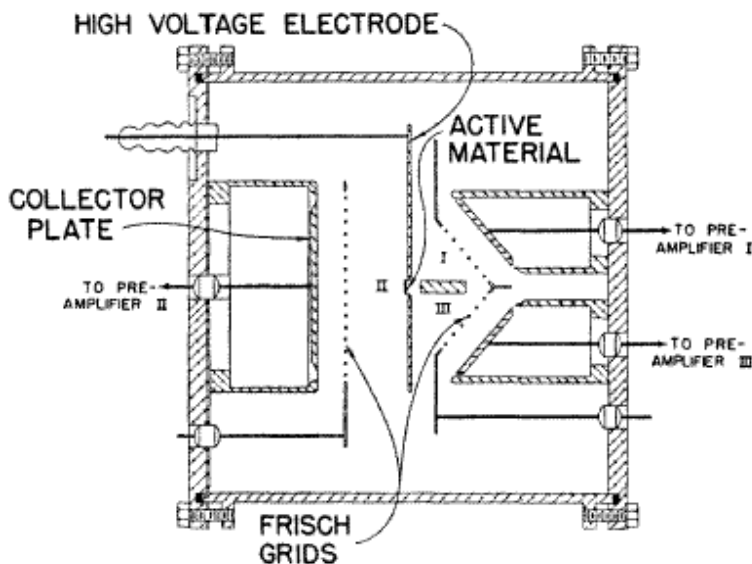


Figure 1.2 Schematic view of the ionization chamber used for the detection of triple fission of ^{235}U . Figure from [Ros50]

Estimation of the probability for tripartition into heavy fragments was done based on the analysis of counting rates for the triple coincidences and for each section of ionization chamber. The obtained frequency of ternary fission is 6.7 ± 3.0 per 10^6 binary fissions.

In 1963-1969 *Muga et al.* conducted series of experiments in order to search for true ternary fission in spontaneous fission of ^{252}Cf and in fission of ^{233}U , ^{235}U , ^{239}Pu , ^{241}Pu induced by thermal neutrons [Mug63, Mug67a, Mug67b, Mug69]. The experimental arrangement consisted of three solid-state detectors with a sensitive area of about 0.25 cm^2 (5mmx5mm) positioned 120° apart in a plane about a fission source. The radial positions of the detectors were fixed at 1.0, 1.5 or 2.0 cm. A scale drawing of the experimental configuration is shown on Figure 1.3. It was expected that fragments of ternary fission should fly away at 120 degrees to each other. The output signals of each of the three detectors were paralleled to a fast triple coincidence system, and only those events in which a fission fragment entered each detector within the resolving time of the coincidence unit (about 20 ns) were recorded. The frequency of the triple-event count rate relative to the single count rates of binary-fission fragments was found to be of the order of $\sim 10^{-6}$ for all systems studied. The masses of the fragments were determined based on the measured values of the kinetic energies in the assumption that total sum of all fragment masses is equal to the mass of the fissioning nucleus. The light-mass fragment distribution is presented on Figure 1.4. The fact of observing light fragments with mass up to 60÷70 is the most intriguing result of these experiments. The authors had considered in detail all possible phenomena and effects which can give rise to triple events:

- ternary fission;
- accidental events;
- instrumental effects;
- scattering phenomena;
- others, e.g. fission with α -particle emission, cosmic-ray showers.

Of all the other possible origins for the observed triple coincidence events, scattering phenomena are the most difficult to eliminate or to distinguish from ternary fission events. A very careful analysis was carried on and the following arguments indicated the absence of scattering phenomena for the case of a symmetrical detector arrangement ($\alpha=\beta=\gamma=120^\circ\pm 7^\circ$):

1. From the dynamics (kinetics) involved it is impossible for the detectors to record a scattering event.
2. The foregoing analysis has been experimentally verified by observing the features of binary-fission fragment scattering. Neither the energy distribution nor the angular dependence of true scattering events is consistent with or able to explain the data collected at the 120° angles.
3. The ratio of the triple events to binary events recorded is independent of the source foil thickness. A linear dependence should be observed if scattering was involved.
4. The energy distribution for $^{236}\text{U}^*$ and $^{234}\text{U}^*$ are markedly different; they should be virtually identical if scattering is the correct explanation.

By the process of elimination it was concluded that the only reasonable explanation for the observed data was a fission process in which three large fragments are formed, i.e., ternary fission.

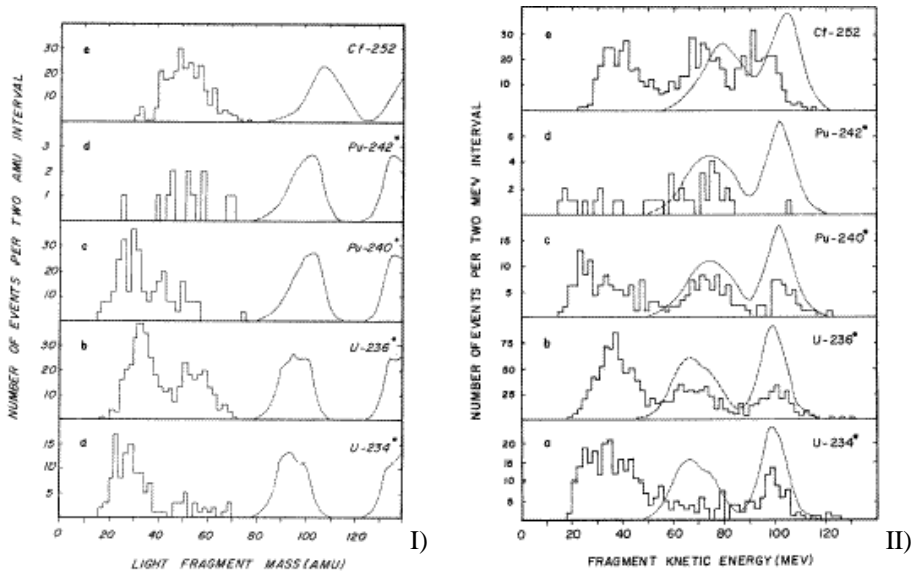


Figure 1.4 I) Light-mass fragment distribution and II) fragment kinetic energy distribution from ternary fission. The broken curve represents the distributions from binary fission. Figures from [Mug67a].

Mass-spectrometric analysis of fission products does not suffer from the limitations of the radiochemical method. It enables detection of stable as well as long-lived radioactive isotopes. The attempt to detect isotopes such as ^{20}Ne , ^{21}Ne , ^{22}Ne , ^{36}Ar , ^{37}Ar , ^{38}Ar , ^{39}Ar , ^{40}Ar , ^{42}Ar in ternary fission of ^{235}U was performed by *Kugler and Clarke* [Kug71]. The investigations of this work have extended the results from radiochemical studies to some mass chains and nuclides not previously studied. Except for ^{20}Ne and ^{40}Ar mass yields shown by *Muga* were from 1 to 6 orders of magnitude higher than those obtained by mass-spectrometric and radiochemical studies. The authors concluded that the negative results obtained in their work and in earlier radiochemical studies suggest that ternary fission at low excitation energies is either absent or occurs much less frequently than indicated by instrumental results. Since mass-spectrometric and radiochemical investigation had eliminated only 12 out of a possible 40 mass chains, the problem of existence of ternary fission at low energy was not satisfactorily resolved.

Twenty years later, the phenomenon of true tripartition was reinvestigated for ^{252}Cf (sf) by the group of *J.P. Theobald* [Sch87], using the powerful detection system "Diogenes". The detector is a toroidal gridded ionization chamber operated with isobutene at a pressure of $1.5 \cdot 10^4$ Pa (115 Torr). This position-sensitive ionization chamber allows the measurement of the angular and energy distributions of the ternary fission fragments with good accuracy. The energy and mass distributions for the observed triple coincidences are shown in Figure 1.5.

The measured energy spectrum of ternary fragments, unlike the mass spectrum, agrees quite well with that found by *Muga et al* [Mug67b]. It is evident from the observed angular distribution and mass spectrum that the measured ternary fission events reveal an asymmetric fission process into a pair of large-mass fragments (A_3 and A_2) accompanied by the emission of a light charged particle (A_1) rather than tripartition into nearly equal masses.

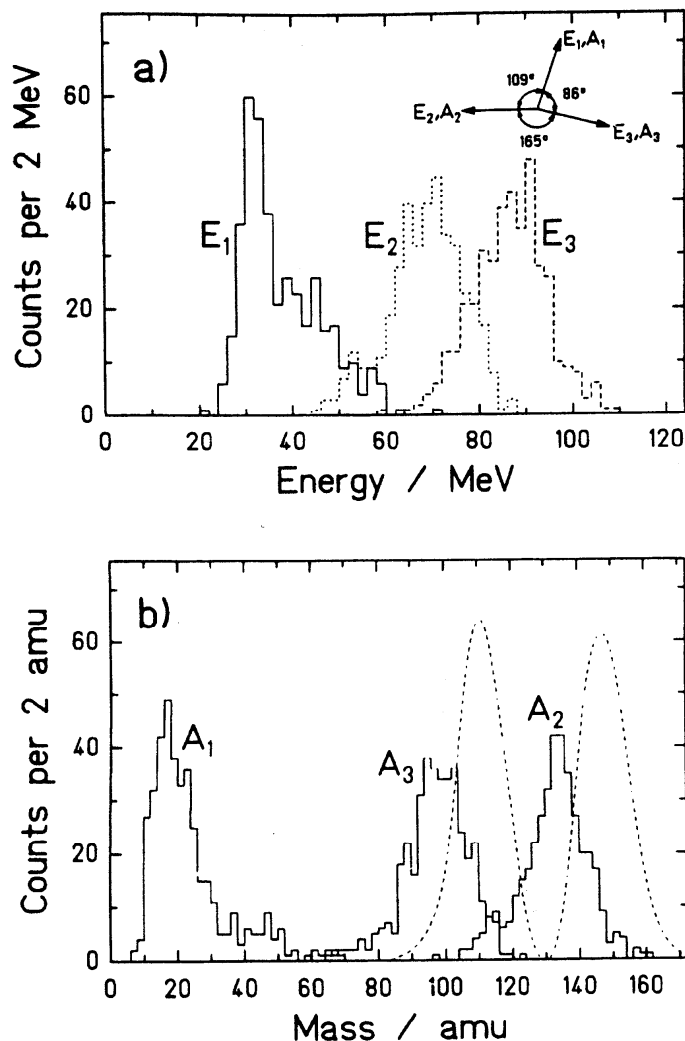


Figure 1.5 (a) Energy spectrum of ^{252}Cf ternary fission events, measured with a low-energy threshold of 25 MeV. The insert indicates the corresponding mean angles. (b) Mass distribution calculated from the measured energies and angles using momentum conservation. The binary fission mass spectrum of ^{252}Cf is presented by dashed lines. Figures from [Sch87].

The mass of the emitted light particles is within the range of $13 \leq A \leq 23$ and the atomic mass number Z_1 must be ≥ 6 for depositing the measured energy E_1 within the gas volume of the detector. The corresponding emission probability for this mass region is about 10^{-6} . For the possible true ternary fission with lightest masses in the range $30 \leq A \leq 70$ it was estimated an upper limit of $8 \cdot 10^{-8}$ per binary fission, which is about one order of magnitude lower than the one observed by *Muga et al.* The probability for symmetric tripartition ($70 \leq A < 95$) was found to be $< 2 \cdot 10^{-9}$.

1.4 Intermediate excitation energies

Positive results for the existence of tripartition at intermediate-energy range were obtained by *R. H. Iyer and J. W. Cobbe* [Iye66, Iye68] in 1966-1969. The scheme of the target assembly is shown in Figure 1.6. Uranium-238 target T was irradiated with ^3He and ^4He ions at energies ranging 20÷120 MeV. Various excitation energies were obtained using degrading foils A in front of target.

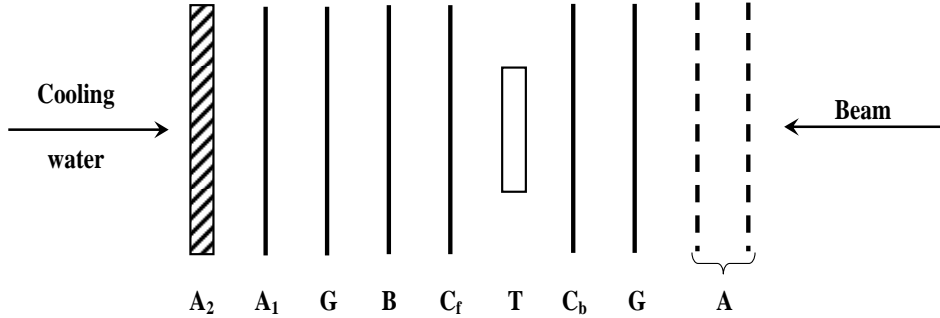


Figure 1.6 Schematic diagram of target assembly. A – energy adjusting foils; G – silver guard foils; C_f, C_b – forward and backward silver catcher foils; T – uranium target foil; B – blank silver foil; A₁ – high-purity aluminum foil; A₂ – aluminum foil.

The absolute cross sections for formation and yields were measured in target foil and in catcher foils C_f and C_b by standard chemical procedures. Excitation functions for the formation and yields for ^{24}Na , ^{28}Mg and ^{38}S were determined. These isotopes were chosen since they are far from any possible binary products at these energies, and also because they are neutron-excess species which can only be formed either in fission or by a limited number of spallation reactions (spallation is the process in which a heavy nucleus emits a large number of nucleons as a result of being hit by a high-energy projectile). Analysis of blank silver foil B irradiated along with the target assembly indicated that no nuclides were produced in detectable amounts by nuclear reaction on impurities in the catcher foils under the condition of the experiments.

Figure 1.7 illustrates the sharp dependence of the ratio of ternary to total binary fission yields of ^{28}Mg and ^{38}S on the energy of the compound nuclei $^{242}\text{Pu}^*$ ($Z^2/A=36.5$) and $^{241}\text{Pu}^*$ ($Z^2/A=36.6$) produced by helium-ion excitation. If it is assumed that these species are typical and representative of the ternary process in heavy elements, then it is possible to make estimates on order of magnitude of the probability of observing ternary fission in similar compound nuclei. At an excitation energy of 6.5 MeV, corresponding to the thermal neutron induced fission of ^{235}U ($Z^2/A=35.9$ for $^{236}\text{U}^*$), the ratio of ternary to binary fission cross section is expected to be of the order of $<10^{-12}$ and orders of magnitude smaller than the 10^{-6} reported by *Muga* for representative products.

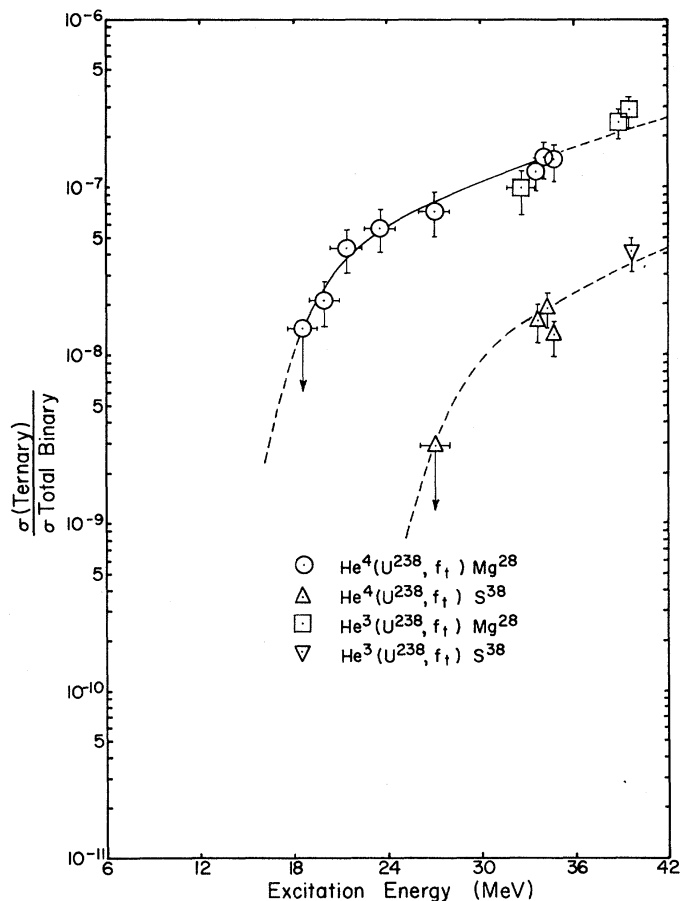


Figure 1.7 The ratio of ternary to total binary fission cross section as function of excitation energy for ^{238}U excited with ^3He and ^4He ions. Figure from [Iye66]

1.5 Polar emission in fission

It is generally believed that light charged particles, which once in a few hundreds of cases accompany fission, are born somewhere in the vicinity of scission and subsequently accelerated and focused almost perpendicularly to the fission axis by the Coulomb field of the fission fragments [Hal71]. This process, called equatorial emission, is described by the classical three-charged-points model. The emission of charged particles moving almost along the fission axis was observed by *Piasecki et al.* [Pia70] and called “*polar emission*”. This phenomenon cannot be explained by the three-charged-points model, since according to it the particles which start from the region between the two fission fragments should always be deflected off the fission axis by the Coulomb field. The nature of polar emission is still unclear although many hypotheses have been advanced.

E. Piasecki and *L. Nowicki* with colleagues did few experiments and compared the experimental results available from other groups with some theoretical models concerning the nature of polar emission [Pia70, Pia79, Now82, Kor85]. To determine the intensity of polar emission the authors used some convention setting the

borderlines: at 25° and 155° (the angles being measured with respect to the light fragment trajectory). This way they obtained the P/E ratios of the polar to equatorial emission intensities for protons, deuterons, tritons, ^4He and ^6He . These ratios decrease with increasing particle mass. The difference between the intensities of emission of various particles in polar emission and in conventional tripartition is remarkable, e.g. ^6He nuclei were never observed at the extreme angles, although over 5000 polar events were recorded by the Polish group alone (in tripartition, the intensity ratio $^6\text{He}/^4\text{He}$ is about 0.02). On the other hand, the protons, which are observed in conventional tripartition with intensities about hundred times lower than those of the alphas, constitute about one third of all polar particles. Knowing the P/E values one can determine the probability of polar emission. Using the experimental data on the α -particle yield in ternary fission Nowicki *L et al.* [Now82] obtained 15 and 18 polar α -particles per 10^6 fissions in ^{252}Cf and ^{236}U , respectively. However, the authors noted that these results can be substantially biased by systematic errors, since the P/E ratio in the uranium case was determined with fairly low accuracy due to a poor knowledge of the angular distribution in the polar region. Thus, it can not be excluded that polar emission probabilities may differ from the values given above by a factor of 2.

The kinetic energy E_3 spectra (in the lab system) of polar protons, tritons and α -particles emitted along the light (L) and heavy (H) fragment trajectory from $^{252}\text{Cf}(sf)$ are shown in Figure 1.8.

The energy of polar particles is definitely higher than that emitted in conventional tripartition although it seems that this energy changes smoothly on passing from "equatorial" to the "polar" range of angles.

The kinetic energy of the fission fragments which are accompanied by a polar particle is lower than in bipartition. The decrease of energy of the fragment moving at the same direction as the polar particle is explained partially by the recoil effect due to particle emission (near the moment of scission or later). However, since a similar decrease of the energy for the fragment moving in opposite direction to polar emission is also observed, it can mean that polar emission "prefers" those bipartition events in which the scission configuration is more then usually stretched.

Various theoretical approaches have been presented to explain polar emission, most of them however conflicting with the experimental observations. One of the hypotheses explaining the nature of polar emission is the evaporation hypothesis according to which the polar charged particles are evaporated from the accelerated excited fission fragments and focused along the fission axis by the kinematic effect. This hypothesis describes some of the experimental data quite well, but some observations are certainly in disagreement with this proposed mechanism, e.g. the angular distribution with respect to the fission axis, which according to the evaporation hypothesis should be much flatter than that experimentally observed especially for protons. The mean energies of polar α -particles and tritons are substantially lower than the values predicted theoretically. In [Pia79, Now82, Kor85] the authors examined few other hypotheses concerning the nature of polar emission and concluded that some of them are false but the others are quite promising, for example, the pre-scission emission model. This model suggests that the α -particle clustered in the neck remains for some time in the nucleus while the latter is deforming towards scission, and gains its kinetic energy through the one-body mechanism (i.e. by collisions with the moving walls of the neck) until the emission is energetically possible.

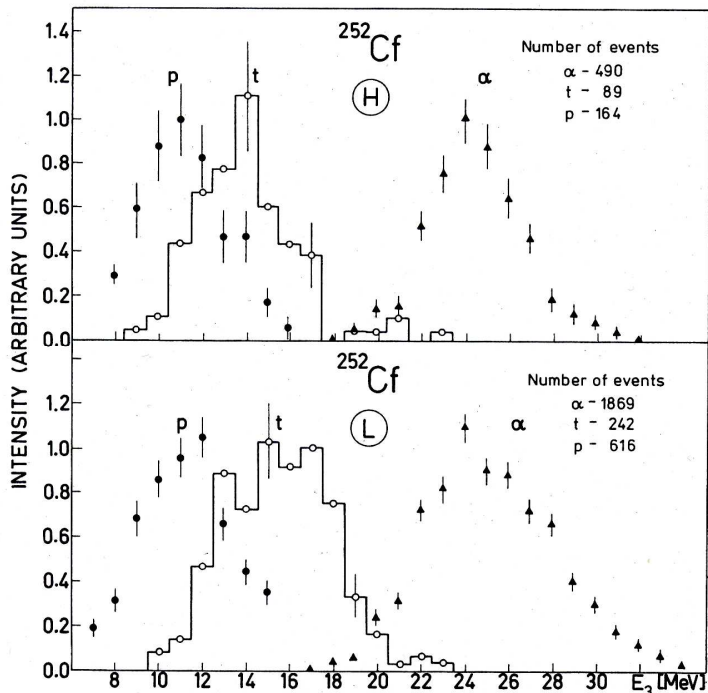


Figure 1.8 Energy spectra (in the lab system) of polar protons, tritons and α -particles moving along the light (L) and heavy (H) fragment trajectory. The spectra are normalized to unity in the peak. For simplicity the triton spectra are presented in the form of histograms. Figure from [Now82].

During this process, after several reflections from the potential wall, some clusters (or protons) could move to the polar tips, being subsequently emitted from this region of lower Coulomb barrier. Of course, such a mechanism needs a very long mean free path in the nuclear interior, which can not, however, be excluded.

In many experiments devoted to study polar emission there were high energy thresholds due to using ΔE - E telescopes and thick detectors to register the fragments moving at the small angle to the particle trajectory and to protect the telescope from fission fragments and strong α -radioactivity of the source. In such systems the energy threshold is very rapidly rising with the increase of the charge of the identifying particle. Thus studying characteristics of fission with creating massive third particles is impossible in the method mentioned above and is a real task which could be solved at some other setups and with different approaches.

1.6 Cluster radioactivity and cold fission

Cluster radioactivity as a rare spontaneous decay mode of heavy nuclei has been intensively studied in recent years [Pri89, Gön93, Ogl01]. In this new type of radioactivity any emitted nuclear species with masses heavier than $A = 4$ (α -particles) and lighter than $A \approx 60$ (fission fragments) are called “clusters”. The heavy fragments are grouped in the vicinity of the double magic ^{208}Pb , and this allows speaking about the known domain of cluster decay as “lead radioactivity”. This type of radioactivity

is far from being unique. Many other combinations of daughter nuclei are allowed energetically to be emitted; they include the formation of the products of comparable masses. This process is known as cold fission. However, cluster radioactivity is a very rare process: the observed partial life times lie in the interval $10^{11} \div 10^{27}$ s. This corresponds to a probability of $10^{-10} \div 10^{-17}$ for those α -decays. Estimates show that many cluster decays should have lifetimes even more than 10^{100} s.

In all known cases, except for one, the products of cluster radioactivity are formed in their ground states. From this point of view cluster radioactivity is much closer to alpha-decay than to spontaneous fission, the process in which the both fragments are deformed and strongly excited. For this reason correct comparison of both processes can be done only if cold fission is meant because here the fragments are formed in their ground or low-lying excited states. However, cold spontaneous fission itself is studied even worse than cluster radioactivity. The question of what is the mechanism of cluster radioactivity and whether it resembles either α -decay or fission was widely discussed.

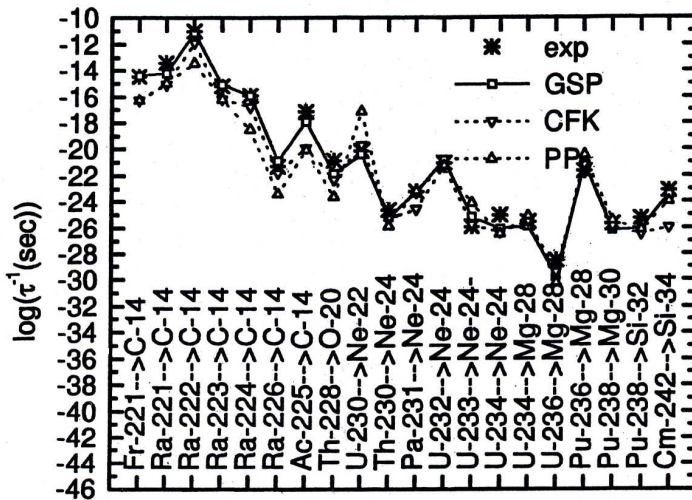


Figure 1.9 Cluster decay probabilities. GSP, CFK and PP are predictions of models by Greiner-Sandulesku-Poenaru, Chuvilski-Furman-Kadmenski and Pik-Pichak correspondingly. Figure from [Ogl01].

In Figure 1.9 cluster decay probabilities of all known decays are shown as a function of the emitted fragment masses. The dependence is rather irregular, which can partly be explained by incompleteness of the data. Still two tendencies are seen. Firstly, the probability for emission of a particular cluster is biggest when the heavy partner is ^{208}Pb ($^{222}\text{Ra} \rightarrow ^{14}\text{C}$, $^{232}\text{U} \rightarrow ^{24}\text{Ne}$, $^{236}\text{Pu} \rightarrow ^{28}\text{Mg}$) which correlates with the maximum Q-values of these decays. Secondly, the probability diminishes with light fragment masses at first fast (approximately by 10 orders of magnitude from ^{14}C to ^{24}Ne) and then does not change in average (from ^{24}Ne to ^{34}Si).

Comparison of the data with predictions of three models (phenomenological by Greiner-Sandulesku-Poenaru, semi microscopic “fission like” by Pik-Pichak and microscopic “ α -decay-like” by Chuvilski-Furman-Kadmenski) is also shown in Figure 1.9. Though the physical grounds of all three models differ very strongly, their predictions coincide among themselves and reproduce the data with the accuracy of

1 - 2 orders of magnitude. Thus, simple comparison of theory with experimental periods of half-lives does not allow to draw an unambiguous conclusion about the mechanism of the process.

The authors of [Ogl01] made a survey of mass distributions of cold decays for a series of nuclei and drew some conclusions. Cold decays are distributed over the whole available range of masses. The phenomenon known today as “cluster radioactivity” is only a particular case of their more general family. It is not distinguished either by the nature of its origin, or by its probability in comparison with the other modes. One can speak about “lead”, “tin” and “calcium” activities depending on the vicinity of Z- and N- values to the corresponding magic numbers. The most wide-spread activity is the “tin” one due to the fact that the ratio 82/50 is close to the average N/Z ratio of the decaying parent nuclei (this provides in average the maximum Q-value). “Tin” activity drifts from very asymmetric one in the parent mass region $A \sim 150$ to symmetric fission for ^{264}Fm . Another source of enhancement of the decay probability is the formation of fragments having prolate static deformations. Orientation of the big axis along the direction of movement results in lowering of Coulomb barrier and diminishing the path under it. As a result, the authors conclude that one cannot distinguish between cold fission and different types of cluster radioactivity. However, the dynamics of fragment formation in different parts of mass spectra can be different.

Alpha-radioactivity and fission usually are described by completely different formalism reflecting a different physical picture of what happens, and these extremes are applied to the description of cluster radioactivity. Alpha-decay is considered to be a non-adiabatic process. It means a sudden formation of a cluster inside the mother nucleus which then makes attempts to penetrate the barrier. The fission-like process, on the contrary, is described as an adiabatic one. It includes the pre-scission phase where the matter flow takes place and fragments are overlapping. Their final formation happens only after the system goes through a sequence of geometrical shapes whose parameterization is a part of the adopted theoretical approach. The existing data and theoretical calculations indicate that cluster (at least “lead”) radioactivity and cold fission have different mechanisms, probable non-adiabatic and adiabatic correspondingly. The transition between both mechanisms takes place at the fragment masses in the vicinity $A = 35$.

Summing up, the main conclusions about cluster radioactivity and cold fission are:

- The shapes of cold decay mass distributions mostly depend on two properties of the emitted fragments:
 - 1 the vicinity of their proton and (or) neutron numbers to the magic ones;
 - 2 the existence of static deformations: prolate static deformations of fragments result in lowering of Coulomb barrier and diminishing the path under it.
- Besides “lead radioactivity” one can distinguish some others like “tin” or “calcium” ones with “tin” radioactivity expected to be the most wide-spread.
- A cold fission region of mass spectra depends mainly on the interplay between deformation and shell effects.
- Emission of the lightest clusters is governed by non-adiabatic (α -decay-like) mechanism; emission of heavy fragments in cold fission region is adiabatic. The transition between both mechanisms seems to take place at fragment masses $A \sim 35$.

1.7 Indications for collinear tripartition of different nuclear systems

Most of ternary particles are emitted about perpendicular to the fission axis, but there are experimental indications for collinear tripartition, when the fissioning system has collinear configuration, i.e. elongated three-body chain-like configuration, and after scission fragments fly away along the axis of the system. The main object of this work is searching for collinear multi-body decays with creation of massive particles. We formulated this task based on the results from the papers reviewed below.

The collinear ternary fission has been intensively studied in the recent few decades by different groups. As far back as 1963 the sequential (cascade) ternary fission was studied in reactions ^{238}U , $^{197}\text{Au} + ^{22}\text{Ne}$ (185 MeV) and ^{209}Bi , $^{238}\text{U} + ^{40}\text{Ar}$ (310 MeV) [Kar63]. It was shown that the excitation energy of a heavy fragment is enough for a second scission to occur. In other work [Glä83] the authors describe the results of kinematically complete experiments which have been performed on the two- and three-body exit channels in the reactions $^{84}\text{Kr} + ^{166}\text{Er}$ and $^{129}\text{Xe} + ^{122}\text{Sn}$ at 12.5 MeV/u. Three-body events occur here with an unusually high probability and arise from a fast two-step mechanism where a sequential fission-like process follows a deep inelastic collision with preferentially very large energy losses. The angular distribution of fission fragments is consistent with an orientation of the fission axis approximately collinear with the axis of the system at the first scission, and the mass distribution of the fission is asymmetric with the heavier mass emitted preferentially opposite to the direction of the third particle. All together particular features of these three-body events present consistent evidence for a new phenomenon of non-equilibrium fission.

Another work [Van00] has studied the final states produced by $^{32}\text{S} + ^{59}\text{Co}$ and $^{32}\text{S} + ^{63}\text{Cu}$ dissipative collisions at $E \sim 5.6$ A·MeV that indicate the presence of three-body fragmentation processes in the reaction. Besides the already observed sequential binary process, analysis of the data revealed the presence of prompt ternary break-up of the composite system. The decay appears to occur in a collinear configuration, one of the produced fragments originating from the neck which connects the other two. In spite of the large energy dissipation some events show structural effects, i.e. the possible presence of clustering phenomena in reactions: at least one fragment is an α -like nucleus.

Collinear tripartition of ^{238}U nuclei induced by relativistic protons was reported in [Sol96]. This group used a source of spontaneously fissioning ^{252}Cf for energy and time calibration. A part of the calibration data was used to search for the spontaneous collinear tripartition [Kra99]. Unfortunately, the authors of [Kra99] were looking only for symmetric (both in masses and in charges) collinear tripartition with a slowly moving third fragment.

$$^{M_0}\mathbf{Z}_0 \rightarrow ^{M_1}\mathbf{Z}_1 + ^{M_3}\mathbf{Z}_3 + ^{M_2}\mathbf{Z}_2,$$

where $M_1=M_2$, $Z_1=Z_2$ and M_3 is at rest for $Z_3 \neq 0$. The mass of the inner third fragment was also limited by the condition $M_3 > 75$ a.m.u., which corresponds to the events of collinear tripartition found in the disintegrations of ^{238}U induced by 1 GeV protons. It was concluded that no effect has been observed for $M_3 > 75$ a.m.u. at the level of $7.5 \cdot 10^{-6}$ with respect to the probability of the binary fission process.

Very recently the evidence for collinear deformed system was obtained at the fragment spectrometer FOBOS installed at FLNR of JINR, Dubna [Her02]. Ternary

fission of heavy hot composite systems with excitation energies of 1.5–2.5 MeV/amu has been studied in the reactions of ^{14}N (53 AMeV) with ^{197}Au and ^{232}Th . The comparison with calculations for various scission configurations shows the averaged values of TKE measured for the anisotropic component to be in agreement with the assumption of a collinear stretched scission configuration with the light fragment positioned in between the two heavier ones. From the present investigation and from the comparison with previous data it was concluded that there exists a ternary fission mode out of a collinear deformed system very similar to the classical ternary fission observed in spontaneous fission. In particular, authors of this work have shown that this mode extends up to almost mass-symmetric ternary decays.

Thus the existence of collinear tripartition of different nuclear systems is an experimental fact and could be considered as the base for looking for collinear multi-body decays with creation of massive particles that is the aim of this work.

1.8 Theoretical studies of multi-body decays

In 1963 *Strutinsky* studied equilibrium forms of nucleus in a liquid drop model and showed [Str63], that along with ordinary configuration with one neck there are more complicated configurations with two and even three necks (Figure 1.10).

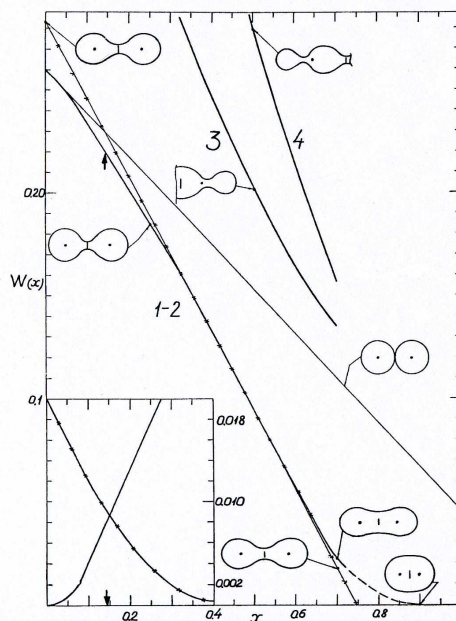


Figure 1.10 The potential energy of absolute equilibrium shapes $W(x)$ versus x for the conventional sequence of shapes (1 and 2), two-neck shapes (3) and three-neck shapes (4). Here x is the conventional liquid drop model parameter, which is proportional to nuclear charge Z and mass number A of the nucleus $x \sim Z^2/A$. The energy W is determined as the difference of potential energy of the nucleus with a given deformation and that of the initial sphere. Figure from [Str63].

These configurations can lead to triple fission. Note that the figures of unconditional equilibrium for the case of two necks are obtained at much higher energies that lead to very low cross sections for ternary fission.

About ten years later, *Diehl* and *Greiner* [Die73, Die74] considered the fissioning of a nucleus into three equal fragments in the liquid drop model in the cases of prolate and oblate pre-scission configuration (Figure 1.11).

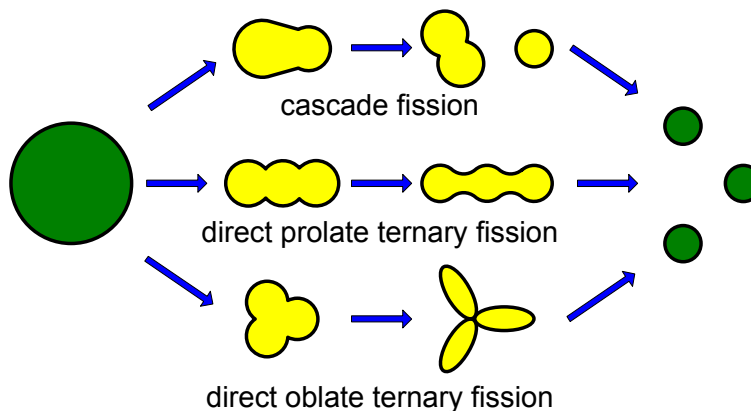


Figure 1.11 Schematic view of possible modes of ternary fission

It was found that the fission barrier in the case of oblate configuration is higher than that in the prolate configuration. The height of fission barrier rapidly decreases with increasing fissility parameter. Thus prolate (collinear) configurations are more profitable energetically for ternary fission. Decreasing the ternary fission barrier with the increase of the mass of the fissioning nucleus is well agreed with the observed experimental growth of the ratio between ternary and binary yields at increasing Z^2/A of compound nucleus.

Recently more general multicluster accompanied fission was analyzed by *Poenaru* who emphasized the strong shell effect corresponding to the doubly magic heavy fragment ^{132}Sn [Poe99]. Some typical pre-scission configurations for α -multicluster accompanied cold fission of ^{252}Cf are shown in Figure 1.12. As it can be seen from the figure, it is clear that the potential barrier for the “polar emission” is much higher than that of the emission from the neck. This explains the experimentally determined low yield of the polar emission compared to the “equatorial” one. As it should be, the compact configuration possesses the maximum total interaction energy, hence, it has the lowest chance to be observed.

From results of calculations the authors draw the important conclusion that the multiple clusters should be formed in a configuration of the nuclear system in which there is a relatively long neck between the light and heavy fragment. The second significant remark is that the minimum barrier height for ternary decay modes of ^{252}Cf is always obtained when the heavy fragment in calculations is the doubly magic ^{132}Sn .

The elongated prolate configuration with two necks for the fissioning ^{252}Cf nucleus was demonstrated recently in our work [Pya03] where the shell corrections were taken into account. This result was obtained in more detailed calculations of the potential energy surface of the ^{252}Cf nucleus carried out in the framework of the procedure presented in [Pas71, Pya97] based on the Strutinsky method.

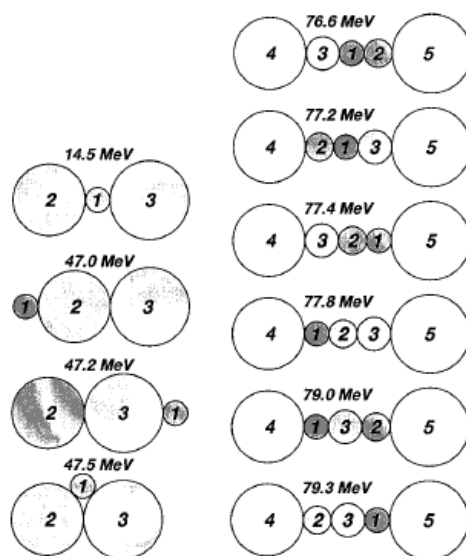


Figure 1.12 Aligned and compact configurations for α accompanied cold fission of ^{252}Cf with doubly magic ^{132}Sn heavy fragment (left-hand side), and aligned configurations with three clusters between the light and heavy fragment for $\alpha+{}^6\text{He}+{}^{10}\text{Be}$ accompanied cold fission of ^{252}Cf with ^{132}Sn heavy fragment (right-hand side). The corresponding energies are shown. Figure from [Poe99].

Figure 1.13 depicts the shape of the fissioning nucleus at the bottom of the “symmetry” valley with the quadrupole moment $Q_2 = 7.52$ a.u. The system that fissions in the vicinity of the bottom of the potential valley constitutes two magic nuclei (clusters) connected by a neck. In Figure 1.13(a), these clusters are the deformed magic nuclei of ^{108}Mo ($\beta_2 \sim 0.58$). In the calculations, the shape of the system was varied in such a way that the value of Q_2 remained constant while the mass-asymmetry η changed starting from the value corresponding to the valley’s bottom. By definition, $\eta = (M_1 - M_2)/Mc$, where $M_{1,2}$ is the mass of the system concentrated, respectively, on the left and on the right sides of the varied boundary, which divides the nuclear body into two parts (marked by vertical lines in Figure 1.13), and Mc is the mass of the fissioning nucleus. As a result, the new shape of the system shown in Figure 1.13(b) was revealed for the first time. The energy of the system is only slightly higher (by ~ 2 MeV) than the corresponding value at the bottom. The distinguishing feature of the shape observed is the double waist which vividly divides the system into three parts of comparable sizes namely $^{108}\text{Mo}_{66}$, $^{98}\text{Sr}_{38}$, $^{46}\text{Ar}_{28}$. Magic numbers are marked at the bottom of the element symbol. Thus, all three constituents are the magic nuclei. It would appear reasonable to identify the double rupture of such a configuration as the true ternary fission (ternary cluster decay) so long sought.

Ternary decay of low or middle excited nucleus via chain-like pre-scission configuration into magic fragments of comparable masses seems to be reasonable from a theoretical point of view. It is also reasonable to search for experimental manifestations of such decay channel analyzing almost collinear multi-body events.

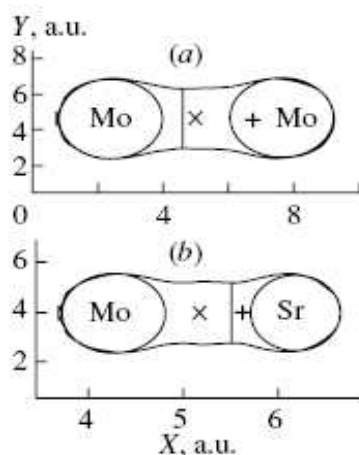


Figure 1.13 The shape of the nucleus at the bottom of the “symmetric” valley ($Q_2 = 7.52$ a.u., $\eta = 0.074$) (a); the same system at the point $Q_2 = 7.52$ a.u., $\eta = 0.208$ (b). See text for details.

1.9 Conclusions

From theoretical calculations based on the liquid drop model [Die73, Die74] it was found a preference for prolate over oblate saddle-point shapes for ternary fission. It could be in this case that after two simultaneous scissions of the fissioning system massive central fragment can stay almost in rest (or can have a low kinetic energy). Sequential ternary fission can also lead to the formation of a fragment having low kinetic energy. As a result, in order to register such fragment the detection system should have low energy threshold. This was not provided in the latest experiment [Sch87]. The placement of detectors in experiments [Mug63, Mug67a, Mug67b, Mug69 and Sch87] was not optimized, because fission, where fragments fly away at 120° is unlikely due to high height of fission barrier for oblate pre-scission shape of nucleus. Recent calculations, which take into account shell effects [Poe99, Pya03], strengthen conclusions about chain-like pre-scission configuration of fissioning nucleus obtained in the frame of the liquid drop model.

While in most known conventional ternary fission emission of light charged particle occurs in the plane almost orthogonal to the fission axis, the collinear ternary fission was also observed experimentally by different groups: [Kar63, Glä83, Van00 and Her02]. Polar emission also can be considered as collinear fission with creation of the light third particle. The study of the fission with creation of the third massive particle in polar emission experiments was not possible due to high registration thresholds of the detection systems.

From a number of clusters (nuclei with closed neutron or proton shells) involved in the decay the heavy cluster radioactivity and cold fission are one-cluster decay. The question whether there are cluster decays with multiplicity two or even three arises. Searching for such decay is much closer to the classical task of finding true ternary fission. So far there are no accepted proofs of this process for low excited systems. Thus, searching for the collinear multi-body decays of low excited nuclear systems with creation of massive third particle when at least one of fragments is magic nucleus is an actual scientific problem.

2 Experiment at modified FOBOS setup

In the early experiments at the spectrometer FOBOS some unusual structures in the mass-mass plot were obtained in the reactions $^{248}\text{Cm}(\text{sf})$ and $^{252}\text{Cf}(\text{sf})$. These structures had the yield level of $\sim 10^{-5}$ – 10^{-6} with respect to conventional binary fission and had been treated as an indication for new exotic decay – collinear cluster tripartition (CCT) [Pya00]. The advanced experiment aimed specially at the investigation of CCT phenomenon for the ^{252}Cf nucleus has been performed at the modified spectrometer FOBOS. This experiment allowed us to test the model of the CCT process which implies the three-body chain-like configuration at scission: after scission two outside fragments fly apart along the chain axis while the central fragment stays almost at rest and constitutes the isotropic source of post-scission neutrons of a high multiplicity (~ 10) in the laboratory system. In order to improve the quality of the data in comparison with the previous experiments at the FOBOS setup, some modifications have been introduced into the experimental scheme. To symmetrize the detector arms a special three-electrode avalanche counter start detector with an internal ^{252}Cf source was developed. The ordinary FOBOS setup has been covered with the belt of neutron detectors to verify the idea of the high neutron multiplicity in the CCT events. Because energy losses of fission fragments in the foils of the gas detectors is quite large special attention was devoted to techniques and methods of calibration of FOBOS gas filled detectors and to the development of an original mass reconstruction procedure.

2.1 Original FOBOS setup

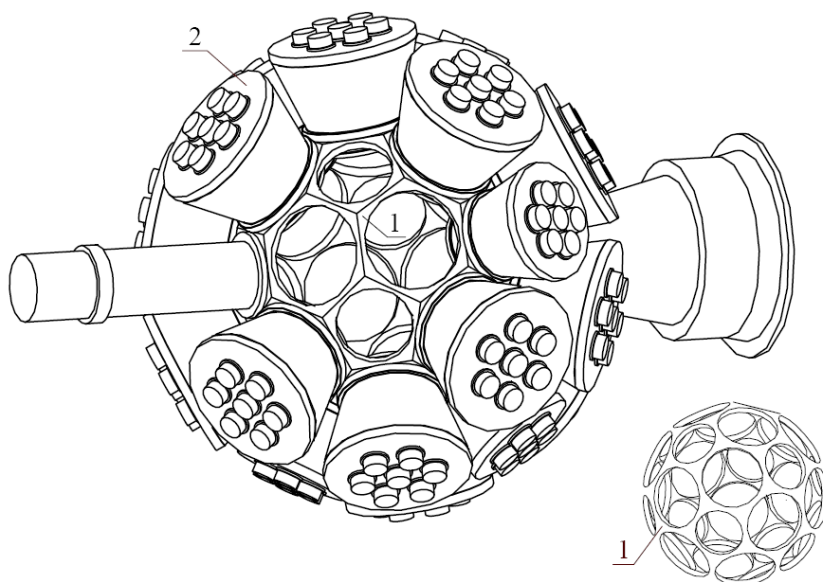


Figure 2.1 General layout of the FOBOS spectrometer. 1 – monolithic skeleton, 2 – detection module.

The experiment at the modified FOBOS setup was based on the constructive elements of the original FOBOS setup. FOBOS [Ort98] is a 4π spectrometer installed at the Flerov Laboratory of Nuclear Reactions (FLNR) of the Joint Institute for Nuclear Research (JINR) in Dubna, Russia. This spectrometer was specially designed for reaction studies in direct kinematics, i.e., for reactions where a light projectile impinges upon a heavy target nucleus. FOBOS is able to register charged reaction products only, ranging from protons up to heavy residues (HRs). A spherical detector design was conceived in order to cover most of the solid angle around the target, and consists of a 32 face truncated isocahedron in which 20 of the faces are regular hexagons and 12 are regular pentagons, respectively. The general layout of the FOBOS spectrometer is shown on Figure 2.1.

The detection system of the FOBOS spectrometer consists of three consecutive shells of particle detectors. The inner detector shell, consisting of 30 position-sensitive avalanche counters (PSACs), and the relatively long flight path of 50 cm between the target and shell, provides the means for a very precise time-of-flight (TOF) and coordinate (X, Y) measurement of fragments with $Z \geq 2$. The second detector shell, consisting of 30 axial Bragg ionization chambers (BICs), measures the stopping power of the fragments along their path within the gas volume (Bragg curve). From the TOF and the residual energy E_R information, the fragment masses (m_i) can be calculated by making suitable corrections to the energy losses in the penetrated detector materials. Adding to this the coordinate information, the momentum vectors (p_i) of each fragment can be derived “event by event” in an independent manner. This feature is a necessary condition for exclusive measurements. For the detection of energetic LCPs ($Z = 1-2$) a third, more granular, scintillator shell of CsI(Tl) detectors is arranged behind the BICs. The PSACs and BICs are not sensitive to low ionizing fast LCPs and, consequently, the passage of these particles through these detectors does not affect the registration of other fragments. The third shell of scintillator detectors was not involved in the experiments devoted to the investigation of the collinear cluster tripartition in spontaneous fission of ^{252}Cf .

2.2 Modified FOBOS spectrometer

The experimental layout of the modified FOBOS spectrometer is shown in Figure 2.2. Due to the low cross-section of the process under study and some additional requirements addressed to the spatial arrangement of the detectors involved, the two-arm configuration containing five big and one small standard FOBOS modules in each arm was used. Every module includes a position-sensitive avalanche counter and a Bragg ionization chamber. Such scheme of double-armed TOF-E (time-of-flight-energy) spectrometer allows to measure the energies and the velocity vectors of the coincident fragments to be detected and covers $\sim 29\%$ of the hemisphere in each arm. In order to provide “start” signal for all the modules only wide-aperture start-detector capable to span a cone of $\sim 100^\circ$ at the vertex could be used. Known micro-channel plate based detectors fail to meet this strict requirement. The relatively low energies of the fragments to be detected arisen both from physics of the process under study and energy losses in the rather thick entrance windows call for the minimization of the thickness and/or number of foils on the flight path of a fragment. The next problem to be solved is connected with the danger of an accidental disintegration of the source in the inner space of the spectrometer due to the very thin

($\sim 50 \mu\text{g}/\text{cm}^2$) backing used. It means that some kind of the source encapsulation is desirable.

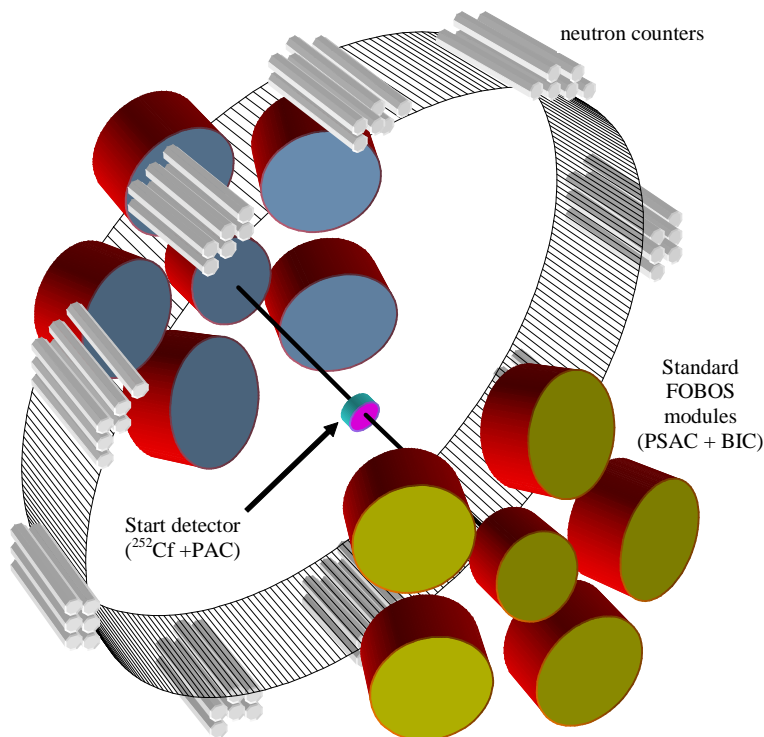


Figure 2.2 Schematic view of the modified FOBOS setup.

All the above mentioned, partially discrepant, requirements were satisfied in the special designed three-electrode start avalanche counter in which a central electrode (cathode) is combined with the fission fragment source of ^{252}Cf [Ale00]. The additional advantage achieved in such a schema consists in minimization of the error of the velocity determination which occurs when only one start-detector located in one of the time-of-flight arm at some distance from the fragment source is used.

According to the model of the CCT process proposed in [Pya00] the middle fragment of the three-body pre-scission chain borrows almost the whole deformation energy of the system. Being presumably in rest it would be an isotropic source of post-scission neutrons of a high multiplicity (~ 10) in the lab system. On the contrary, the neutrons emitted from the moving fission fragments are focused along the fission axis. In order to exploit this phenomenon for revealing the CCT events the “neutron belt” was assembled in a plane being perpendicular to the symmetry axis of the spectrometer, which serves as the mean fission axis at the same time (Figure 2.3).

The centre of this belt coincides with the location of the FF source. The neutron detector consists of 140 separate hexagonal modules [Sok97] comprising a ^3He -filled proportional counter, a moderator, a high-voltage input and a preamplifier. The counters operate under a gas pressure of 7 bar, being 50 cm in length and 3.2 cm in diameter. The moderator is made of polyethylene. The spacing between the parallel planes of a module is 5 cm. The neutron counters are composed into 8 arrangements of 16 counters each and one of 12 counters and they cover altogether $\sim 35\%$ of the

complete solid angle of 4π . Two such arrangements are mounted at the main FOBOS vacuum chamber near the target node. The electronics of the “neutron belt” is operated in the slave mode being triggered by the event selector of the gas part of the FOBOS detector. The number of hited ^3He neutron counters was added to the data stream as an additional parameter for each registered fission event.

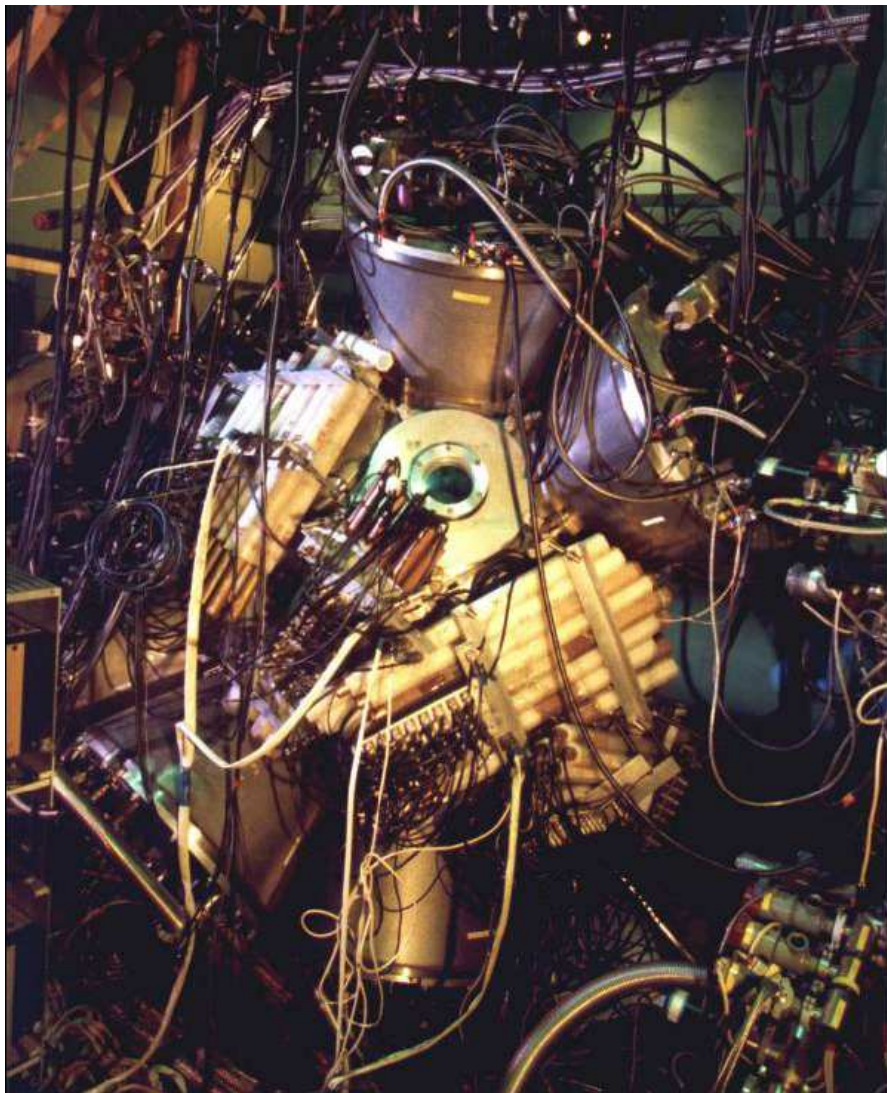


Figure 2.3 The overall view of the spectrometer FOBOS surrounded by the belt of neutron counters.

The registration efficiency for those neutrons emitted from an isotropic source was found to be very close to its geometrical limit, while the registration efficiency for neutrons emitted from the fission fragments registered by the FOBOS modules amounted to $\sim 4\%$ because they are focused along the fission axis which is perpendicular to the plane of the neutron counter belt. The registration probability for more than one neutron from ordinary spontaneous fission in this geometry amounts to

1%, however, the same probability for the CCT events runs up to 85%. The registration probabilities for more than two neutrons are 0.3% and 62%, respectively. Such a comparison argues, obviously, in favour of searching the CCT events among those with the multiple numbers of fired neutron counters.

2.3 FOBOS detector module

The base of the detection system of the FOBOS spectrometer is a standard detector module. Every module consists of position-sensitive avalanche counter, Bragg ionization chamber and a set of scintillator detectors. The latter were not used in the experiment at modified FOBOS spectrometer. Figure 2.4 shows the sketch of general layout for the detector module.

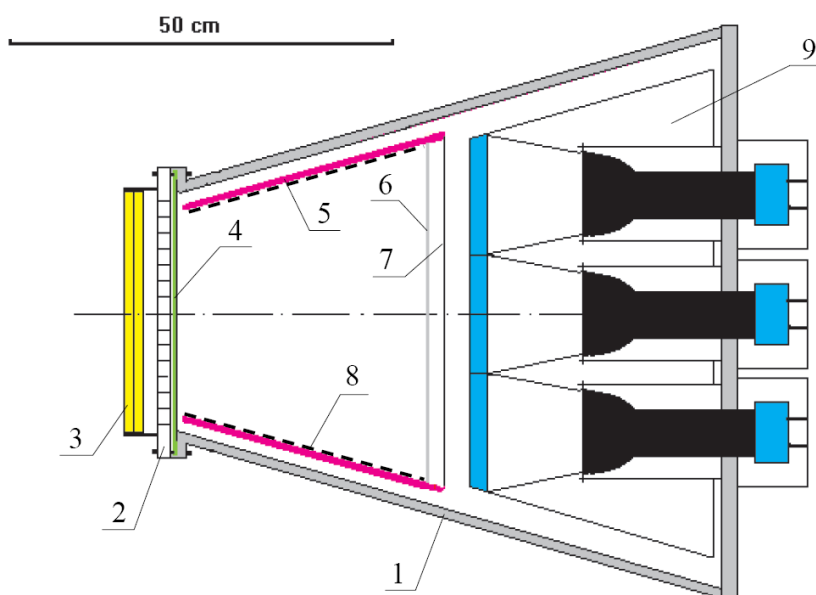


Figure 2.4 Sketch of the general layout of a detector module. 1- body of the BIC, 2 – support grid for entrance window, 3 – PSAC, 4 – entrance window foil (cathode), 5- teflon cone, 6 – Frish grid, 7 – anode, 8 – HV-divider, 9 – scintillator shell.

Because of the main attention in this chapter will be devoted to analysis of experimental information obtained from gas-field detectors (PSAC and BIC), these detectors will be described below in more detail.

2.3.1 Position-sensitive avalanche counters.

The operation of position-sensitive avalanche counters is based on the principles described in [Sei88]. Three thin Mylar foils ($1.2 \mu\text{m}$) are used as cathode and PSAC windows. The central cathode-foil is covered by $40 \mu\text{g}\cdot\text{cm}^{-2}$ thick Au layers and delivers the timing signal. Two perpendicular wire-planes (made of $30 \mu\text{m}$ thick Au-coated W, spaced by 1 mm) are positioned at a distance of $3 \text{ mm} \pm 50 \mu\text{m}$ on both

sides of the common cathode. They serve as anode coordinate grids. The window foils are glued to special frames, which can be changed individually in the case of gas leakage. The transparency of the PSAC amounts to 92%.

Pairs of neighbouring coordinate wires are connected to conductive strips which are capacitively coupled to a wound read-out delay-line of $1.4 \text{ ns}\cdot\text{mm}^{-1}$ specific delay and 560Ω impedance. The delay lines of the two coordinate grids are matched with resistors at one end and coupled to special read-out amplifiers at the other end. The cathode read-out circuit delivers an amplified current signal for timing and a charge signal for pulse-height analysis. All electronic channels are protected against damage if spark discharges occur in the counters. The surface-mounted circuits and the delay lines are placed in non-sensitive areas directly inside the PSAC frames. The spatial resolution of the PSACs amounts to $\Delta x = \Delta y \approx 1.5 \text{ mm}$. The general scheme of the PSAC read-out is shown in Figure 2.5.

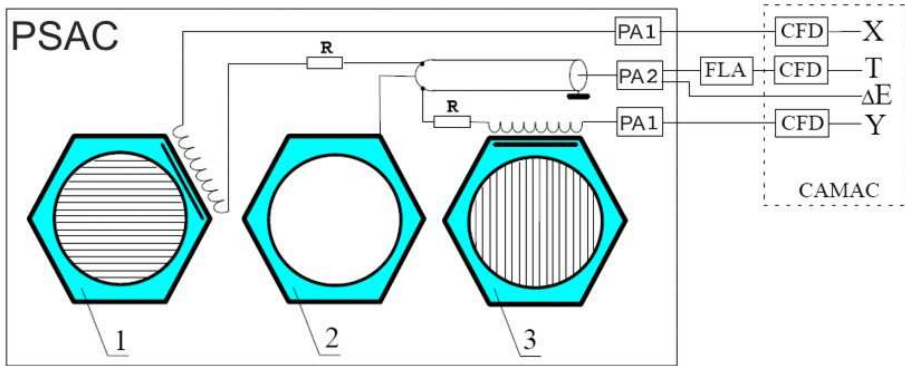


Figure 2.5 Principal scheme of the PSAC read-out. Delay lines are capacitively coupled to the X- and Y-wire planes. Three preamplifiers (PA) for the coordinates and timing signals are directly mounted to the PSAC frame. A fast linear amplifier (FLA) for the timing signal (TOF) drives the long cable line to the front-end electronics in the measurement hall. A CAMAC module contains three constant fraction discriminators (CFD).

The counter gas is pentane at a pressure between 200 Pa and 800 Pa. The voltage (typically $\approx 500 \text{ V}$) is set about 5 V below the onset of spark discharges, which may be induced by feed-back effects after the passage of highly ionizing particles. This voltage level guarantees an effective registration of heavy fragments with a lower threshold of $\approx 0.05 \text{ AMeV}$. The efficiency of registration for α -particles drops for energies $\geq 1.5 \text{ AMeV}$ because of the decrease of the energy loss in the sensitive volume. The time resolution of the detector at registration of α -particles is about 500 ps.

2.3.2 Axial ionization chambers

The principle of a BIC was first described in [Gru82]. Since the electric field is parallel to the direction of the incoming particles, the registered pulse-shape of a fragment stopped within the gas volume of the BIC represents an image of the specific energy loss along the ionization path characterized by the Bragg curve. The integral of the electronic charge created is proportional to the residual energy (E_R) of

the fragment, and the maximum of the ionization-density distribution in the stopping path is a smooth function of Z .

The entrance windows of the large and small BICs, made of 1.5-3 μm thick aluminized Mylar, have diameters of 385 mm and of 285 mm, respectively. The sensitive depth of the BICs is 250 mm. To withstand the pressure of the working gas, the delicate window foil, which at the same time serves as cathode, has to be supported by twofold structure - a concentric heavy carrier of transparency of 94% and an adjacent etched Ni-mesh having a cell dimension of 2.7 mm. Cells smaller than 3 mm are necessary because, otherwise, the extremely thin foils would not hold gas pressures up to 100 kPa needed to stop most of the intermediate mass fragments within the sensitive depth. This mesh, however, reduces the transparency of the entrance window to 75%, causing the most serious restriction with respect to the effective solid angle ($\Delta\Omega$) of the spectrometer. The PSAC foils and the BIC window foil create together a dead layer for fragment spectroscopy of $\approx 0.7 - 0.9 \text{ mg}\cdot\text{cm}^{-2}$.

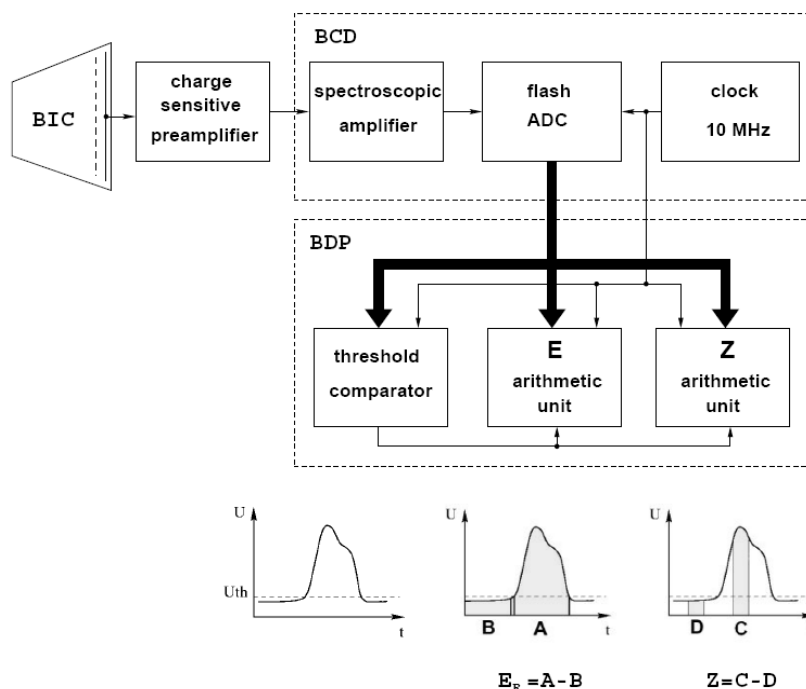


Figure 2.6 Principle of the digital-processing method of the BIC signal. (BCD – Bragg-curve digitizer unit, BDP – Bragg digital-processor unit).

The shaping of the axial electric field is performed by 5 mm spaced Cu-strips coated on the inner side of the conical Teflon insulator. The voltage divider provides equal potential steps. The Frisch grid is placed 10 mm in front of the anode. It consists of two perpendicular wire-planes (50 μm thick Cu-Be spaced by 1 mm). The anode is a 10 μm thick aluminized Mylar foil. The positive voltage is fed to the anode and the Frisch grid via a passive filter and an attenuator to achieve optimum field strength relations. In typical experiments the BICs are filled with a P-10 gas-mixture (90% Ar + 10% CH_4) at a pressure of 20 – 40 kPa and operated with an anode voltage of 1.5 – 3 kV. At the design limit of 100 kPa this voltage reaches 8 kV.

Conventionally, the charge signal of a BIC is split and shaped by two different time constants to deduce the E_R - and Z-information. In our case, the long electron drift-time (up to 4 μs) would cause a considerably large ballistic deficit. Therefore, a new processing method has been developed which derives the E_R - and BP-signals directly from digitized signal samples. The electronic setup of this method has been described in [Ort89], and its principle is shown on Figure 2.6.

The read-out system consists of a charge-sensitive preamplifier, a Bragg curve digitizer (BCD) and a Bragg digital processor (BDP). The BIC-signal is shaped by a short time constant ($\tau = 0.2$ or $0.4 \mu\text{s}$) in a spectroscopic amplifier and further digitized by an 8-bit flash ADC with a quartz-stabilized sampling frequency of 10 MHz. When a signal is recognized by the threshold comparator, two arithmetic units are activated calculating the values for E_R and BP. The algorithms are schematically displayed in the bottom of Figure 2.6. The hatched areas indicate the sums over the samples. The control logic (not shown on Figure 2.6) organizes the coincidence condition with respect to the PSAC, a pile-up inspection, and the connection with the first-level trigger. The digital-processing system (two CAMAC modules per FOBOS module) is very simple to operate, faster than a conventional one by a factor of ≈ 10 , and about two times less expensive.

2.4 Calibration procedures

The whole data analysis relies on the accuracy of the calibration. The detector systems measure only electrical signals and without a reference they have no significance. All detectors have to be calibrated to match the proper regions of the parameters for the current measurement. The difficulties of precise reconstruction of the fragment masses due to large energy losses in the foils of the gas detectors become apparent as some asymmetry in the mass-mass correlations of the events presumably linked with the CCT observed in previous data obtained on FOBOS setup [Pya97]. This has enforced on improvement of time and energy calibration procedures, which are extremely important in discussions of the data reliability. Therefore a detailed description of these procedures is given below.

2.4.1 Checking the stability

The first stage in data processing of any experiment consists of checking the stability of all measured parameters for the time of experiment and, if it is needed, making corrections. The stability of E and T channels for each FOBOS module was checked by calculating the mean value and the dispersion of data in spectrum. If there were some doubt moments regarding the stability of the data, the former was checked the second time by fitting the spectrum with two Gaussians and determining the parameters of these Gaussians. For a large amount of data such procedure of double check allows to automate the difficult process of checking the stability for critical spectra. To avoid routine work special software was developed for both methods. Some small corrections were done for some modules, but this procedure is trivial and does not need special attention.

2.4.2 Coordinate calibration of the PSACs

The absolute coordinate calibration of the PSACs is performed by using coordinate scatter plots of events measured in coincidence with the BICs positioned behind them. The supporting structure of the window foil of the BIC generates a shadowed zone with a decreased rate (Figure 2.7).

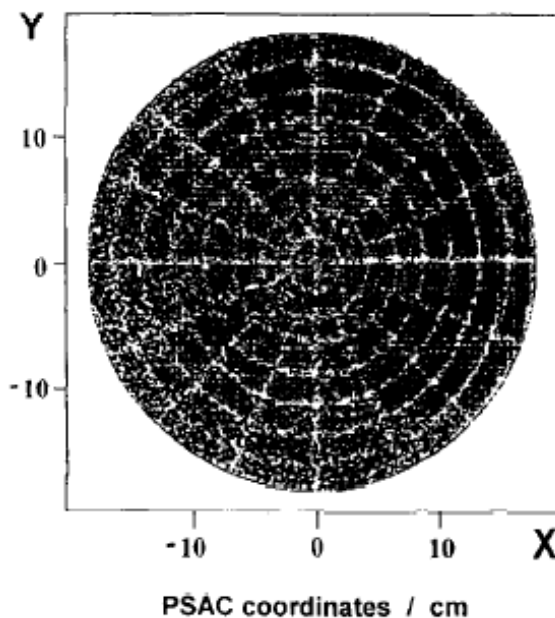


Figure 2.7 Shadow zone in the coordinates scatter plot of a PSAC imaging the supporting structure of the window foil of the BIG. The plot is generated by correlated events in the PSAC and the BIG positioned behind it.

A geometrical model of the supporting structure is adjusted to the center and to the dimensions of this image to achieve a complete agreement with the shadowed zone. This procedure gives the intrinsic scales, which are used to define the module-oriented coordinates (x , y) of the registered event. The polar and azimuthal angles (θ , φ) of the particle with respect to the target position can be calculated in a straightforward manner with reference to a special table. The uncertainties (Δx , Δy) lead to errors $\Delta\theta = \Delta\varphi \approx 0.2^\circ$.

2.4.3 Time calibration of the PSACs

The TOF calibration has been performed by fitting the experimental mass distribution of ^{252}Cf to that known from the literature. There are several variants of Mtt spectrum (i.e. obtained with TOF-TOF method) for $^{252}\text{Cf}(\text{sf})$ available in publications but they have some discrepancy at least in the form of the distribution as it is shown ,for instance, in Figure 2.8.

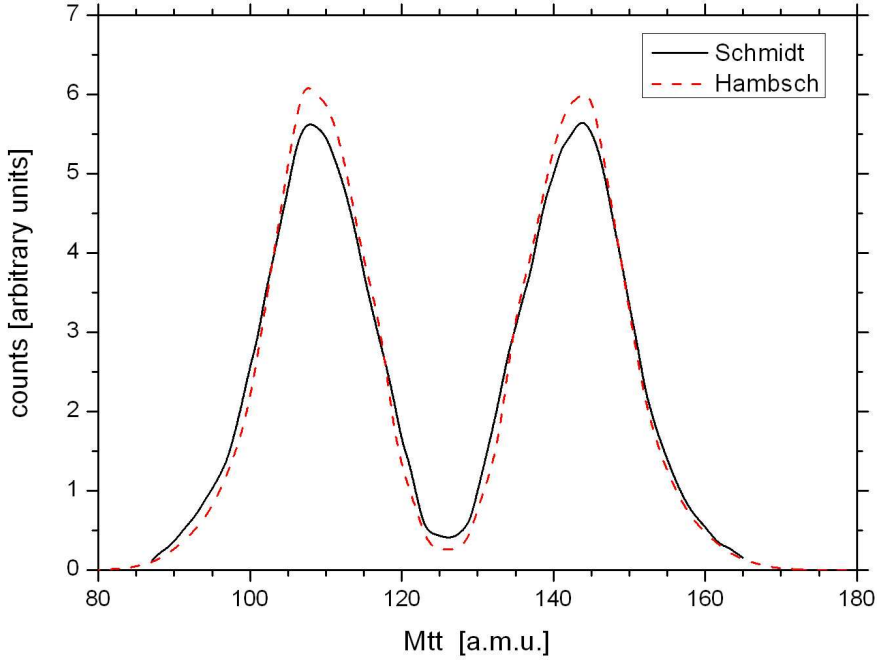


Figure 2.8 Comparison of two Mtt spectra reported in literature. Black solid line is [Sch83], red dashed line is [Ham97].

Between the data from [Sch83] and [Ham97] we have chosen the former. This is data from a more complex study of $^{252}\text{Cf}(\text{sf})$ (the experiment made by Hamsch [Ham97] was focused on the study of the far asymmetric mass region).

In order to extract the coefficients of the TOF calibration we fit the experimental distribution of TOF-masses for ^{252}Cf to that taken from [Sch83]. The free parameters for the fitting were the effective thickness of an absorbing matter on the particle flight-path (the thicknesses of the start-detector foils and the radioactive source backing) and the time calibration constants. Figure 2.9 shows a good agreement between our experimental distribution and the one taken as reference from the literature.

As it can be seen from Table 2.1, the parameters of the experimental mass spectrum $Y(M_{\text{tt}})$, namely the positions of gravity centers and the widths for light and heavy peaks, are also well consistent with the reference values taken from [Sch83].

Table 2.1 Comparison of the parameters for experimental and literature Mtt distributions.

Parameter	Experiment at modified FOBOS setup	Literature data [Sch83]
$\langle M_L \rangle$, a.m.u.	108.56 ± 0.22	108.55
$\langle M_H \rangle$, a.m.u.	143.44 ± 0.35	143.53
σ_{M_L} , a.m.u.	7.04	7.16
σ_{M_H} , a.m.u.	7.04	7.16

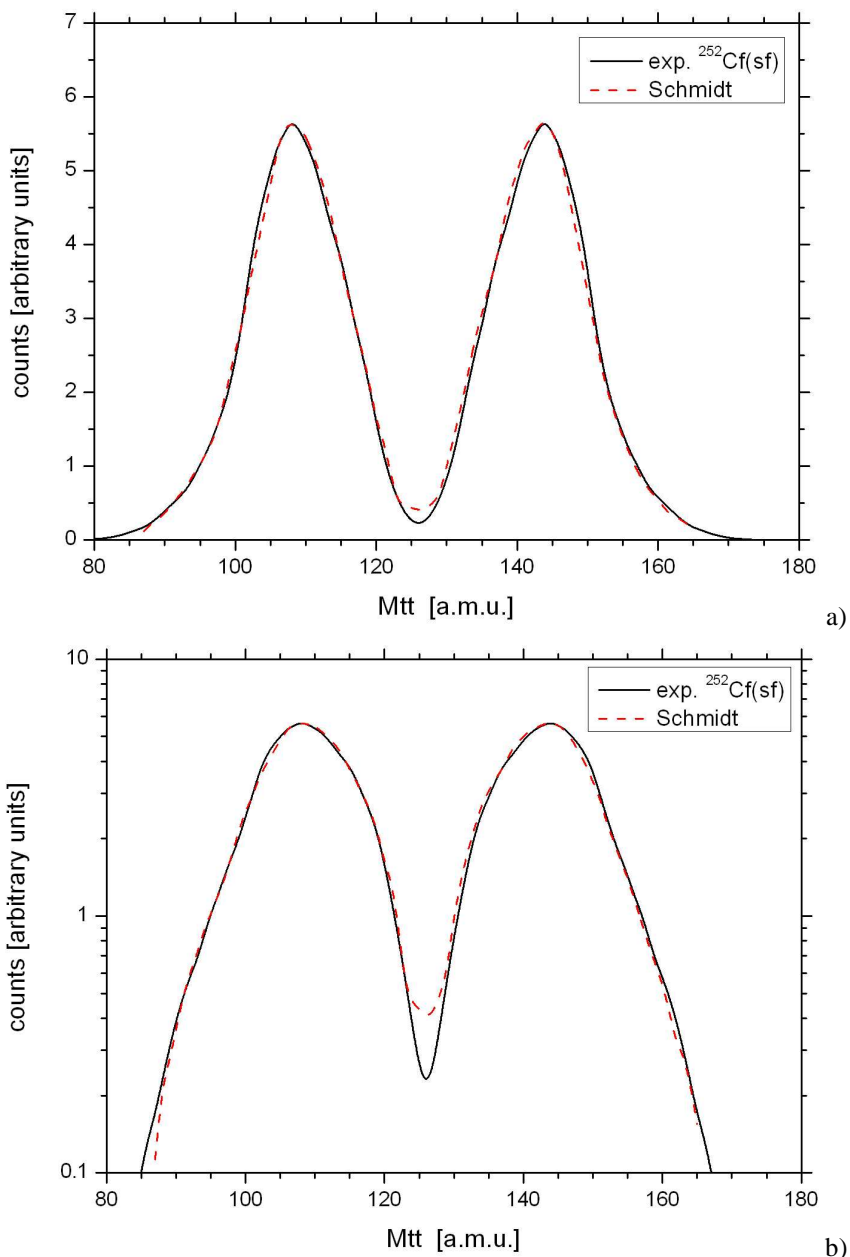


Figure 2.9 Comparison of the mass spectrum of the fission fragments of $^{252}\text{Cf}(\text{sf})$ obtained by the TOF-TOF analysis with that taken from the literature [Sch83]. a) linear scale, b) the same as a) in logarithmic scale.

As an additional check of the mass calibration we performed the comparison of parameters for the experimental velocity distribution with the data known from literature [Whe63, Kie92]. The mean values and the standard deviations of velocities of light and heavy fragment from our experiment and those from other measurements are listed in Table 2.2.

Table 2.2 Mean values and standard deviations of the fragment velocity distribution from spontaneous fission of ^{252}Cf in comparison with reference data from literature.

Parameter	Experiment at modified FOBOS setup	Literature data	
		[Whe63]	[Kie92]
$\langle V_L \rangle$, cm/ns	1.375 ± 0.007	1.375 ± 0.007	1.369 ± 0.009
$\langle V_H \rangle$, cm/ns	1.037 ± 0.005	1.036 ± 0.005	1.035 ± 0.007
σ_{v_L} , cm/ns	0.071	0.067	0.064
σ_{v_H} , cm/ns	0.083	0.080	0.078

2.4.4 Energy calibration of the BICs

In order to improve the mass calibration in the framework of the TOF-E method the procedure aimed to restore the fragment energy has been refined. This task is especially difficult for the slow CCT fragments since they lose up to 70% of their initial energy. The final M_{te} mass spectrum obtained by the TOF-E analysis is given in Figure 2.13.

The mass resolution achieved in the frame of the TOF-E method is known to be much worse than that obtained by the TOF-TOF analysis. However, in the case of incomplete kinematics, e.g. for the CCT events, the TOF-TOF method becomes unusable since it exploits the momentum conservation law of the binary reaction products. Taking into account that the middle non-observable fragment deposits almost the third part of the initial mass the detection of such a large mass deficit doesn't require any perfect mass resolution.

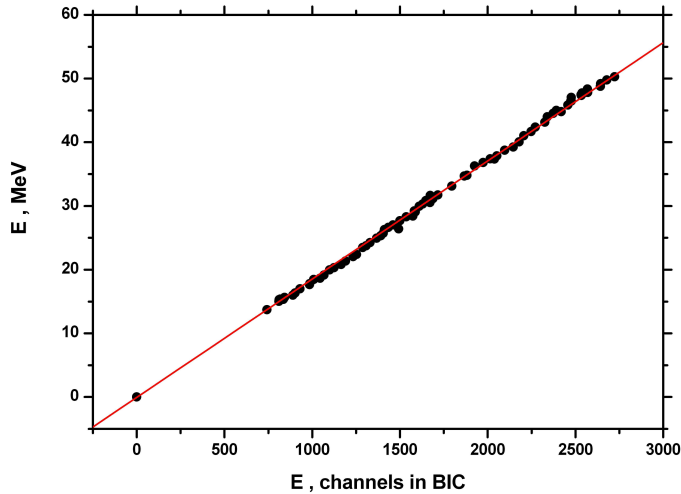


Figure 2.10 The correlation obtained between the raw energy signals in the Bragg chamber (in channels) and the FF energy calculated from the TOF-TOF analysis corrected for the post-fission neutrons and for the entrance foils (in MeV).

On the other hand, any systematical shift in the mass calibration must be excluded in order to draw correct physical conclusions. To obtain a proper energy calibration of the Bragg ionization chamber we used improved transport calculations

based on having good resolution M_{tt} masses. The idea of these calculations is the following. We calculate the energy of the ion before the entrance to the BIC from the M_{tt} mass obtained from the TOF-TOF analysis and corrected to the post-fission neutrons, and from the velocity of the ion. Then this energy is decreased by the value corresponding to energy loss in the entrance foils of gas detectors. When there is enough statistics accumulated we calculate for one M_{tt} mass the mean value of the measured energy in BIC (in channels) and complementary the mean value of the energy calculated (in MeV) for this statistics. Similar calculations for the whole range of M_{tt} masses result in an almost perfect correlation (see Figure 2.10) between the energy measured in the Bragg chamber and the estimated one.

Such a straight line could be expected as the calibration dependence only, if both the energy-loss table used is correct and if there is no significant amplitude defect in the ionization chamber which is exactly the case.

The correlation line obtained crosses the point of origin thus additionally confirming the quality of the calibration. This constraint automatically follows from the algorithm the Bragg processor uses to integrate the fragment-track charge in the chamber [Ort98]. This linear dependence means that the energy calibration is unambiguous and non-shifted and this is essential for the search for the CCT fragments with their unusual mass-to-energy ratio.

2.5 Reconstruction of the fragment mass

Once the calibration procedures presented above are performed, both the velocity of the fragment before entering the BIC and its energy deposited in the gas volume become known. The mass of the fragment is restored from these quantities according to the algorithm illustrated in Figure 2.11 which shows dependences of the energy deposited in the BIC $E_{cal}(M | V=const)$ on the fragment mass M for different fixed velocities V before the entrance in the BIC (for instance, 1.4 cm/ns, see the upper curve).

One calculates actually the energy E_{in} of the fragment with the given mass M and the velocity V . The energy E_{cal} of the fragment after crossing the entrance window of the BIC is obtained applying the table of energy losses. Let's assume E_{ch} and V_{in} to be the energy of the fragment deposited in the BIC and, respectively, its actual velocity before the BIC entrance. In order to restore its mass we examine descending along the curve $V_{in}=const$ in Figure 2.11 mass-by-mass until the following condition is met for the first time:

$$E_{ch} < E_{cal}(M | V_{in})$$

This procedure is complicated by some discontinuities in the $E_{cal}(M, V)$ function caused by imperfect energy losses tabulations as exemplified in Figure 2.12 by triangles.

To avoid such a gap we applied smoothing by means of a cubic polynomial patching of the initial dependence $E_{cal}(M | V)$ in the vicinity of the gap by equalizing both the values and the first derivatives at the edges. Such a method has been proven to be the best one for this purpose. The smoothed values are marked in Figure 2.12 by circles. The mass spectrum obtained with this procedure is compared in Figure 2.13 with the known one [Wah88].

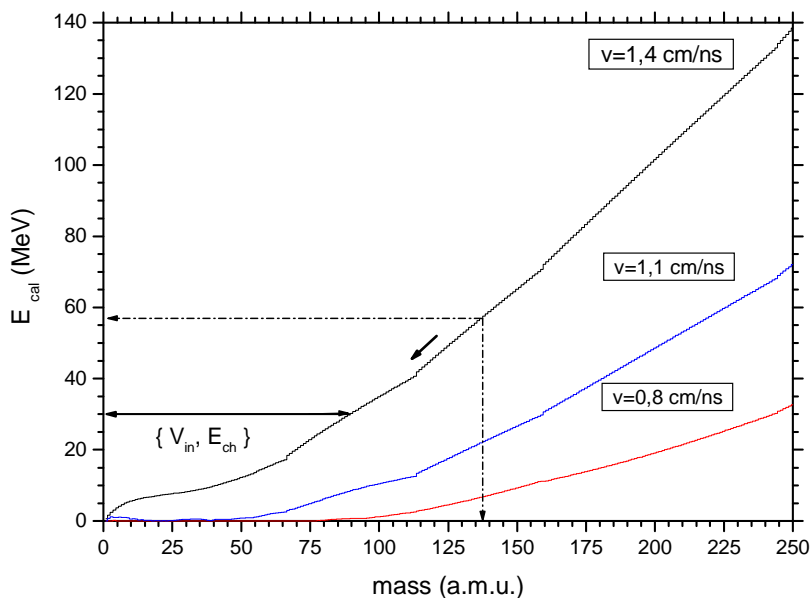


Figure 2.11 Illustration of the mass restoration procedure. See text for details.

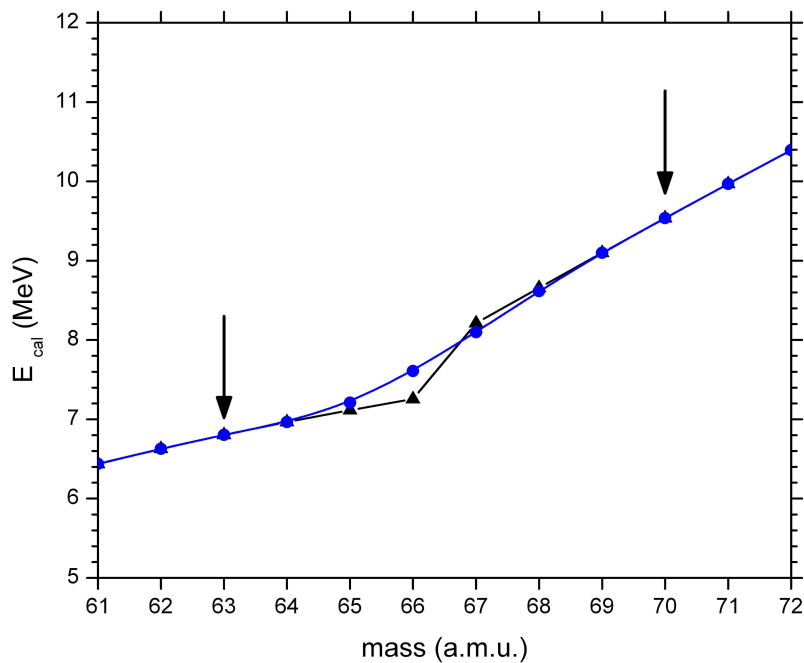


Figure 2.12 Smoothing of the gaps in the table of the energy losses. The values calculated using the initial tabulations are shown by triangles; the smoothed ones are shown by circles. Arrows mark the points of “stitching” of the initial $E_{\text{cal}}(M | V=\text{const})$ dependence with the smoothed one.

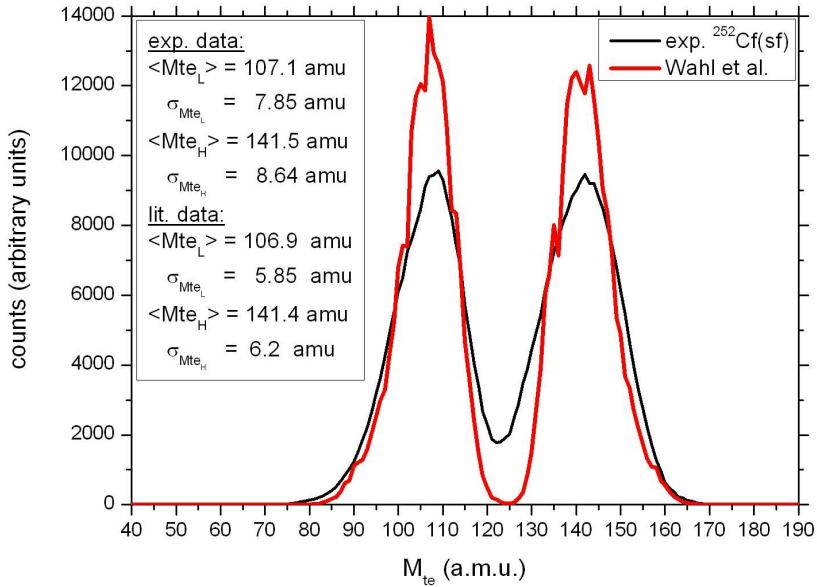


Figure 2.13 Comparison of the FF mass spectrum obtained by the TOF-E analysis with the literature data [Wah88].

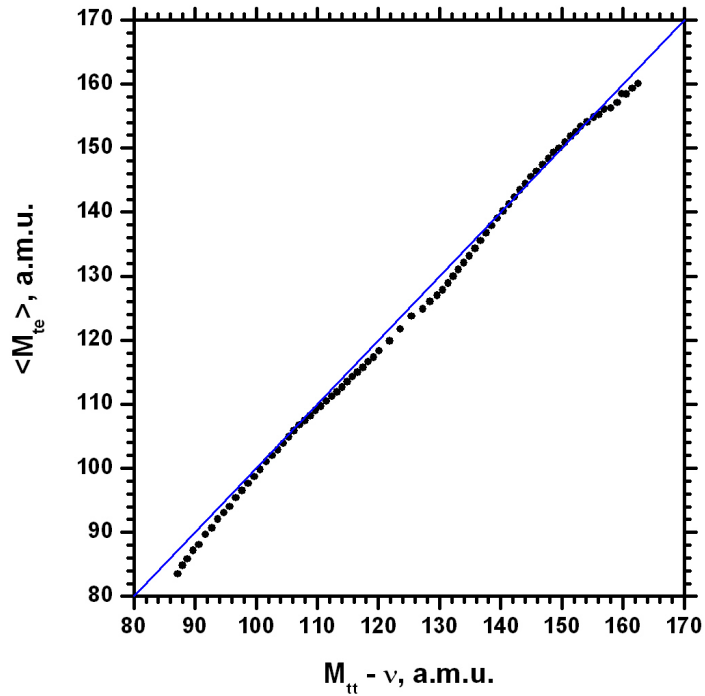


Figure 2.14 The correlation of mean value of post-neutron experimental mass $\langle M_{te} \rangle$ versus mass M_{tt} obtained in TOF-TOF analysis (the shift due to neutron emission has been already taken into account).

There are no shifts in the peak positions, which is important for identification of the CCT events. This fact is demonstrated as well by Figure 2.14 where the dependence of mean value of post-neutron experimental mass $\langle M_{te} \rangle$ versus mass M_{tt} obtained in TOF-TOF analysis looks like a straight line (the shift due to neutron emission has been already taken into account). There are only small offsets from the straight line in the vicinities of low yields around the symmetry region and at the ends of the spectrum, but these distortions do not change the whole picture of the quality of the mass reconstruction procedure.

2.6 Results

The mass-mass plot of the coincident fragments with the high multiplicity of neutrons (at least 3 of them should be detected) is shown in Figure 2.15(a,b). It is easy to recognize the rectangular-shaped structure (marked with the arrows at Figure 2.15(b)) below the locus of conventional binary fission. This structure becomes more conspicuous relative to background (Figure 2.15(b)) if the velocity cut shown in Figure 2.16 is applied to the distribution. The clearing effect can be explained in the following terms.

Fragments scatter both at the electrodes of the “stop” avalanche counter and at the supporting grids of the ionization chamber that provides the main part of the faulty events which imitate the CCT effect searched for. Indeed, the mass of the heavy fragment calculated from the true velocity value but from incorrect (reduced) value of the energy diminishes proportionally to the latter. Therefore a pair of the fragments originated from conventional binary fission could reveal the mass defect similar to that characterizing a CCT event. However, if one rejects the events corresponding to the sufficient mass asymmetry determined by means of the ratio of the velocities which occurred beyond the velocity-window selected (Figure 2.16), a notable part of the scattered events under consideration are also discriminated automatically. This selection cuts off a part of the binary events loci and the tails of these loci in the direction of smaller masses due to velocity gating.

A special attention should be paid to the rectangle in Figure 2.15(b). Three sides of this rectangle are lying on masses corresponded to magic nuclei (clusters). The corresponding magic numbers are marked in this figure at the bottom of the element symbols. More complicated structures (marked by the arrows a, b, c in Figure 2.15(c)) are observed in the mass-mass plot if the events with 2 fired neutron counters are also taken into play. Omitting for a moment physical treating of the structures observed, we attract an attention to the specific feature of some lines constituting the structures “b” and “c”. The sum of the masses along them remains constant, see the dashed line in the lower left corner of Figure 2.15(c) for comparison. It should be especially stressed that the structures shown in Figure 2.15 manifest themselves only in one spectrometer arm on the side of source backing.

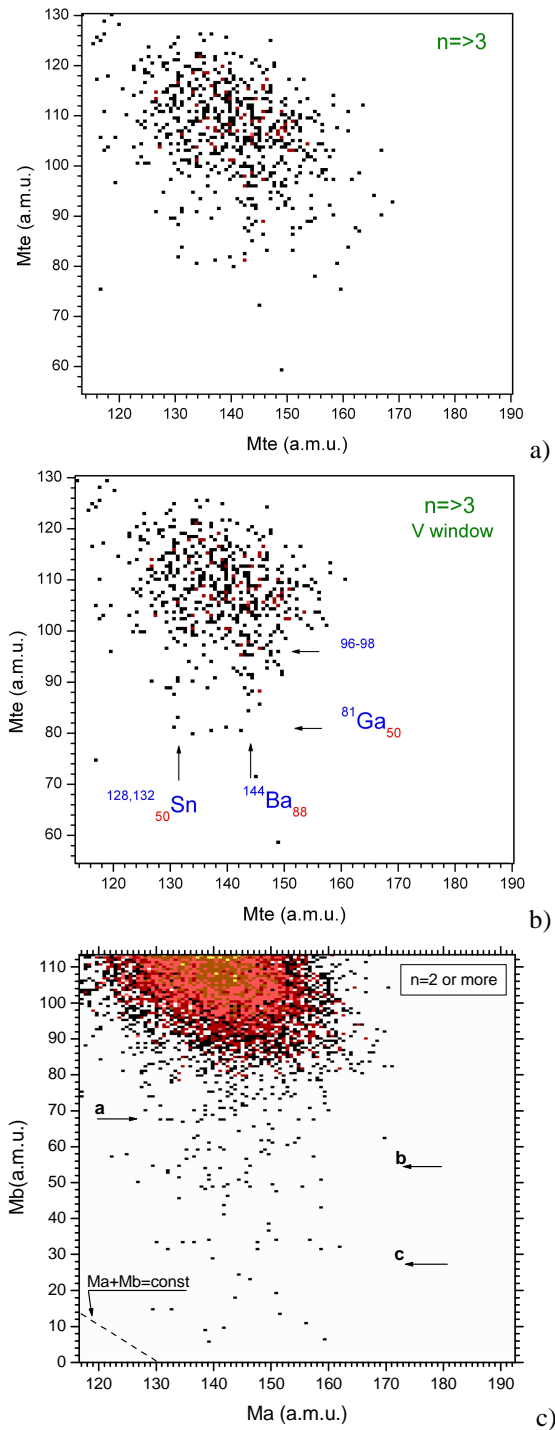


Figure 2.15: a) The mass-mass plot of the complementary fragments with at least 3 neutrons detected; b) The same plot after filtering the fragment velocities in the rectangular box shown in Figure 2.16; c) The same as (a), but the lowest number of hit neutron counters let down to 2.

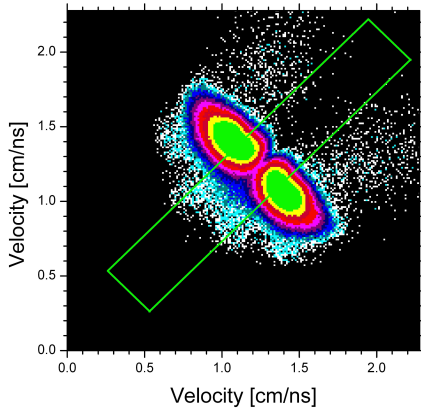


Figure 2.16 Velocity matrix of the complimentary fragments. The events falling into the rectangular box were used to compose the final mass-mass plot in Figure 2.18 (a).

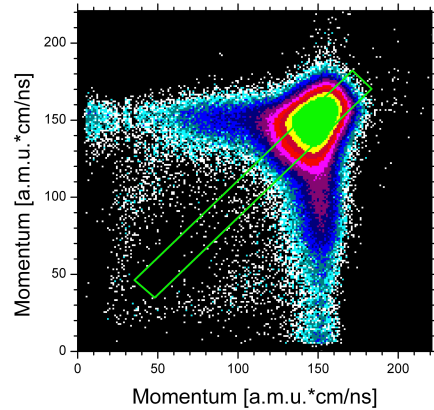


Figure 2.17 Momentum-momentum plot. The events falling into the rectangular box were used to compose the final mass-mass plot in Figure 2.18.

Figure 2.18(a) represents a similar structure to that shown in Figure 2.15(a) except that it is not gated by neutrons and both the velocity and the momentum windows are used here to reveal the mass-symmetric partitions. The corresponding momentum distribution of the fragments and the selection applied are shown in Figure 2.17. The plot in Figure 2.18(b) obtained on conditions of the momentum selection solely is not so clear.

However, as in the previous case the rectangular structure observed is bounded by the magic fragments, namely ^{68}Ni (the spherical proton shell $Z=28$ and the neutron sub shell $N=40$) and, probably, ^{84}Se (the spherical neutron shell $N=50$). Each structure revealed maps an evolution of the decaying system onto the mass space. The events at the lower left corner of the rectangle attract special attention as they form well-separated blocks in the matrices of the experimental observables (velocity and energy). Table 2.3 exemplifies the parameters of three most symmetric events.

Table 2.3 Experimental parameters of the most symmetric events.

Parameter	symbol	units	Event			
			$N_{\#1}$	$N_{\#2}$	$N_{\#3}$	
Number of hited neutron counters	mult	counters	0	0	1	
Velocity	arm "a"	V_a	cm/ns	1.147	1.102	1.135
	arm "b"	V_b	cm/ns	1.173	1.141	1.23
TOF-TOF mass	arm "a"	Mt_{t_a}	a.m.u.	127.4	128.2	131.1
	arm "b"	Mt_{t_b}	a.m.u.	124.6	123.8	120.9
Momentum	arm "a"	P_a	a.m.u.*cm/ns	79.6	80.7	7.8
	arm "b"	P_b	a.m.u.*cm/ns	84.7	78.3	83.4
TOF-E mass	arm "a"	Mt_{e_a}	a.m.u.	69.4	73.2	69.4
	arm "b"	Mt_{e_b}	a.m.u.	72.2	68.6	67.8
Emission energy	arm "a"	$E_{t_e_a}$	MeV	47.5	46.3	46.5
	arm "b"	$E_{t_e_b}$	MeV	51.7	46.5	53.4
Total kinetic energy	TKE _{t_e}	MeV	99.1	92.7	99.9	

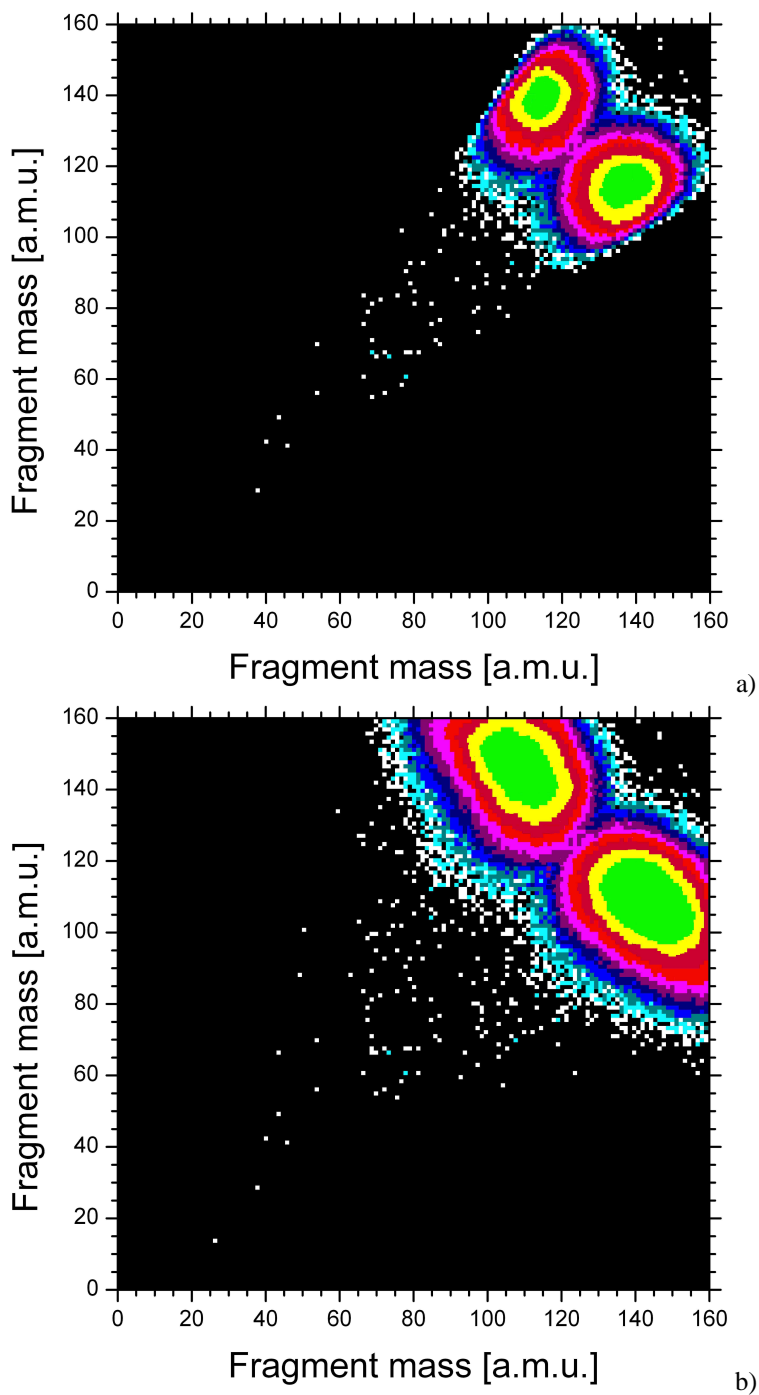


Figure 2.18 a) The mass matrix of the complimentary fragments selected by requirement of their approximately equal velocities and momenta; b) the same matrix if only momentum selection is assumed.

One can judge from Table 2.3 that the cluster masses obtained by the TOF-E analysis are located in the vicinity of the mass numbers 68-72. Both nuclei are attributed presumably to the magic Ni isotopes. The content of neutrons for the fragments whose masses are close to 72 complies then with the prediction of the unchanged charge density hypotheses. The surprising fact is that the evaluated TKE value even for the extremely elongated configuration like Ni-C-Zn-C-Ni chain exceeds the experimental findings (~ 100 MeV). The next point to be stressed is that the observed neutron multiplicity (the number of hited neutron counters in Table 2.3) is low and, hence, the number of emitted neutrons could not be high. This contradicts the expectations put forward earlier. The discrepancies reported may be an indication of more complicated decay scenario to be restored.

2.7 Conclusions

Among 2 million binary fission events from $^{252}\text{Cf(sf)}$ we have extracted over 30 correlated pairs of FF with clear mass deficit of about 100 atomic mass units. 20 of these FF pairs are organized into a distinct and well-separated rectangular-shape structure in a mass-mass plot gated by velocities and momenta. The corners of the rectangle are bounded by the magic fragments, namely, ^{68}Ni and, probably, $^{84}\text{Se}/^{86}\text{Kr}$. These FF pairs exhibit also a lowered TKE. We interpret the events in the rectangular structure as originating from the three-fold decay of an elongated ^{252}Cf nucleus dominated by the 3 clusters: ^{68}Ni , ^{84}Se and ^{86}Kr . We have found that these FF pairs can be accompanied by an increased number of isotropically emitted neutrons, but we did not obtain a very high neutron multiplicity (~ 10) as it was expected. It could mean that the middle fragment is not staying at rest, but slowly moving along the fissioning axis.

Gating on 3 neutron detectors flashed in coincidence with registration of FFs reveals the other rectangular structure in the mass-mass plot. This structure is also bounded by clusters and contains about 20 points.

Summarizing, it can be said, that in the experiment at the modified FOBOS setup we have obtained the indication of the multi-fragment (at least ternary) collinear decays of the initial nucleus into fragments of comparable masses. We have called such decay a Collinear Cluster Tripartition.

3 Off-beam experiments at JYFL and at JINR

Taking into account the results obtained in the experiment at the modified FOBOS setup, it had been decided to verify the idea of collinear cluster tripartition of the $^{252}\text{Cf}(\text{sf})$ in several independent experiments at different setups. We had also tried to find the CCT events in the data from the previous experiment made at the standard FOBOS setup. One goal for these studies was to check the kinematic scheme, which supposes that scattering processes separate the two CCT partners moving unidirectionally, and only one of them is likely to be registered.

The first experiment Exp#1 at the FOBOS setup was performed using two standard FOBOS modules and micro-channel plate (MCP) based time-pick-off detector delivered “start” signals. Dispersing materials for Exp#1 were the construction elements of the FOBOS setup, namely, the grid on entrance windows of Bragg ionization chambers with 70% transparency.

In order to verify whether the dispersive scattering through a transparent foil can give rise to the separation of the CCT partners we have performed a special experiment Exp#2. Here we used a different TOF-E spectrometer based on one MCP “start” detector and two PIN diodes and 5 μm thick aluminum foil had been placed just near the active ^{252}Cf layer for dispersive purposes.

In the third experiment Exp#3 two pairs of the MCP-based timing detectors provided signals for measuring TOFs with flight paths of 8 cm each. The fragment energy was measured by PIN diodes. The separation of the two lighter partners of the tripartition decay was achieved by scattering in dispersive foils and by blocking one of the two fragments (scattered at a very small relative angle) in the collimators or in the grids of the MCP electrostatic mirrors with a total transparency of about 70%.

These three experiments enable us to find a new island of high yields for exotic decay modes called by us collinear cluster tripartition in the mass-mass distribution of the fragments originated from $^{252}\text{Cf}(\text{sf})$.

3.1 Experimental details

The Exp#1 experiment was carried out in 1997 at the FOBOS setup at the FLNR and about $13 \cdot 10^6$ coincident binary fission events were recorded. A scheme of the experiment is shown on Figure 3.1.

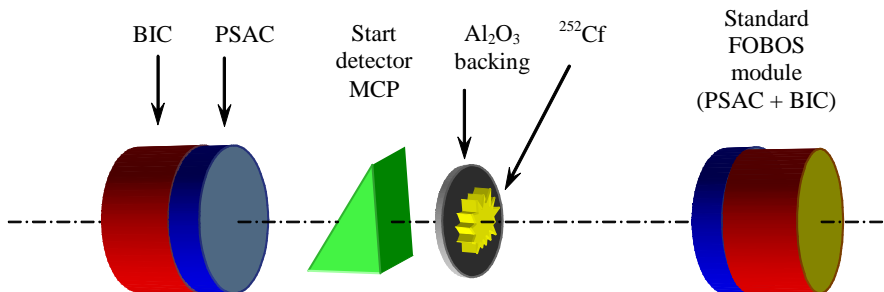


Figure 3.1 A scheme of experiment at FOBOS setup.

The time-of-flight of the fragments was measured over a flight path of 50 cm between the “start” detector based on the micro channel plates (MCP) placed next to the ^{252}Cf source and the “stop” position-sensitive avalanche counters (PSAC). The latter provided through the measurements of the position also the fragment emission angle with a precision of 0.2° . The energies of the coincident fragments that passed through the PSACs were measured in the Bragg ionization chambers (BIC) with the entrance windows supported by a grid with 70% transparency. The geometrical structure of the grid is hexagonal; the side view is shown in Figure 3.2a.

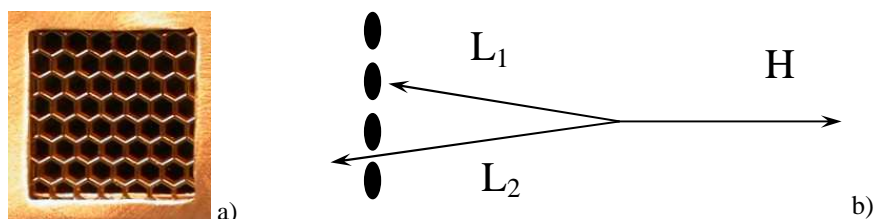


Figure 3.2 a) Side view of FOBOS grid; b) the scheme of detecting of the tripartition partners.

This mechanical structure of the detectors is essential for the registration of the effect. The ^{252}Cf source is mounted on Al_2O_3 backing of a thickness $50 \mu\text{g}/\text{cm}^2$, the other side was free or coated with a layer of Au of $20\text{-}\mu\text{g}/\text{cm}^2$ thickness. In Figure 3.2b the primary heavy fragment (H) is emitted to the right from the free side of the ^{252}Cf source; the two light fragments (L_1 and L_2) are emitted to the left in the same direction. As explained below, scattering processes will separate the two light fragments in a small angular separation, and only one of them is likely to be registered. If both fragments enter, only the total energy is measured.

A similar source of ^{252}Cf was used in a further experiment, performed at the Accelerator Laboratory of the University of Jyväskylä (JYFL). In this experiment Exp#2 (Figure 3.3) we used a different TOF-E spectrometer based on one MCP “start” detector and two PIN diodes, the latter providing both time and energy signals.

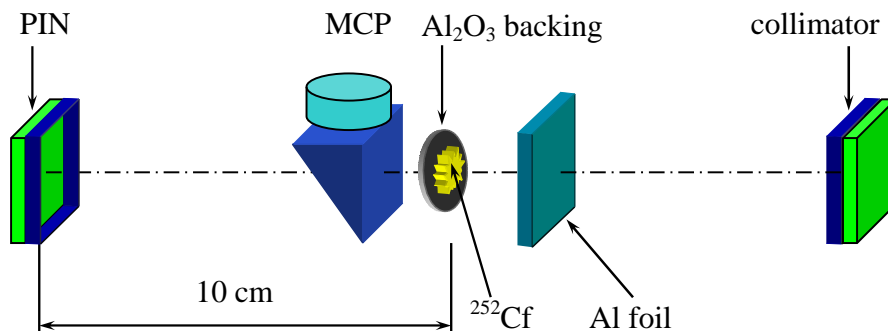


Figure 3.3 A scheme of the experiment Exp#2 in the Small Experimental Chamber.

An active area of each PIN diode was bounded by the collimator. The flight paths here were 10 cm for each detector arm. An Al foil, $5 \mu\text{m}$ thick, has been placed just near the active ^{252}Cf layer. The experimental setup was mounted inside of the Small Experimental Chamber. In this experiment, $2 \cdot 10^6$ binary events were registered.

The experimental setup for the third experiment Exp#3 was installed on the special support rail inside the Large Scattering Chamber facility at JYFL. The setup is shown on the photo below.

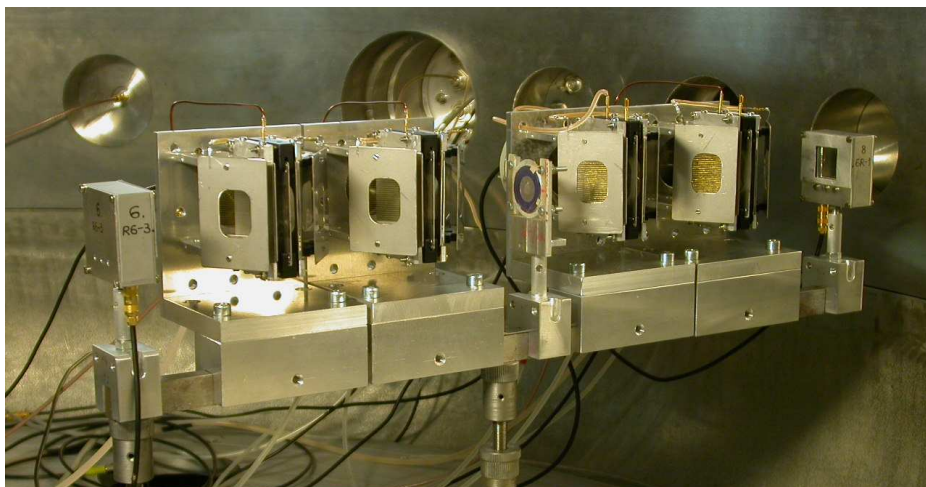


Figure 3.4 Photo of experimental setup for the third experiment Exp#3.

A thin ^{252}Cf source was placed in the middle of a symmetric setup with 4 MCP detectors and 2 PIN diodes, as shown on Figure 3.5.

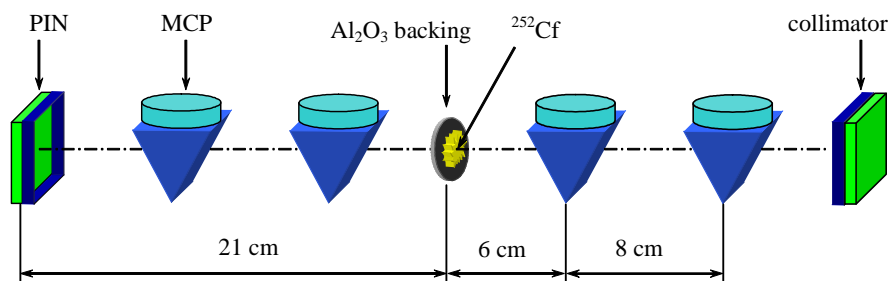


Figure 3.5 A scheme of the setup for the third experiment Exp#3.

The MCP detectors provided TOF signals with a resolution of about 120 ps. Two PIN diodes gave not only energy but also high quality time signals. Therefore, instead of the standard “2·TOF + 2·Energy” detection scheme we had “6·Time + 2·Energy”. With so many extra parameters it is possible to do additional crosschecks for data consistency. This extra information also can be used as a filter for selection of interesting parts from the total amount of the data or for cutting evident bad events, for example, events from scattering. Most parameters were stored at least twice using for instance TAC+ADC together with TDC. The total transparency of each arm amounted to 70% due to the grids of the electrostatic mirrors (four per detector) of the MCP detectors, instead of two as in the other experiments. The experiment took about 50 days and $2 \cdot 10^6$ of fully registered fission events were collected.

3.2 Calibration procedures

For all three experiments the calibration was done for all T and E tracts together with checks on the stability for all parameters. For the Exp#1 the procedures of time-of-flight, energy calibration and mass reconstruction were similar to those done for the experiment at the modified FOBOS setup. For the experiments Exp#2 and Exp#3 the time calibrations were done properly with precise ORTEC time calibrator and using 6.1 MeV alphas from ^{252}Cf as TOF reference. In Figure 3.6 the Mtt spectrum from the experiment Exp#3 is compared with the data from [Sch83].

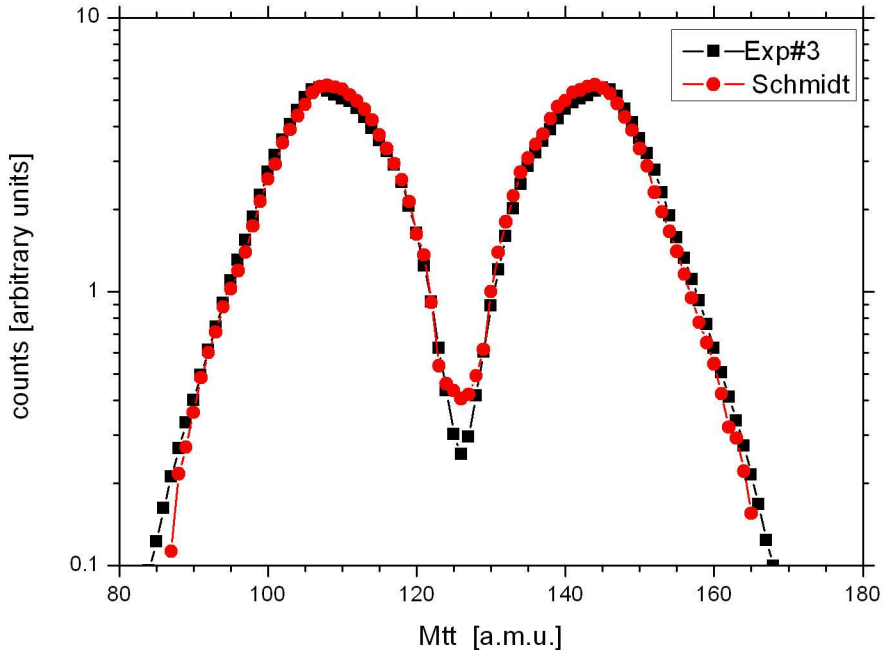


Figure 3.6 Comparison of the mass spectrum of the fission fragments of ^{252}Cf (sf) obtained by the TOF-TOF analysis in Exp#3 with that taken from the literature [Sch83].

Here we see, that in spite of the fact that the TOF bases in the experiments were comparatively small (for instance, ~ 20 cm for Exp#3) and that we did not take into account the plasma delay in silicon detectors (considered as constant), we got a quite satisfactory agreement of the experimental spectrum with the one published in the literature. The energy calibration for the experiments Exp#2 and Exp#3 was done as nonlinear interpolation based on 3 points: positions of 6.1 MeV α -peak, light and heavy fragments in energy spectrum. With this procedure for the energy calibration we have obtained a satisfactory agreement of the light peak for the Mte spectrum with the light peak in Wahl data [Wah88]. Apparently, the pulse-height defect for this peak is not so large and had been taken into account by our calibration procedure, while for the heavy peak (above ~ 124 a.m.u.) a shift of about 2.5 a.m.u. had been observed. The mass spectrum of fission fragments with correction for heavy masses is presented in Figure 3.7.

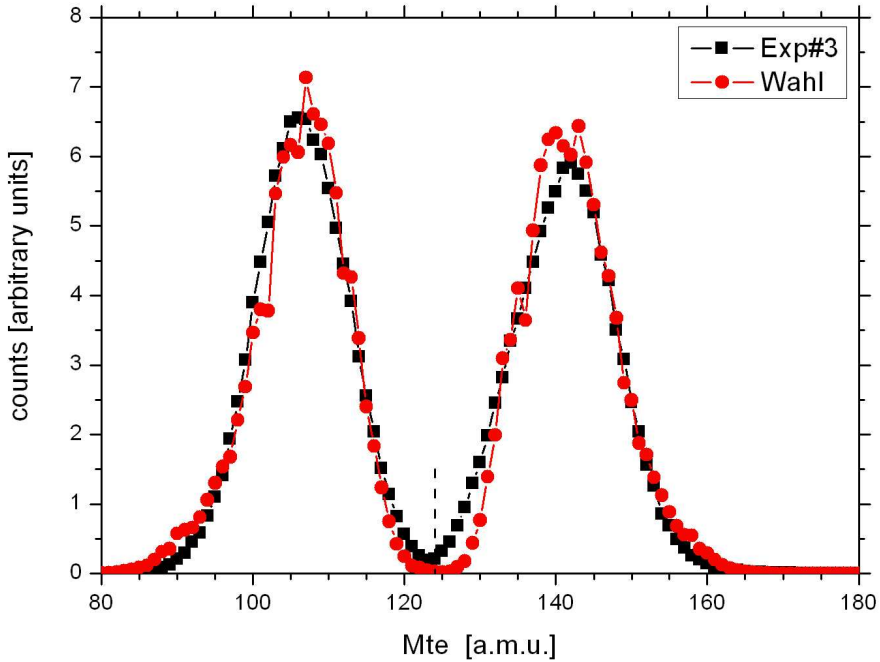


Figure 3.7 Spectrum of Mte masses from the experiment Exp#3 in comparison with the literature data [Wah88].

3.3 Results

Let us start from the results obtained in the Exp#3. Analyzing the plot of the fragment mass versus time-of-flight in one of the spectrometer arms (Figure 3.8a) we have focused on the group of points bounded by the contour W1. They lie far from the loci of binary fission including the tails connected with scattering of the fragments at the elements of start detector. The density of the points increases in the direction of decreasing of fragment energy. The mass-mass plot of the events selected with the gate W1 for approximately half of full statistics ($9.6 \cdot 10^5$) is shown in Figure 3.8b. The vertical line centered at mass 144 a.m.u. attracts attention (marked by the arrow). A similar plot for full statistics is presented in Figure 3.8c. Figure 3.8d depicts a possible treating of the figure, namely the points within contour W2 seems lie on the lines $M_a + M_b = \text{const}$ (tilted lines in Figure 3.8d) and are bounded from the left side presumably by the magic $^{95}\text{Rb}_{58}$ nucleus (shell minimum “B” in [Wil76]). The corresponding projection of the area W2 is shown in Figure 3.9, where $dM = M_{cf} - (M_a + M_b)$ is the mass of undetected fragment. Experimentally evaluated mass resolution for one arm of setup does not exceed 2.8 a.m.u. (full width at half maximum) and thus the peak structure in Figure 3.9 is significant.

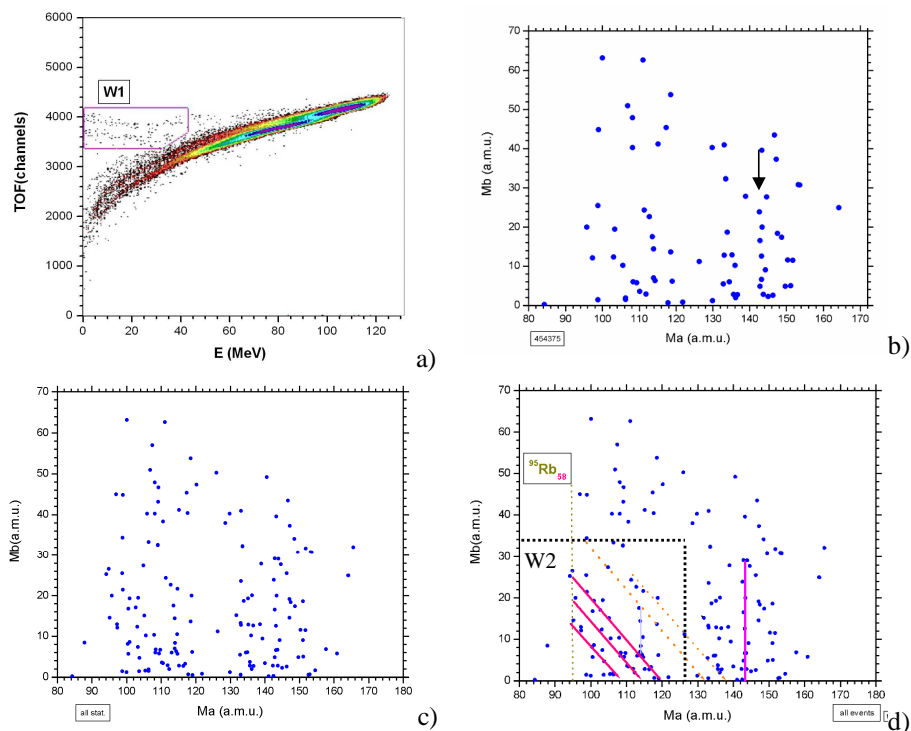


Figure 3.8 Time-of-flight vs. energy in one of the spectrometer arms (a); mass-mass distribution of the coincident fragments selected by W1 window (approximately half of full statistics) (b); all events from W1 gate (c); most pronounced linear structures (d). See text for details.

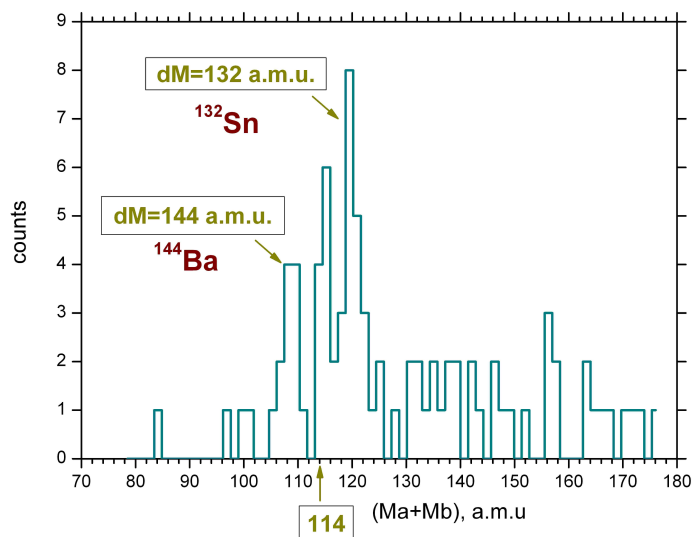


Figure 3.9 Projection of a part of mass-mass matrix (area W2 in Figure 3.8d) obtained along the direction $M_a+M_b=\text{const}$. The mass of undetected fragment $dM=M_{\text{cf}}-(M_a+M_b)$.

It is obvious that the undetected (third) fragment can be a magic one, however another decay scenario showing up clustering likely also takes place (see, for instance, the line centered at 114 a.m.u. — presumably ^{114}Ru linked with the shell minimum “C” in [Wil76]). It should be stressed that at least the deformed magic nucleus of $^{144}\text{Ba}_{88}$ manifests itself both as “missing” fragment (Figure 3.9) and really detected (vertical line in Figure 3.8d). The yield of the events from the window W1 is about 10^{-4} per binary fission. Unfortunately, the spectrum in Figure 3.9 suffers from low statistics, but the reliability of this structure was confirmed in other experiments with high statistics, namely in Exp#1 and Exp#2, by the same effect of an enhanced yield corresponding to a missing mass.

In Figure 3.10, it is shown in a logarithmic scale the two-dimensional (2D) distribution of the two registered masses of the coincident fragments in the experiment Exp#1 at the FOBOS setup. Only collinear events in both identical spectrometer arms with a relative angle of $180 \pm 1^\circ$ were selected; this value is within the angular resolution, and it is in the range of a typical angular spread for conventional binary fission fragments.

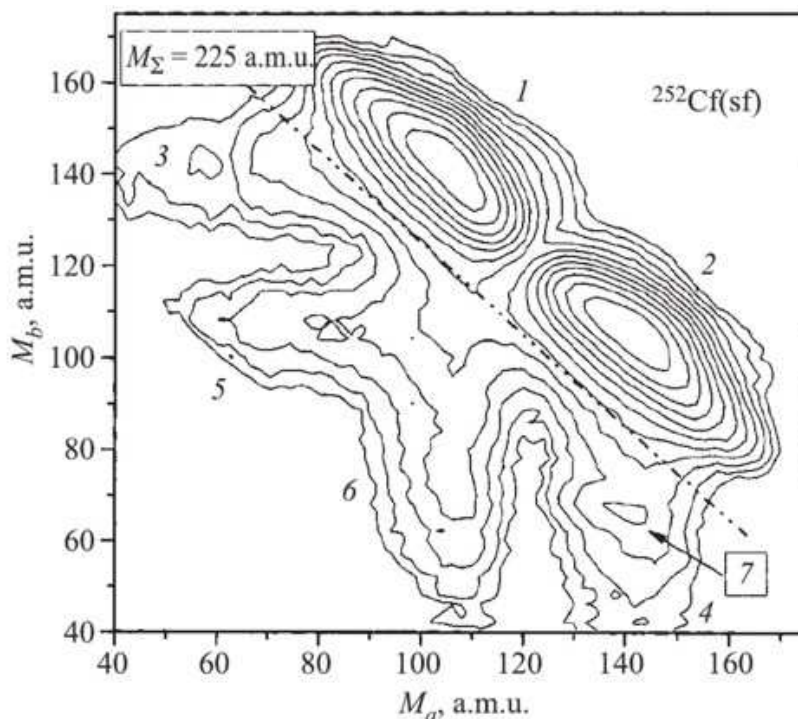


Figure 3.10 Contour map (in logarithmic scale) of the mass-mass distribution of the collinear fragments detected in coincidence in the opposite arms (marked by letters *a* and *b*) of the spectrometer (Exp#1).

The “tails” in the mass distributions marked 3-6 extending from the loci (1 and 2) used to mark the conventional binary fission are mainly due to the scattering of the fragments on both the foils and on the grid edges of the “stop” avalanche counters and the ionization chambers. The only small but important asymmetry between the two arms to be emphasized consists in a very thin source backing for the “rear side” and the “start” detector foil located in the arm *b* only (Figure 3.1). An astonishing

difference in the shapes of the “tails” (3 and 4) attracts attention. There is a distinct bump, marked (7), on the latter “tail” (4), oriented approximately parallel to the line defining a constant sum of masses, $M_a + M_b = \text{const}$, i.e., tilted by 45° with respect to the abscissa axis. The explanation of this bump is the essence of our analysis. The bump is located in a region corresponding to a large “missing” mass. In Figure 3.10, the line for the total mass $M_{\text{total}} = 225$ is shown as a border line to separate these interesting events from normal binary fission. A statistical significance of the events in the structure (7) can be deduced from Figure 3.11 where the spectra of total masses $M_{\text{total}} = M_a + M_b$ for the “tails” (4 and 3), spectrum *a* and spectrum *b* respectively, are compared.

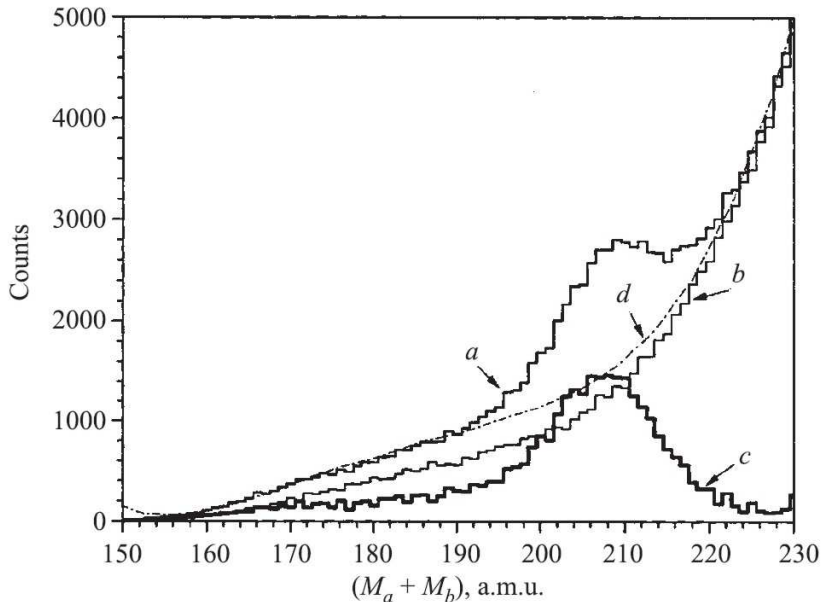


Figure 3.11 Here a bump 7 from Figure 3.10, located below the line of the sum $M_a + M_b = 225$ a.m.u., is analyzed. The spectra of total masses for the “tails” (3 and 4), spectrum *a* and spectrum *b* respectively, are compared. The difference spectrum is marked *c*. Curve *d* is a polynomial fit using the points outside of the gross peak on the spectrum *a*.

The difference between the spectrum of *b* and the “tail” (3) is marked *c*. The integral of these events is $4.7 \cdot 10^{-3}$ relative to the conventional fission events contained in the locus (2) shown in Figure 3.10. The corresponding ratio for the gross peak of the curve *a* (shown by the dashed line) is smaller and amounts to about $2.7 \cdot 10^{-3}$. The background was defined by a polynomial fit (curve *d*) using the points outside the peak.

In order to explain the differences in the “tails” (3 and 4) mentioned above, the following scenario is proposed (the geometry is shown in Figure 3.2b). In ternary fission, the three fragments are emitted collinearly and two of the fragments are emitted in one direction, but become separated with an angle less than 1° after passing a dispersing media, due to multiple scattering [Mey71]. This material is the backing of the source (located only on the side of the “tail” (4)). If both fragments pass on and enter into the BIC, a signal corresponding to the sum of the energies of the two fragments is registered. The event is registered as binary fission with almost usual parameters. In the other scenario, only a proper energy (mass) of one of the light

fragments is measured, because the second one is stopped (lost) in the supporting grid of the ionization chamber.

In order to verify whether the dispersive scattering through a transparent foil can give rise to the effect discussed in Exp#1 experiment, we have performed a special experiment Exp#2 at the Accelerator Laboratory of the University of Jyväskylä (JYFL). An Al foil, 5 μm thick, has been placed just near the active ^{252}Cf layer. This thickness corresponds approximately to a half of the range of a typical heavy fragment. A bump similar to that shown in Figure 3.10 is observed. The result of this experiment is shown in Figure 3.12, which depicts the spectra analogous to those presented in Figure 3.11. The bump obtained with the difference marked *c*, again appears in the arm pointing to the scattering foil. The integrated yield of the spectrum *c* confined within the masses of 180–220 a.m.u. amounts to $2.4 \cdot 10^{-3}$ relative to the corresponding locus of conventional binary fission. These events typically correspond to a mass loss of 40–70 a.m.u., as in the other case, the positions in the mass scale of the peaks *c* agree well in both experiments. This result also shows that the effect of the dispersive scattering considered does not depend on the foil thickness.

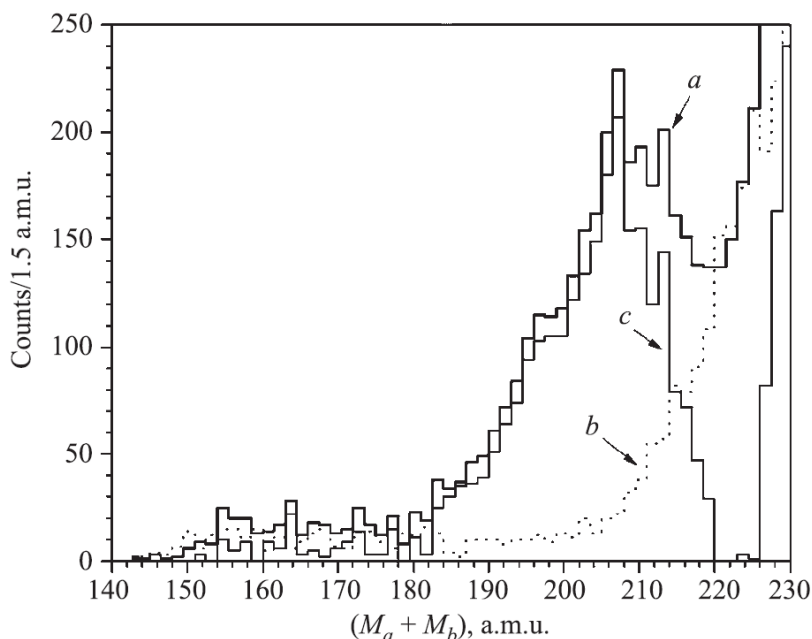


Figure 3.12 Spectrum of sum of masses $M_a + M_b$ from experiment Exp#2, for two registered fragments for the gate similar to the “tail” 4 from Figure 3.10; spectrum *b* corresponds to the “clean” opposite arm free from dispersion foil, *c* is the difference spectrum.

In the third experiment Exp#3 the separation of the two lighter partners of the tripartition decay was achieved by scattering in a dispersive foils and the blocking one of the two fragments (scattered at a very small relative angle) in the collimators. We observe again the bump in the sum spectrum of $M_{\text{total}} = M_a + M_b$ confined within 180–220 a.m.u. as shown in Figure 3.13.

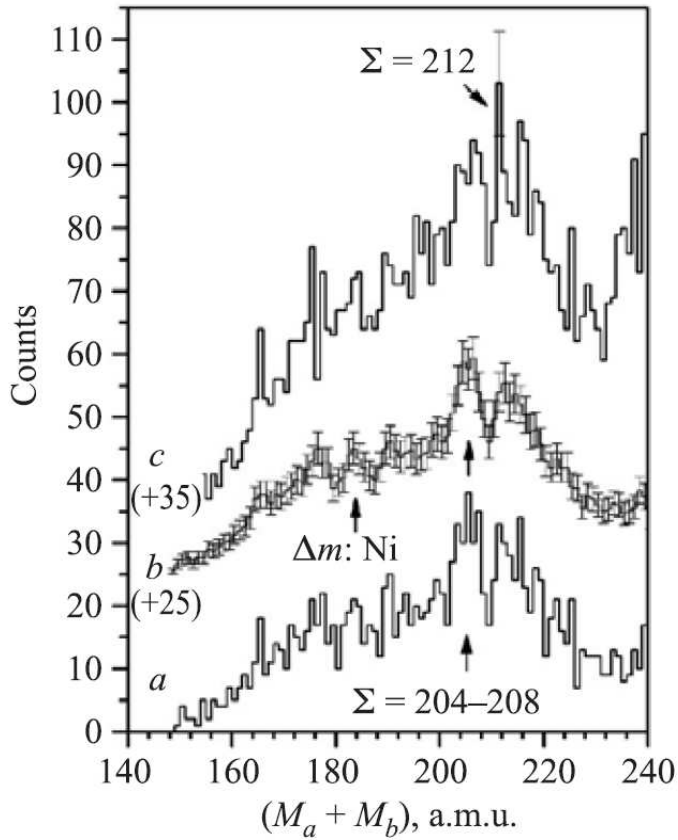


Figure 3.13 Spectrum of the sum of masses of two detected fragments obtained in the third experiment Exp#3: from the arm facing the source backing (*a*); the same spectrum smoothed by means of averaging of counts in three adjacent channels (shifted up by 25 counts) (*b*); the sum of spectrum *a* and a complementary spectrum obtained in the second arm of the spectrometer (shifted up by 35 counts) (*c*). The sums marked in the panels correspond to different pairs of magic nuclei (see text). The peak in spectrum *b* marked by arrow is due to the doublet of “missing” $^{70,68}\text{Ni}$ fragments.

Spectrum *a* corresponds to the arm facing the source backing, which acts as scattering medium. The additional yield mass in the same mass range as previously, relative to binary events, amounts to $2.7 \cdot 10^{-3}$. The best mass resolution among our experiments (< 2.5 a.m.u.) was achieved in this case. This is due to the better measurement of TOFs by the MCP detectors and the absence of straggling in the energy channel. Unfortunately, the spectrum suffers from low statistics; this is partially overcome by applying a simple averaging procedure on the counts in three adjacent channels (curve *b*). This procedure smoothes the background fluctuations and produces two statistically reliable wide peaks in this spectrum, marked by arrows indicating “missing” $^{70,68}\text{Ni}$ fragments and total masses of two registered fragments amounting to 204–208 a.m.u., respectively. The symmetry of the two spectrometer arms is reflected in the result that the spectrum *a* and the complementary one obtained in the second arm of the spectrometer depicted in Fig. 4 as curve *c* give the same result. The statistically significant regions centered at $M_{\text{total}} = 204\text{--}212$ a.m.u. are marked by arrows in Figure 3.13.

We note that the same effect of an enhanced yield corresponding to a missing mass defined by a region of $M_{\text{total}} = M_a + M_b = 180\text{--}212$ has been observed in the three independent experiments described (in this chapter). The small variation of the yields relative to the total binary events can be traced back to the different geometries. Possible uncertainties of the effect yields referred from the experiments at hand need some comments. A statistical error in any case does not exceed 2.5%. At the same time, a systematical component is hard to estimate. The ratio “number of ternary events per binary fission” is governed via multiple scattering angles by the mass–energy–charge distribution of the ternary decay products unknown in detail. Thus we can only claim that the effect should not be less than $4 \cdot 10^{-3}$ per binary fission.

3.4 Discussion of the results

The experimental observations will be interpreted as a collinear ternary decay with three fragments of a similar mass, a decay which is different than the previously reported ternary fission, where the third light fragment (typically He or Be isotopes) is emitted perpendicular to the axis spanned by the heavy fission fragments [Gön05]. For a more detailed analysis, we come back to the results obtained in Exp#1. The contour map of the two-dimensional mass-mass distribution obtained by subtraction of the “tail” (3) from the “tail” (4), already defined in Figure 3.10, is shown in Figure 3.14a.

This distribution shows the contour of the ternary mass splits more clearly; it is almost free from further experimental background originating from scattered fragments of the normal binary fission. Some features of this 2D plot can be further emphasized by a process, where a second derivative filter is applied, a method which is typically used in the search for peaks in gamma spectra [Mar67, Pya02] (see Figure 3.14b). The scale of the squares is defined in the insert to this figure. The tops of the peaks are found over certain linear sections of $M_a = \text{const}$ with intersections with the discrete diagonal lines, as marked in Figure 3.14b; they correspond to the total masses $M_{\text{total}} = \text{const}$ with values 204, 208 and 212 a.m.u., respectively. The listed peaks have already been marked in Figure 3.13. Thus, the bump (7) seen in Figure 3.10 and in Figure 3.14a consists mainly of the three overlapping ridges oriented along the lines $M_{\text{total}} = \text{const}$.

From the observed mass spectra, we will have to consider a ternary fission process with one heavier and two lighter fragments. The missing masses in the sum spectra of the experiment Exp#1 suggest subsystems with particular masses. The same mass values are observed as distinct peaks in Figure 3.13 (from Exp#3); these are also seen as ridges in Figure 3.14b. We note that from these data the shell closures [Wil76] in proton and neutron number are decisive for the formation of the emitted subsystems. In the Figure 3.14a the ridges obtained in the analysis of the two-dimensional mass-mass distribution by applying the second derivative filter are marked by the dashed lines to show positions of these ridges. As can be deduced from the figure, the ridges go through crossing points corresponding to different combinations of two fragments with “magic” nucleon numbers (marked by the dot-and-dash arrows). These marked points could be related to mass values with magic subsystems well-known from binary fission [Wil76, Roc04] as follows: $204 \rightarrow {}^{70}\text{Ni} + {}^{134}\text{Te}$ or ${}^{72}\text{Ni} + {}^{132}\text{Sn}$ (“missing” ${}^{48}\text{Ca}$), $208 \rightarrow {}^{80}\text{Ge} + {}^{128}\text{Sn}$ and for $M_{\text{total}} = 212 \rightarrow {}^{80}\text{Ge} + {}^{132}\text{Sn}$, ${}^{78}\text{Ni} + {}^{134}\text{Te}$ or ${}^{68}\text{Ni} + {}^{144}\text{Ba}$.

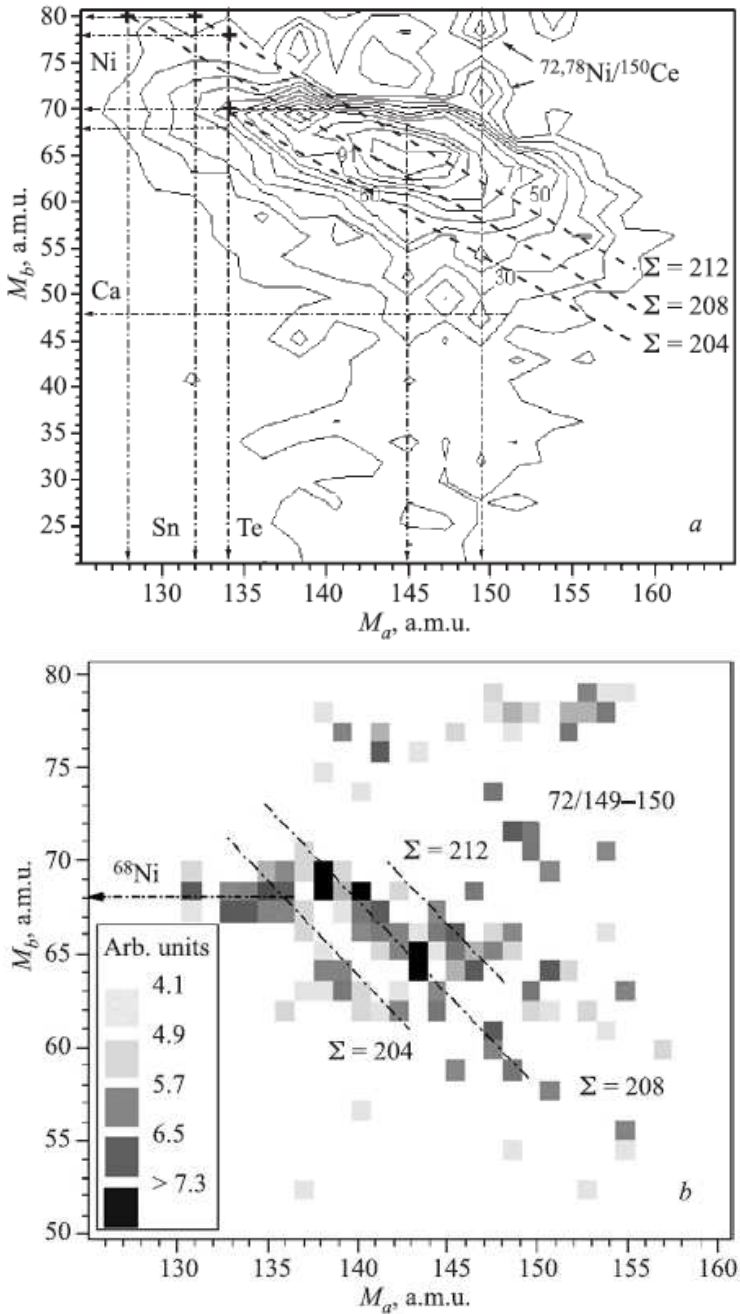


Figure 3.14 a) The figure depicts as a 2D-contour map (M_b versus M_a) the difference between the “tails” (3 and 4) of the events measured with the FOBOS-detector system shown in Figure 3.1; note the expanded scale for the lighter mass fragments. Dashed lines tilted by 45° with respect to the M_a axis correspond to the fixed total mass of detected fragments (see the text for more details). Part b) is the same as a) but passed through a filter which emphasizes the two-dimensional structures.

It should be noted that the “missing” fragments excluding Ni + Sn split are not magic. The ridges discussed are crossed as well by the horizontal ridge (seen via bunching of contour lines in Figure 3.14a), this effect can be linked with the isotopes $^{68,70}\text{Ni}$, which are also magic [Roc04]. This observation would imply that the detected light fragment from the two L_1 , L_2 fragments (see Figure 3.2b) is always a Ni isotope. Due to the symmetry of the detector setup, namely to the fact that the two L_1 , L_2 fragments are always detected in coincidence with the same heavy fragments, one must also observe events with a “missing” Ni fragment. This is indeed observed: the peak corresponding to “missing” masses of 70 and 68 a.m.u. is well-seen in Figure 3.13 (curve *b*). Thus the different peaks in the “missing”-mass spectrum consistently correspond all to the ternary decay scenario proposed.

Inspecting the lower part of Figure 3.14a, we observe a gross bump, which is well bounded by the mass of the double magic nucleus of ^{48}Ca . Further there is a strong manifestation for the formation of the deformed magic ^{150}Ce nucleus, which is seen as two peaks (all in all 355 events) in the upper right corner of Figure 3.14a ($^{72,78}\text{Ni} / ^{150}\text{Ce}$). Also a weak trace of a vertical ridge in the vicinity of the well-known magic $^{144}\text{Ba}_{88}$ nucleus should be noted.

Completing this section, we would like to stress that the observation of structures for the masses of the emitted fragments and the “missing” masses corresponding to known shells must be seen as a decisive argument in favor of the physical origin of the effect of tripartition. No experimental feature can emphasize these mass values; the experiment does not “know” magic numbers. The role of the nuclear shells in the effect observed appears in analogy with known molecular-like states in light alpha-cluster nuclei, which can also form strongly deformed hyperdeformed resonances. Recent theoretical studies of multicluster accompanied fission [Poe99] and binary clusterization of the ^{252}Cf nucleus [Cse04] emphasize the role of double magic nuclei of ^{132}Sn and ^{48}Ca in these processes. One more strong argument in favor of real physical origin of the effect follows from the Figure 2.15 which shows mass-mass distributions for increased number of emitted neutrons: rectangular structures at masses 70 and 80 a.m.u. associated with the bump are also observed only in one spectrometer arm on the side of the source backing.

3.5 Conclusions

The results presented in this chapter were obtained in three different experiments and show that they are consistent with a hypothesis of a new type of spontaneous decay, namely, collinear cluster tripartition of the ^{252}Cf (sf).

The results also confirm the proposed kinematic scheme which allowed one to distinguish two CCT partners flying almost in the same direction: scattering processes separate fragments in a small angular separation, and only one of them is likely to be registered. A “spatial discrimination” let us measure a mass of the “lucky” fragment correctly if it was faster than the lost one. If both fragments enter to the detector, only the total energy is measured and we reject such event.

The experiments presented revealed a new area of the CCT manifestation in the mass-mass distribution of the decay fragments. The probability of this effect is estimated to be not less than $4 \cdot 10^{-3}$ with respect to the normal binary fission. Presumably, the ternary decay of nuclear molecules based on heavy magic clusters such as isotopes of Ni, Ge, Sn, Ba, Te gives rise to the effects observed.

4 In-beam experiment at JYFL

In our previous experiments we have got indications of an unusual decay mode of ^{252}Cf (sf) which was treated as “collinear cluster tripartition”. So far experimental manifestations of this decay channel were obtained in the frame of the “missing mass” method. It means that only two almost collinear fragments were detected in coincidence and they were much smaller in total mass than initial nucleus. It is reasonable to suppose that “missing” mass corresponds to the mass of undetected fragment (or fragments) flying almost along a common fission axis bearing in mind that two detected fragments prove to be almost collinear. The results obtained in previous experiments show that shell effects in the fragments play a key role in the process of interest.

In contrast to the “missing” mass method direct detection of all decay partners is, of course, a more convincing approach and is the main idea of the in-beam experiment. This approach should be realized at a setup of high granularity. Such kind of spectrometer installed at the JYFL, Jyväskylä, Finland was chosen to study the reaction $^{238}\text{U}+^4\text{He}$ (40 MeV) as an example of “pure” fusion-fission reaction. For the purpose of our experiment only light ion induced fission can be considered. There are three main reasons for that:

- straightforward geometry of the setup when $m_{\text{projectile}} \ll M_{\text{target}}$;
- full separation between beam and the fragments;
- the warranty that the observed effects are related to fission and not any other reaction channels.

At the same time the fissioning system should be as heavy as possible to have a larger set of clustering configuration. Since ^{238}U and ^{232}Th were the only suitable targets available for us, the choice of the reaction with ^{238}U becomes quite obvious. Among few light projectiles satisfying the conditions mentioned above, we have decided to take ^4He . The other good candidates would have been proton or deuteron, but they produce much more activation of the experimental area, while ^4He has the additional advantage of increasing the mass of the compound nucleus. Moreover, multiple manifestations of collinear tripartition were obtained in our previous experiments only for the spontaneous fission of ^{252}Cf . Thus, the goal of this experiment is to observe for the first time the collinear multicluster decay of middle excited compound system of $^{242}\text{Pu}^*$. Therewith a much higher FF rate in the beam experiment would allow us to increase the statistical significance of the obtained results.

4.1 Experimental setup

The experimental setup was assembled as a double arm TOF-E spectrometer and includes two arrays of PIN detectors with 19 elements each (only 32 detectors were under operation till the end of the experiment), two MCP (micro-channel plate)-based start detectors and a specially designed target holder (Figure 4.1). Each PIN diode provides both energy and timing “stop” signals. Thus both TOF-TOF (time of flight) and TOF-E (energy) methods for measuring of a mass of fission fragments (FF) can be used.

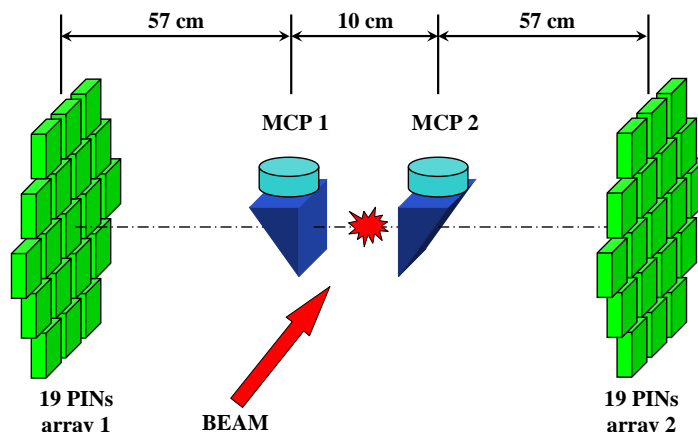


Figure 4.1 Sketch of the experimental setup

The experimental setup was installed inside the Large Scattering Chamber, which has a diameter of about 1.5 m, thus it was possible to improve the accuracy and resolution of our measurements by increasing the base for TOF measurements up to the maximum possible distance of 57 cm. Two MCP-based start detectors were placed at 5 cm from the point of intersection between the beam and the target. This distance allows installing the special target holder and in the same time protects the MCPs from accidental hits by ions from the beam.

The size of the individual PIN-diode is $3 \times 3 \text{ cm}^2$, the depth of the depletion zone is about $200 \text{ }\mu\text{m}$. The MCP aperture is 30 mm (the diameter of the entrance window) and the thickness of the carbon converter foil does not exceed $30 \text{ }\mu\text{g}/\text{cm}^2$. Uranium target consists of 99.99% of ^{238}U (the rest is $^{235,234}\text{U}$) evaporated on a $50 \text{ }\mu\text{g}/\text{cm}^2$ thick Al_2O_3 backing. Uranium spot has the diameter about 9 mm and the thickness of $175 \text{ }\mu\text{g}/\text{cm}^2$.

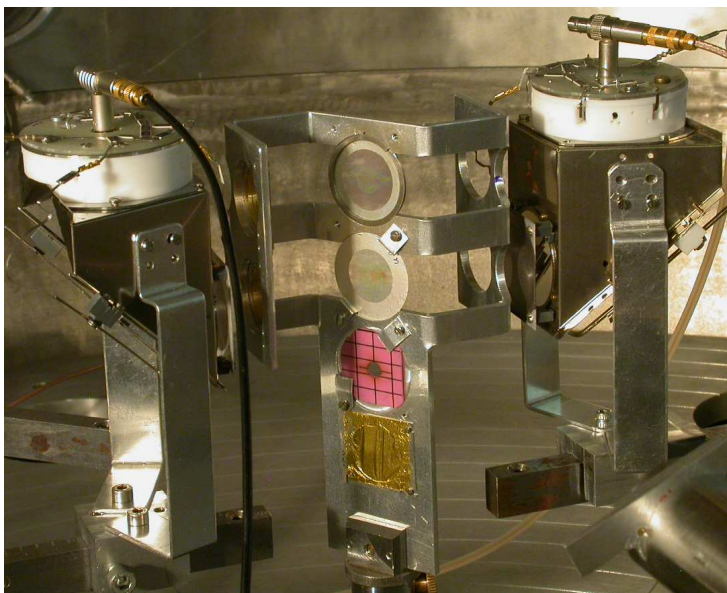


Figure 4.2 Special designed target holder and MCP-start detectors in the center of reaction chamber

A special designed target holder with two targets and two gold foils of 1 and 2 μm thickness was installed at the central axis of the reaction chamber (Figure 4.2). The construction of the target holder permits, by simply rotating it and without opening the reaction chamber, to place a gold foil in front of one of the “start” detectors. The gold foils serve as dispersion media for increasing the probability of detecting two fragments in adjacent PIN’s which are flying originally in almost the same direction. Such events were observed in our previous experiments. In the working position the angle between the target and beam direction is 60° . The experimental setup was installed on the special supports inside the LSC. The overall view of the spectrometer is shown in Figure 4.3.



Figure 4.3 View of the experimental setup inside the reaction chamber. Only the right array of PIN detectors is seen.

The K130 cyclotron at the Accelerator Laboratory of the University of Jyväskylä supplied the ^4He -ion beam with energy 40 MeV. The beam was focused on the target into a spot of 5 mm in diameter. The beam collimators were 9 mm (first) and 10 mm (second). The RF was 14.820 MHz what gives ~ 67 ns interval between bunches.

4.2 Stability of data parameters

To be sure that our results are significant and there are not any artificial effects created by variations in the electronics the stability of each E and T channels was checked for all data. This was done by calculating the mean value and the dispersion of the data in spectrum. Whenever we had some doubts about the stability of the data, we crosschecked it by fitting the spectrum with two Gaussians and calculating the fit parameters. Bearing in mind that we had large amounts of data, to speed up the process, we developed a special software perform automatically crosschecks of the stability of parameters.

4.2.1 Checking stability by mean value and dispersion of critical spectra

In this method the spectrum for each 2000 events in data files is collected and the mean value and dispersion for this group of events is being determined. After processing all data the plots “Mean value versus group of events” and “Dispersion versus group of events” are created and the decision about the stability of the data is concluded. The typical plots for one E-channel are presented on Figure 4.4 and Figure 4.5.

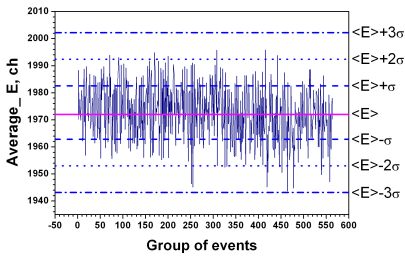


Figure 4.4 “Mean E value” plot

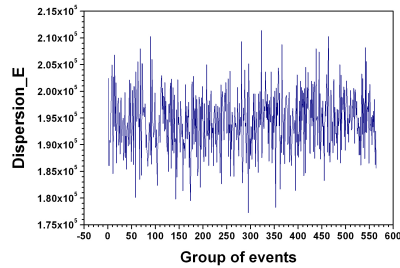


Figure 4.5 "Deviation of E" plot

In Figure 4.4 the mean value $\langle E \rangle$ and $\langle E \rangle \pm 1$, ± 2 and ± 3 standard deviations are shown. As one can see from the graph, the data is stable; the deviations of the data from the mean line are due to statistics. A similar procedure was done for all E and T channels. In case of instability the decision about necessity to do the correction for data was taken based on the stability check of the same data done by the two Gaussian fit method presented below.

4.2.2 Checking stability by two Gaussians fit

If the mean value method discussed above reveals, for instance, some peculiarity in the plot “Mean value versus group of events”, which can be due to some noise events, in order to improve the diagnostics for instability and, if necessary, to make corrections to the raw data we developed a second method for stability checks.

The idea behind this method is the following: both spectra of T and E have a form of two-humped distribution. The stability of data is checking by means of controlling the peak positions for light and heavy fragments in spectrum. In that way a spectrum for each 2000 events in data files is fitted by two Gaussians and positions and areas of both peaks are determined. If the position of peaks and the ratio of peak areas are stable, than we conclude that the data is stable.

The procedure of checking the stability by two independent methods does not reveal any big problems in data for both E-channels and T-channels for all PIN detectors. The data for E-channel for all detectors are completely stable in a range of 30-40 channels ($\pm 2\sigma$ from mean line), which correspond to ≈ 1.14 – 1.52 MeV. For T-channel we have full stability ($\pm 2\sigma$ from mean line) in 15-20 channels (0.7–0.8 ns). Thus no corrections were necessary and we could start to calibrate the T- and E-channels and do subsequent data analysis.

4.3 Calibration of T-channels

Calibration of each time (T) channel consists in determination of two calibration parameters for linear transformation from channel numbers to nanoseconds. The channel width of the time-to-digital converter was accurately determined with the help of a precise time-calibrator “Ortec-462” and did not constitute a problem. Determination of the offset (T0) in time scale is a more delicate task. It was achieved using calibration spectra provided by a ^{252}Cf spontaneous fission source. The basic idea of the procedure used is to find such coefficients T0 that the spectra of calculated quasi-masses (M_{tt}) and quasi-velocities for fission fragments of ^{252}Cf are consistent with those known from the literature [Sch83]. The plasma delay in the time response of the PIN diodes being included in the value of T0 is assumed to be the same for all fission fragments detected in a particular PIN, or, in other words, the difference in plasma delays for light and heavy fragments is ignored. This approximation seems to be of minor influence on the results due to rather long flight paths used in the experiment.

4.3.1 Procedure for determination T0

To find the offset T0 for the linear transformation from channel numbers to nanoseconds we developed a code which uses the MINUIT minimization procedure from the CERN program library. The main idea for the procedure of determination of T0 is described below.

The formula for conversion of time from channels to nanoseconds is:

$$TOF[ns] = (TOF[ch] + T0) * dT/dk \quad (4.1)$$

Coefficients $T0$ and dT/dk are parameters for the minimization procedure. As the first approximation for our minimization procedure we took dT/dk determined from procedure with time-calibrator. In our procedure we can fix the value of the parameter or leave to be variable. We tried different combinations for obtaining the best results. In the end we have found that unfixed values of parameters dT/dk are very closed to that obtained with time-calibrator. The procedure starts with some initial value for the minimization parameter $T0$ and determines velocities of FF:

$$V = \frac{L_{TOF}}{TOF} \quad (4.2)$$

Masses of fission fragments are calculated based on TOF-TOF method using determined velocities:

$$M_1 = \frac{M_{total}}{\left(1 + \frac{V_1}{V_2}\right)} \quad (4.3)$$

$$M_2 = \frac{M_{total}}{\left(1 + \frac{V_2}{V_1}\right)} \quad (4.4)$$

After processing of some amount of data the spectra of velocity and of mass are created and the minimum of a criterion function is being looked for. The criterion function looks like:

$$\begin{aligned} F = & \alpha_1 \left[\frac{1}{n-r} \sum_i \frac{(M_T(i) - M(i))^2}{M_T(i)} \right] + \\ & + \alpha_2 [(\langle ML_T \rangle - \langle ML_1 \rangle)^2 + (\langle MH_T \rangle - \langle MH_1 \rangle)^2 + \\ & + (\langle ML_T \rangle - \langle ML_2 \rangle)^2 + (\langle MH_T \rangle - \langle MH_2 \rangle)^2] + \\ & + \alpha_3 [(\langle VL_T \rangle - \langle VL_1 \rangle)^2 + (\langle VH_T \rangle - \langle VH_1 \rangle)^2 + \\ & (\langle VL_T \rangle - \langle VL_2 \rangle)^2 + (\langle VH_T \rangle - \langle VH_2 \rangle)^2] \end{aligned} \quad (4.5)$$

where α_i are the coefficients which allow to regulate the contribution of different parts into the criterion function, $M_T(i)$ and $M(i)$ – normalized counts in channel number i in literature and experimental spectra, $\langle M \rangle$ and $\langle V \rangle$ are mean values for mass and velocity, L and H – light and heavy FFs. Parameters with index “T” – mean values of the peaks from literature spectra, parameters with digit index – mean values of the peaks from the experimental V and M_{it} spectra for arms “1” and “2”.

Using the minimization packet MINUIT [Min] the program tries to minimize the criterion function by varying input parameters T0 (for both arms). As output we obtain the appropriate coefficients T0 such that the position of peaks for light and heavy fission fragments in the mass and velocity spectra agree well with the literature data and the spectrum for mass is similar to the one taken from [Sch83]. Such procedure was repeated for all pairs of PIN diodes.

4.3.2 Modified procedure for determination of T0

In the process of data analysis it was found that the influence of energy loss of fission fragments in foils of the start detectors and in the source backing on the final results can not be neglected. Even $30 \mu\text{g}/\text{cm}^2$ of carbon foil and $50 \mu\text{g}/\text{cm}^2$ of Al_2O_3 backing may produce a distortion to our results. As it can be inferred from a comparison of the matrices presented in Figure 4.6, even thin absorbers can distort the TKE-Mtt distributions if they were ignored in the calculation.

To take into account all absorbers and to precisely define thicknesses of these absorbers a modified procedure for determination of T0 was designed [Pya06a, Pya07]. This procedure has two minimization cycles:

- an outer cycle for the calculation of the coefficient T0;
- an inner cycle for the determination of values V_{emit} and M_{emit} before degrader used as input values in the outer cycle.

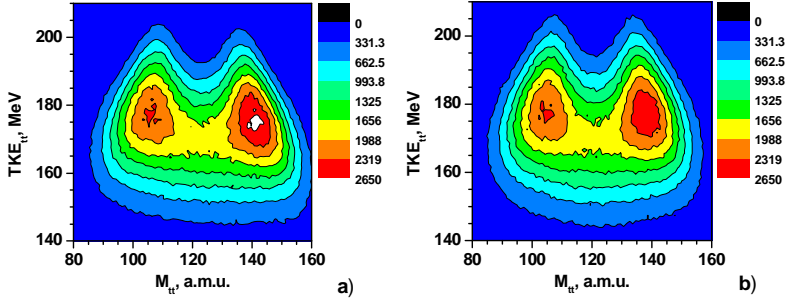


Figure 4.6 a) M_H -TKE matrix of the FF's from ^{252}Cf (sf) obtained when the absorbers were disregarded in the time calibration. b) Similar matrix when they were taken into account.

The outer cycle looks the same as the one in the unmodified procedure for the determination of T0 and is processing the whole amount of data. In the inner cycle we work with individual events and use the Nelder-Mead algorithm to determine proper values of V and M before degrader, the so called V_{emit} and M_{emit} .

The Nelder-Mead method [Nel] is a simplex method for finding a local minimum of a function of several variables. For two variables, a simplex is a triangle, and the method is a pattern search that compares function values at the three vertices of a triangle. The worst vertex, where $f(x,y)$ is largest, is rejected and replaced with a new vertex. A new triangle is formed and the search is continued. The process generates a sequence of triangles (which might have different shapes), for which the function values at the vertices get smaller and smaller. The size of the triangles is reduced and the coordinates of the minimum are found.

The main steps of the inner minimization are:

- 1) take $TOF1_E$ and $TOF2_E$ for arm 1 and 2 from the outer minimization cycle;
- 2) calculate the input values of V and M for the Nelder-Mead method:
 - $V(1)=V_T - \Delta V$;
 - $V(2)=V_T$;
 - $V(3)=M_T + \Delta V$;
 - $M(1)=M_T - \Delta M$;
 - $M(2)=M_T$;
 - $M(3)=M_T + \Delta M$,
 where V_T and M_T are table values for V and M for ^{252}Cf .
- 3) using the energy loss procedure we calculate the energy of FFs after degrader (foils of MCP-start detector and source backing);
- 4) once the energy after degrader is known, we calculate the velocities of the fragments after degrader;
- 5) calculate the current TOF value, TOF_{NM} , using the Nelder-Mead procedure;
- 6) minimize the criterion function:

$$F = (TOF1_E - TOF1_{NM})^2 + (TOF2_E - TOF2_{NM})^2 \quad (4.6)$$

As output from the inner minimization cycle we have proper values of velocity and mass before particles have lost their energy at carbon foils of MCP-start detectors and source backing. These values are used for the outer minimization cycle.

The M_H mass spectrum for the fission fragments of ^{252}Cf , obtained using this algorithm is in a good agreement (see Figure 4.7) with our reference spectrum taken from [Sch83].

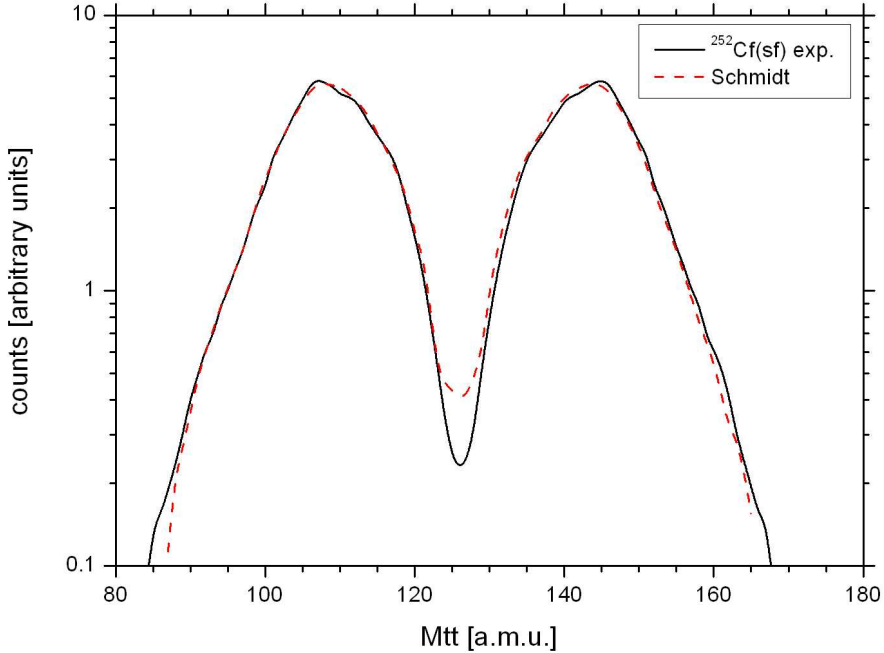


Figure 4.7 Mtt mass spectra for the FF's of ^{252}Cf . Solid line is data from experiment, dashed line presents data from [Sch83].

The table below summarizes the results of the proper time calibration using a ^{252}Cf source.

Table 4.1 Parameters for V and Mtt spectra obtained in proper time calibration compared to published data.

Parameter	All PIN detectors	Literature data		
		[Whe63]	[Kie92]	[Sch83]
$\langle V_L \rangle$, cm/ns	1.373 ± 0.005	1.375 ± 0.007	1.369 ± 0.009	
$\langle V_H \rangle$, cm/ns	1.038 ± 0.007	1.036 ± 0.005	1.035 ± 0.007	
σ_{V_L} , cm/ns	0.067	0.067	0.064	
σ_{V_H} , cm/ns	0.082	0.080	0.078	
$\langle M_L \rangle$, a.m.u.	108.61 ± 0.41	108.39		108.55
$\langle M_H \rangle$, a.m.u.	143.39 ± 0.41	143.61		143.53
σ_{M_L} , a.m.u.	7.03	6.72		7.16
σ_{M_H} , a.m.u.	7.03	6.72		7.16

Here $\langle V_{L,H} \rangle$ and $\langle M_{L,H} \rangle$ denote mean velocities and mean M_{tt} masses for the fission fragments of light (L) and heavy (H) mass groups, respectively; $\sigma_{V_{L,H}}$ and $\sigma_{M_{L,H}}$ are standard deviations of the respective distributions. Averaging was done over all PIN diodes.

We have as well applied another test proven to be very sensitive to the quality of the data. The test deals with the manifestation of the proton odd-even effect in the mass yields. It is known that the FF's having an even nuclear charge number feature

comparatively higher mass yield. In the TKE-Mtt distribution obtained in the frame of the TOF-TOF method the ridges of the enhanced yields of FF masses are dominated by fragments with even nuclear charge numbers [Pya02]. This is illustrated as a regular sequence of vertical ridges in the TKE-Mtt space, see Figure 4.8.

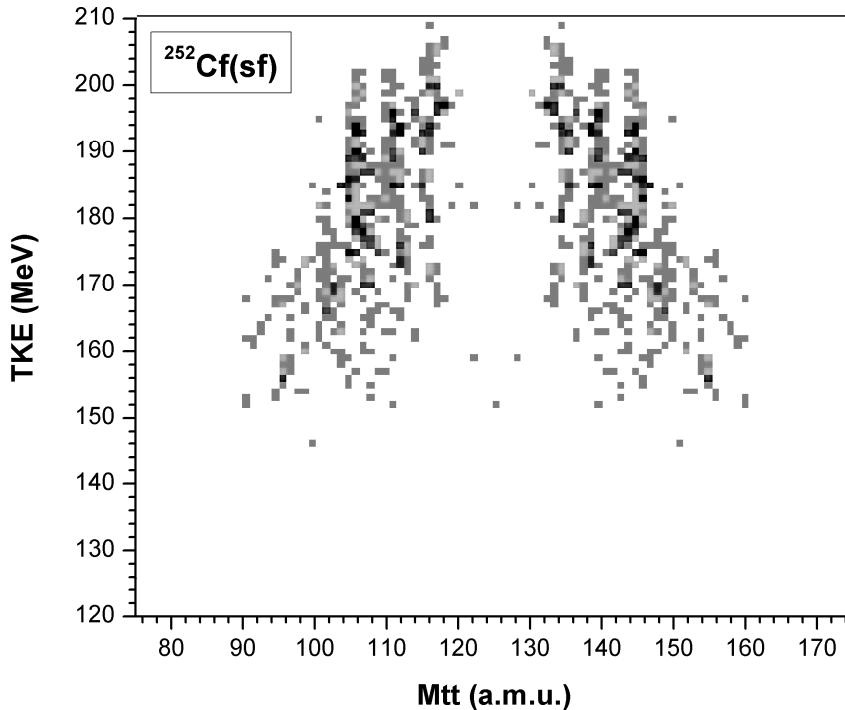


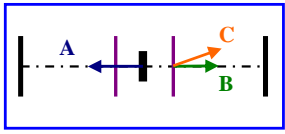
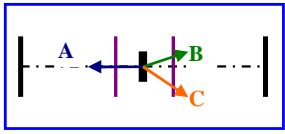
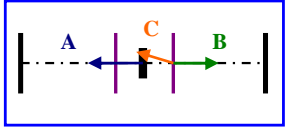
Figure 4.8 Fine structure of the Mtt-TKE matrix of the FF's from ^{252}Cf (sf).

The initial matrix (unsymmetrized) was processed by applying a second derivative filter, thus simultaneously testing the symmetry of the mass distribution [Trz02] obtained by the TOF-TOF method.

4.3.3 Determination of velocity in the multi-body decay

In the multi-body decay the position of the start detector plays a significant role in the determination of velocity for all fragments. In the present setup the MCP-based “start” detectors were placed at 51 mm from the target (Figure 4.1). In the multi-body decay, the fastest of the fragments hitting the “start” detector gives the “start” signal to be common for the corresponding arm. Consequently, only the velocity of this fragment will be measured correctly. Others fragments detected in the same arm get shifted velocity values. True (emission) velocities can be calculated according to the formulae given in Table 4.2 where V^{emis} and V^{exp} are the experimental and the emission velocities respectively. The choice of the proper formula is controlled by the time difference between the signals of start detectors (this parameter was also measured in our experiment).

Table 4.2 Corrections to the fragment velocities for ternary events.

Variant №	Kinematical scheme of the decay mode	Formula for calculation of the emission velocity
1		2 fragments "B" and "C" formed in the MCP detector fly in the same direction: <u>no corrections</u> , i.e. $V_{B,C}^{emis} = V_{B,C}^{exp}$
2		2 fragments "B" and "C" were formed in the target (fragment C is faster): $V_B^{emis} = \frac{61.7}{\frac{V_B^{exp}}{56.6} + \frac{V_C^{exp}}{5.1}};$ $V_C^{emis} = V_C^{exp}$
3		2 fragments "B" and "C" were formed in the MCP detector, but fly in opposite directions: $V_B^{emis} = V_B^{exp};$ $V_C^{emis} = \frac{66.8}{\frac{V_c^{exp}}{56.6} - \frac{1}{\frac{V_B^{exp}}{56.6} - \frac{1}{V_A^{exp}}}}$

4.4 Energy calibration and reconstruction of the FF masses

Energy calibration and reconstruction of the mass of the FF is the most important stage of data analysis, and this is a difficult and sophisticated task, if silicon detectors are used for registration energy of ions. One of the specific problems is the necessity of taking into account the so-called pulse-height defect (PHD). A unified parametric procedure was worked out for simultaneous determination of the real fragment energy (i. e., including the PHD) and Mte mass [Pya06a, Pya07]. Related parameters were obtained by fitting the spectrum of quasi-masses (Mte) to those known from literature.

4.4.1 Pulse-height defect

The response of semiconductor detectors to fission fragments is different than that of light ions, such as protons and alpha particles. The pulse height of a heavy ion is smaller than that of a light ion of the same energy, and the term PHD is used to denote this phenomenon. PHD is commonly defined as the difference between the energy of a heavy ion and that of an alpha particle yielding the same pulse height. Investigation of PHD showed that its value R consists of three components and each of them has a complicated dependence on the mass M and the kinetic energy E of recorded ion:

$$\mathbf{R} = f(\mathbf{M}, \mathbf{E}) = \mathbf{R}_1(\mathbf{M}, \mathbf{E}) + \mathbf{R}_2(\mathbf{M}, \mathbf{E}) + \mathbf{R}_3(\mathbf{M}, \mathbf{E}) \quad (4.7)$$

The quantity \mathbf{R}_1 is due to energy losses in the entrance window of a detector. The component \mathbf{R}_2 results from energy losses at elastic collisions with atoms of crystal lattice in a detector. The third quantity \mathbf{R}_3 is connected with the electron-hole recombination in plasma produced along an ion track.

The difficulties connected with the evaluation of recombination losses and the uncertainties in the widths of detector entrance windows make it necessary to determine the value $\mathbf{R}(\mathbf{M}, \mathbf{E})$ for each given detector experimentally. The most precise solution of the problem is to measure the dependence $\mathbf{R}(\mathbf{E})$ for every studied mass \mathbf{M} with a heavy ion accelerator. This technique is rather expensive though. Therefore, the detector calibration methods are usually based on the application of different empirical expressions for $\mathbf{R}(\mathbf{M}, \mathbf{E})$. The parameters of these expressions are determined either from measurements only for several selected masses and energies or from the parameters of ^{252}Cf spontaneous fission fragment spectra.

At present the PHD for Si-detectors is usually described within the framework of the procedures proposed by *Schmitt* [Sch65], *Kaufman* [Kau74] and *Ogihara* [Ogi86]. These techniques give satisfactory results for the detectors whose parameters are close to those investigated in these original works and in the range of heavy ion masses and energies studied by these authors. In other cases the application of the techniques may lead to visible errors.

In our data analysis we evolved an approach superposing the calculation of both, true energy and TOF-E mass of the fragment. For this purpose we used a new empirical PHD description for PIN diodes derived by *Mulgin* and his colleagues [Mul97].

4.4.2 Calibration of E-channels

There are two steps in the procedure of deducing correct FF energies. The first one consists in energy calibration using α -lines and precise amplitude generator, the second one aims at taking the PHD into account. The usual equation for conversion of channel number to registered energy of a particle is

$$\mathbf{E}[\text{MeV}] = (\mathbf{E}[\text{ch}] - \mathbf{E}_0[\text{ch}]) \cdot d\mathbf{E}/d\mathbf{k}, \quad (4.8)$$

where $\mathbf{E}[\text{ch}]$ is the channel number in which the ion is registered, $\mathbf{E}[\text{MeV}]$ is the energy of the ion deposited in the PIN. Both the scale coefficient $d\mathbf{E}/d\mathbf{k}$ and the zero shift value $\mathbf{E}_0[\text{ch}]$ were determined with the help of a high precision pulse generator PB-5 BNC (Berkeley Nucleonic Corporation) and natural alphas from ^{252}Cf ($E_\alpha = 6.118$ MeV) and from a standard ^{226}Ra calibration source ($E_\alpha = 4.781$ MeV, 5.486 MeV, 6.000 MeV, 7.688 MeV).

During the experiment one block of ADCs was replaced due to the fact that one of the control signals in this block was no longer working. Thus two independent energy calibrations were done for two parts of data: before and after block replacement.

4.4.3 Reconstruction of FF masses

Reconstruction of the mass of the fission fragment is a difficult task due to the influence of the pulse-height defect. The channel number of energy coder in which the ion is registered depends on the energy of the ion and on the pulse-height defect. On the other hand PHD depends on the mass and the kinetic energy of registered particle. We used a specially developed procedure for combined calculations of true energy and TOF-E mass of the fission fragment [Pya06a, Pya07].

For the relation between the energy E_{MeV} and the ion mass M and the channel number E_{ch} in which the ion was registered one can write

$$E_{MeV} = (E_{ch} - E_0) \frac{dE}{dk} + R(M, E_{MeV}), \quad (4.9)$$

where $R(M, E_{MeV})$ is the PDH for this ion. The scale coefficient dE/dk and the zero shift value E_0 were defined as discussed above. *Mulgin* proposed the following empirical expression for the description of the PHD value for PIN diodes [Mul97]:

$$R(M, E_{MeV}) = \frac{\lambda E_{MeV}}{1 + \varphi \frac{E_{MeV}}{M^2}} + \alpha M E_{MeV} + \beta E_{MeV}, \quad (4.10)$$

where λ , φ , α , β are parameters.

Taking into account that

$$E_{MeV} = \frac{MV^2}{1.923} \quad (4.11)$$

where mass M and velocity V are expressed in MeV and cm/ns respectively, we can replace E_{MeV} in expressions (4.9) and (4.10) according to expression (4.11).

As a result a polynomial equation of 3rd order for the determination of mass is obtained:

$$F(M, \{X\}) = 0, \quad (4.12)$$

where $\{X\} = \{\alpha, \beta, \lambda, \varphi\}$ is a vector of the parameters denoted above. Equation (4.12) should be solved in order to calculate the mass of the ion using known values of the ion velocity V and energy E_{ch} expressed in channels under the condition that the vector $\{X\}$ is also known. The numerical components of vector $\{X\}$ suggested in [Mul97] failed to reproduce Mte spectrum of the FF's obtained at our setup for ²⁵²Cf (sf).

In order to find a proper vector of parameters a special iteration procedure was applied. At first, an analytical solution of the expression (4.12) was obtained. This means that a quasi-mass can be calculated in each event using experimental values of V and E_{ch} on the one hand, and the current value of vector $\{X\}$ on the other hand. Then a spectrum of quasi-masses can be collected using sufficient sets of the initial data. Varying the vector of parameters the procedure tries to minimize the criterion function F :

$$F = (\langle ML_T \rangle - \langle ML \rangle)^2 + (\langle MH_T \rangle - \langle MH \rangle)^2 + \mu \sum \left\{ \frac{[Y(M) - Y(M_T)]^2}{Y(M)} \right\}, \quad (4.13)$$

where $\langle ML \rangle$ and $\langle MH \rangle$ are the mean values of light and heavy peaks in the experimental spectrum of mass $Y(M)$. The index "T" denotes values taken from the

spectrum known from the literature. The parameter μ defines a relative weight of the components included in function F .

The reconstruction quality of the Mte masses proved to be acceptable for all PIN detectors. A comparison of the Mte mass spectrum for fission fragments from ^{252}Cf (sf) from our experiment with the Mte mass spectrum taken from literature [Wah88] is presented in Figure 4.9.

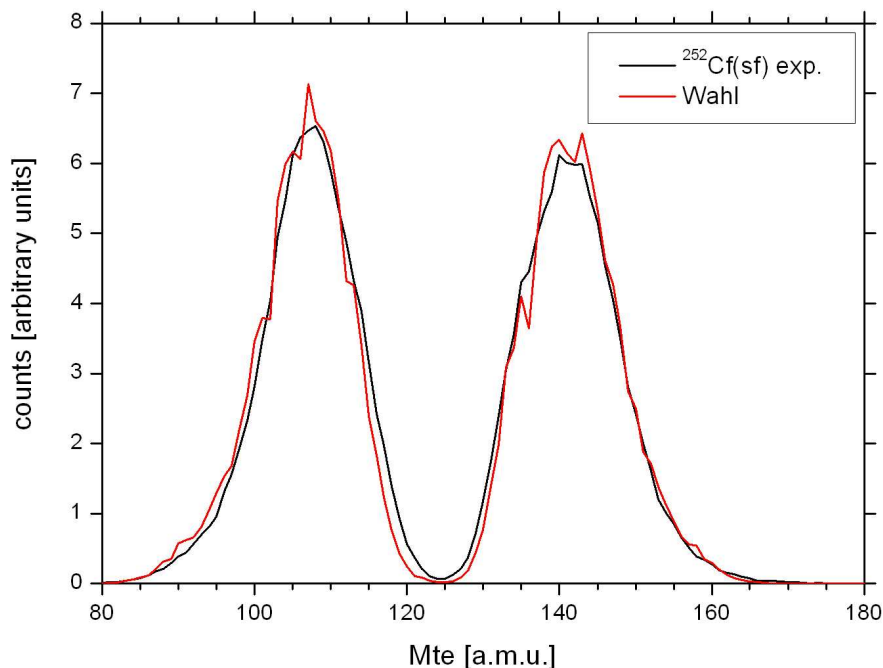


Figure 4.9 Mte mass spectra for the FF's of ^{252}Cf . Solid line is data from experiment, dashed line presents data from [Wah88].

Table 4.3 compares the parameters of the Mte spectra in PINs and the corresponding values taken from [Wah88].

Table 4.3 Comparison of parameters for the reconstructed Mte mass spectrum with literature values.

Parameter	All PIN detectors	Literature data [Wah88]
$\langle M_L \rangle$, a.m.u.	106.66 ± 0.21	106.91
$\langle M_H \rangle$, a.m.u.	141.19 ± 0.48	141.46
σ_{M_L} , a.m.u.	6.0	5.8
σ_{M_H} , a.m.u.	6.5	6.2

Here the averaging for calculation of mean values $\langle M_L \rangle$ and $\langle M_H \rangle$ was done over all PIN diodes.

Another sensitive test of the quality of calculation of the Mtt and Mte masses is presented in Figure 4.10. The mean value of Mte (postneutron experimental mass) was calculated for each Mtt - $\nu(\text{Mtt})$ slot, where the mean number of emitted neutrons $\nu(\text{Mtt})$ is known from the literature [Bud88]. The deviations of the experimental

points in the regions of low mass yields from the expected diagonal line can have physical as well as methodical base and it is under current analysis.

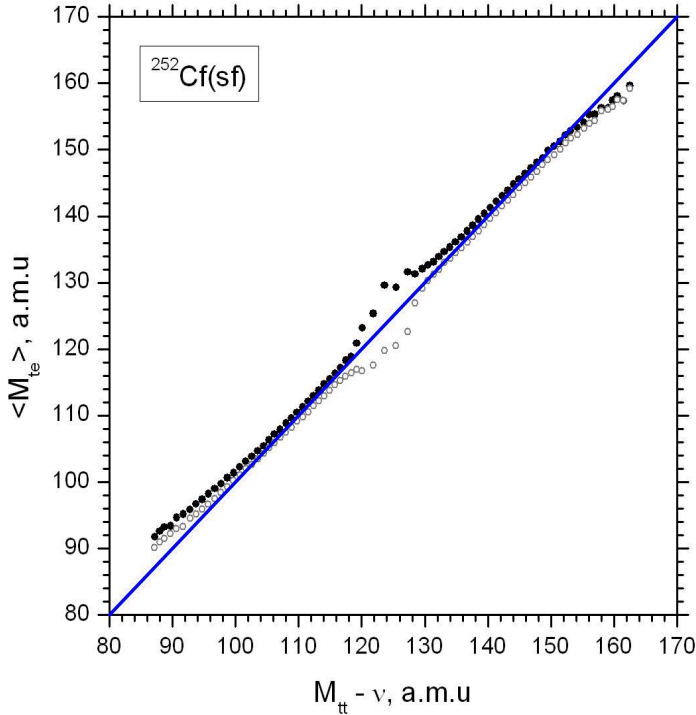


Figure 4.10 The plot $\langle M_{te} \rangle$ versus $M_{tt} - v$. Solid circles are presented data for the spectrometer arm 1, open circles are data for the spectrometer arm 2.

It should be stressed that both time and energy calibration related parameters were obtained by fitting the spectrum of quasi-masses (M_{tt} or M_{te}) to those known from literature. In the calculation of the TOF coefficients also the peak positions in the measured spectra for the velocity were adjusted to literature data. Thus in both T and E channels, just known M_{tt} and M_{te} mass spectra and the mean values of velocity for FFs insensitive to peculiarities of the set up were used as standards for calibrations. This allows us to be sure that each of the 32 detectors was carefully calibrated with respect to T and E [Pya06a, Pya07]. The M_{te} mass spectra for the FF's from the reaction $^{238}\text{U} + ^4\text{He}$ are presented in Figure 4.11.

The mean value obtained for the total mass is 231.7 a.m.u. Contrary to our result, the expected value due to the known mean number of emitted neutrons v_{tot} [Col61, Rub01] is around 236 a.m.u. Thus the spectrum of the M_{te} masses (Figure 4.11) is presumably shifted to lower masses by approximately 2 a.m.u. A systematic shift of 400 ps in the TOF reading in each arm of the spectrometer would be sufficient to cause the mass shift observed. A possible reason for the shift in the TOF measurement compared with the calibration using the Cf source could be the bulk of delta electrons emanating from the target during beam bursts. This effect is well known to influence MCP based start detectors [Kon].

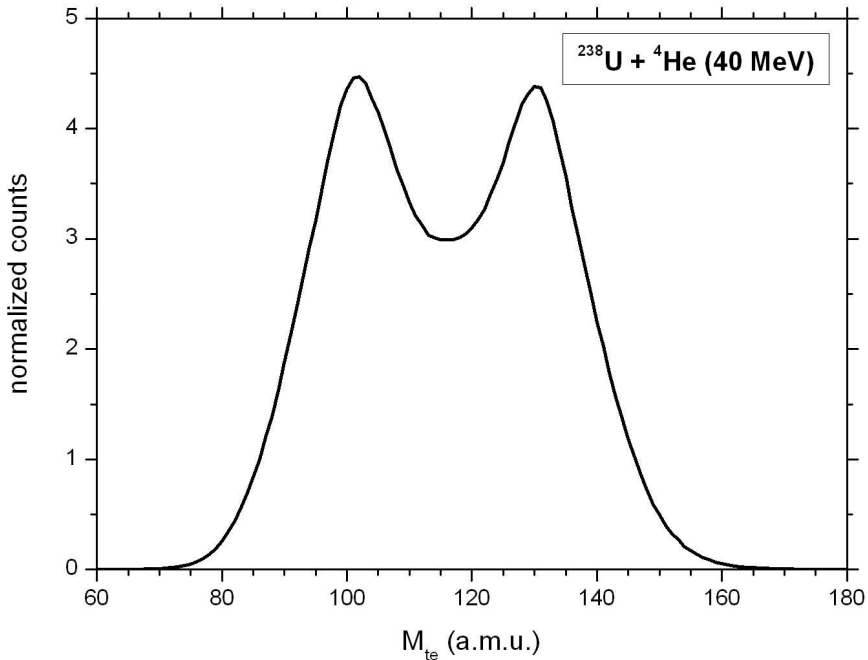


Figure 4.11 Spectrum of the M_{te} masses of the fission fragments originated from the reaction $^{238}\text{U} + ^4\text{He}$ (40 MeV).

Figure 4.12(a) illustrates the correlation between two masses for events with a multiplicity three of detected fragments. By convention, the fragments in each ternary event have been re-sorted in order of decreasing fragment mass number. Namely, M_a denotes the heaviest mass, M_b the next lighter one, and M_c the lightest mass in the triplet. Only two among the three fragments detected in those events are depicted in the scatter plot of Figure 4.12a. No additional gating was used. A pronounced vertical line marked by the arrow is suggested to correspond to the deformed magic nucleus ^{98}Sr . If so, the width of this mass peak on the Figure 4.12b does not exceed 2.5 a.m.u. This value is in fair agreement with the energy resolution measured earlier at the mass separator Lohengrin for the PINs used in our experiment [Spi92].

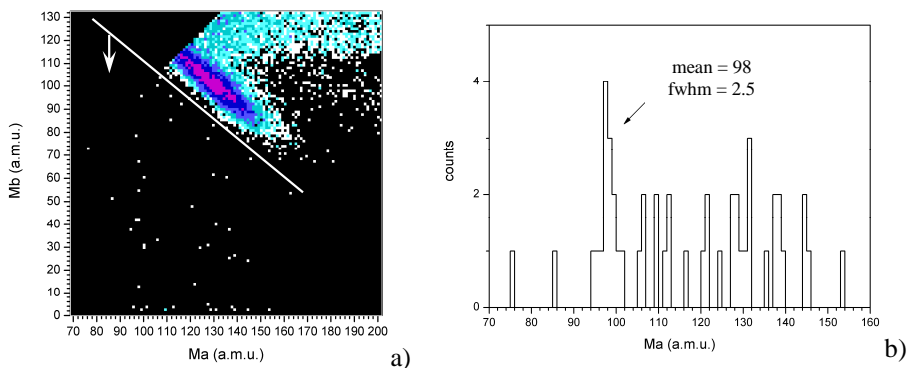


Figure 4.12 a) Mass-mass distribution of fragments in ternary fission of ^{242}Pu . b) Projection onto M_a axis of the events below the white line in (a)

4.5 Experimental results

The analysis of the experimental data we collected is presented below. We tried to reveal the main possible sources of false events, which could be detected as events of the effect under study. An analysis of detected triple events is carried out and one group of interesting points in mass-mass plot is examined in detail.

4.5.1 Possible sources of false events

The main purpose of our experiment was the search for rare multi-body decays of the ^{242}Pu compound nucleus. Due to the geometry of the setup used (Figure 4.1) only decays with almost collinear kinematics of the decay partners can be studied. Let us analyze the main reasons for events with an experimental multiplicity ≥ 3 (i.e. at least three fragments were detected in coincidence).

At first it can be that two binary fission events appear to occur during one beam bunch. The probability of simultaneous registration of four fragments in this case can be estimated using Figure 4.13. The momentum distribution for the FF's from common binary fission is peaked at a momentum of ~ 135 cm·a.m.u./ns (Figure 4.13a), while the coordinates of the center of the locus marked by the arrows in Figure 4.13b are twice as large. Due to this fact random coincidences of two pairs of the fission fragments in one bunch appear with a probability $\sim 6 \cdot 10^{-6}$. If one of four fragments is not registered, the observed triple random coincidences rate has increased probability of up to $2.6 \cdot 10^{-5}$.

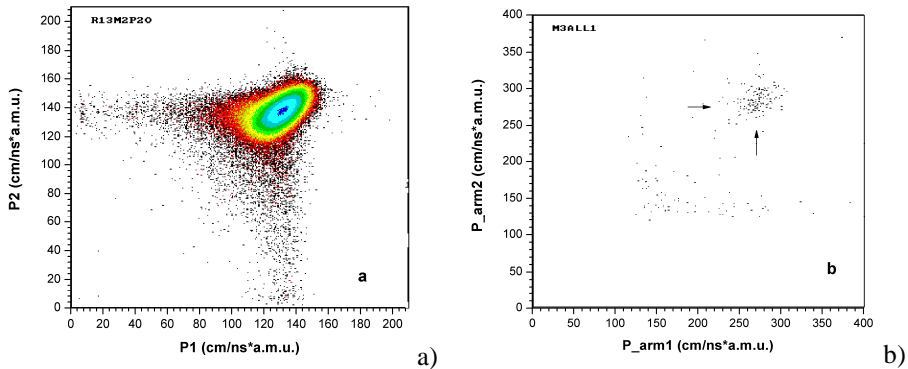


Figure 4.13 a) Momenta of the coincident fragments for multiplicity two. b) Similar plot for multiplicity four. Arrows mark the events linked with random coincidence of four FF's from two binary fissions in one bunch.

Along with random coincidences inside one bunch such possibility exists also for events in adjacent bunches as can be inferred from Figure 4.14. Here, the energy measured in the PIN diodes (E_p) is plotted versus the time-of-flight (TOF) in one of the spectrometer arms (1), for events with multiplicity two. The locus of normal binary fission events is marked by number 1. Bearing in mind that each “start” signal opens a time gate of ~ 200 ns for event registration two additional beam bunches (2 and 3 in Figure 4.14) hit the target during this time. The ratio between the events contained in locus 2 and those in locus 1 is about $1.3 \cdot 10^{-5}$. Evidently random

coincidences related to the events in loci 2 and 3 can easily be rejected. The next set of points to be discussed is marked by number 4. It is linked with light ions scattered off by the beam particles from the backing material of the target (masses corresponded to these events are equal to 27 (aluminum) and 16 (oxygen)). Locus 5 is of the same origin but is generated in the previous beam bunch: if we subtract from the time for these events ~ 68 ns (the interval between bunches), then we obtained the picture equivalent to group 4. It should be noted that we use TOF-E method and thus we determine the real mass of fragment. Both, the loci 4 and 5, are responsible for the major part of the random triple coincidences. In the upper part of the loci under discussion a specific set of points, marked by number 6, is worthwhile to note. Alpha-particles from the beam scattered at approximately 90° on the target are responsible for this structure. When they penetrate the PIN diodes they deposit only part of their initial energy of ~ 30 MeV due to insufficient depth of the depletion layers. The total yield of events in loci 5 and 6 is about $1.4 \cdot 10^{-4}$ compared with locus 1. It should be stressed that occasionally locus 6 superimposes on the position of α -particles originating from conventional ternary fission and polar emission. The “tail” marked with number 7 is predominantly connected with the fragments being scattered on the diaphragm in front of the PIN diodes. For these events we have almost correct velocity and incorrect energy (less, then it is for normal fragments). It means that fragments are scattered close to stop detector, very probably on the diaphragm in front of PIN array. Here, the relative yield is about $3.6 \cdot 10^{-4}$. The events in locus 8 are related with pile up in the energy channel, with a relative probability $\sim 2 \cdot 10^{-5}$.

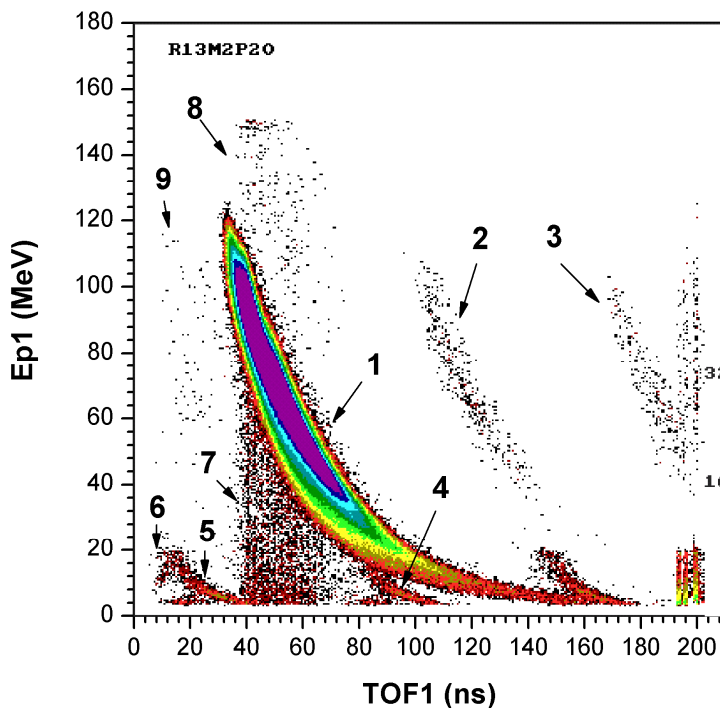


Figure 4.14 Energies E_p measured in the PIN diodes of one of the spectrometer arms (1) versus time-of-flight (TOF), for events registered with multiplicity two. The different groups of events marked by numbers 1-9 are discussed in the text.

Finally, the main part of the points marked by number 9 (relative yield is about 10^{-5}) is due to an incorrect measuring of fragment TOF. Calculations show that if there is head collision, then fission fragment can knock out the ion from the backing or conversion foil and the velocity of this ion will be greater than the fission fragment velocity. Later on, if the mutual angle between fragment and ion is less than aperture of one detector, then these two particles will come in the same detector. We will have incorrect velocity for registered fragment (greater then it should be) and almost right energy as we see in Figure 4.14.

4.5.2 Analysis of ternary events

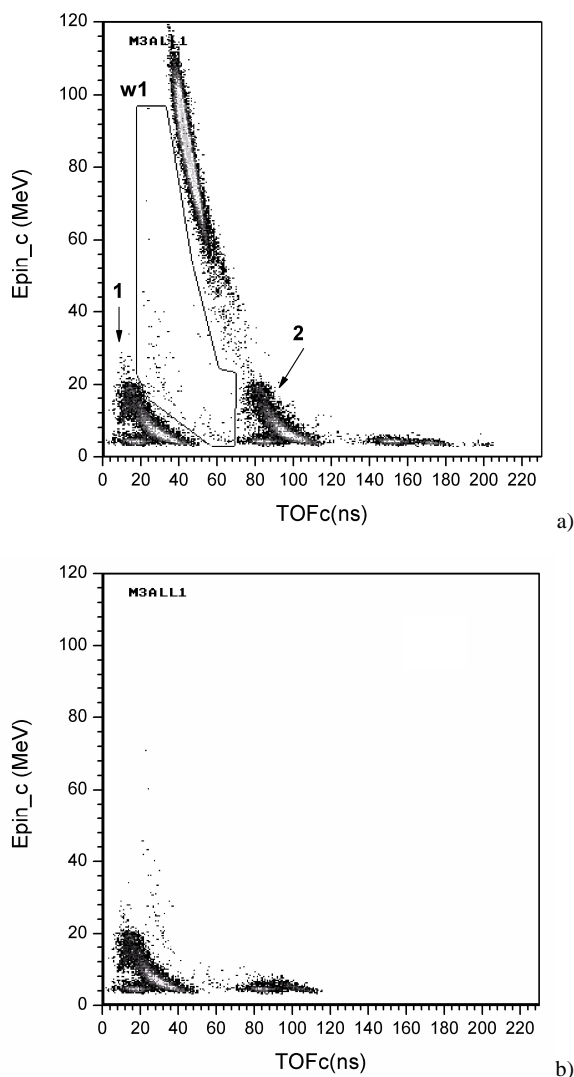


Figure 4.15 a) TOF versus energy detected in PIN for the lightest fragment in each ternary event. b) The same under condition that a total mass of all three fragments detected does not exceed 250 a.m.u.

Analysis showed that the main part of the triple events detected are due to the random coincidences of the FF originated from conventional binary fission with both scattered α -particles from the beam and ions of oxygen and aluminum knocked from the target backing by the beam particles. Such events form pronounced loci in Figure 4.15a (marked by the arrows).

Both loci (1 and 2) are of the same nature but are linked with adjacent bunches. For the sake of convenience the fragments in each ternary event were resorted in order of decreasing of fragment mass namely M_a to be the heaviest one and so on. A long locus in the upper part of Figure 4.15a should be excluded from further analysis. It follows from Figure 4.15b were gating $M_s < 250$ a.m.u. was used. Thus only the events in the window w_1 will be analyzed below. Their projection onto M_c axis is shown in Figure 4.16. As it can be seen from the spectrum the alphas are excluded from further analysis due to the choice of window w_1 .

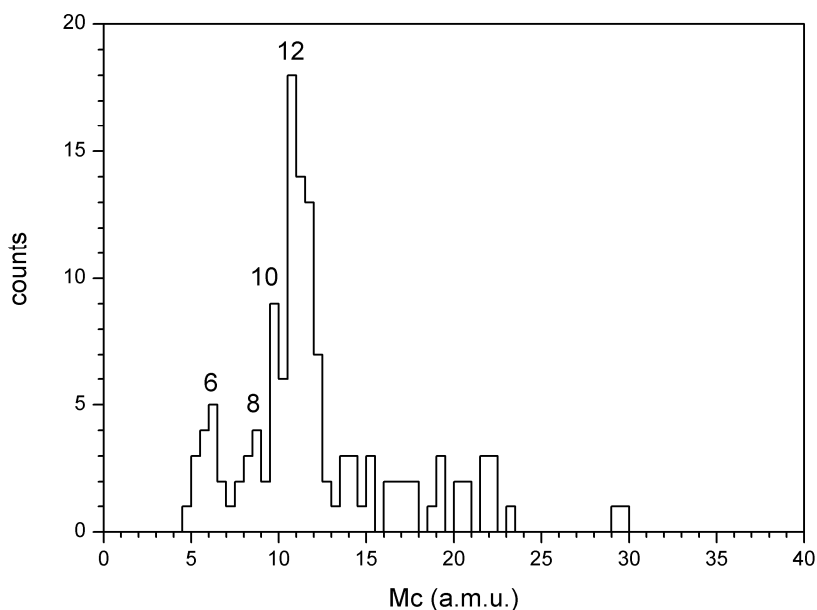


Figure 4.16 Spectrum $Y(M_c)$ for the events included in window w_1 in Figure 4.15a. Each channel on the mass axis corresponds to 0.5 a.m.u. The numbers above the peaks correspond to their centers.

For the search for unusual events Figure 4.17a was used. Here a difference in time when “start” detectors were hit by the fragments flying apart is plotted on vertical axis. This time is known to be approximately proportional to mass ratio of the fission fragments from binary fission.

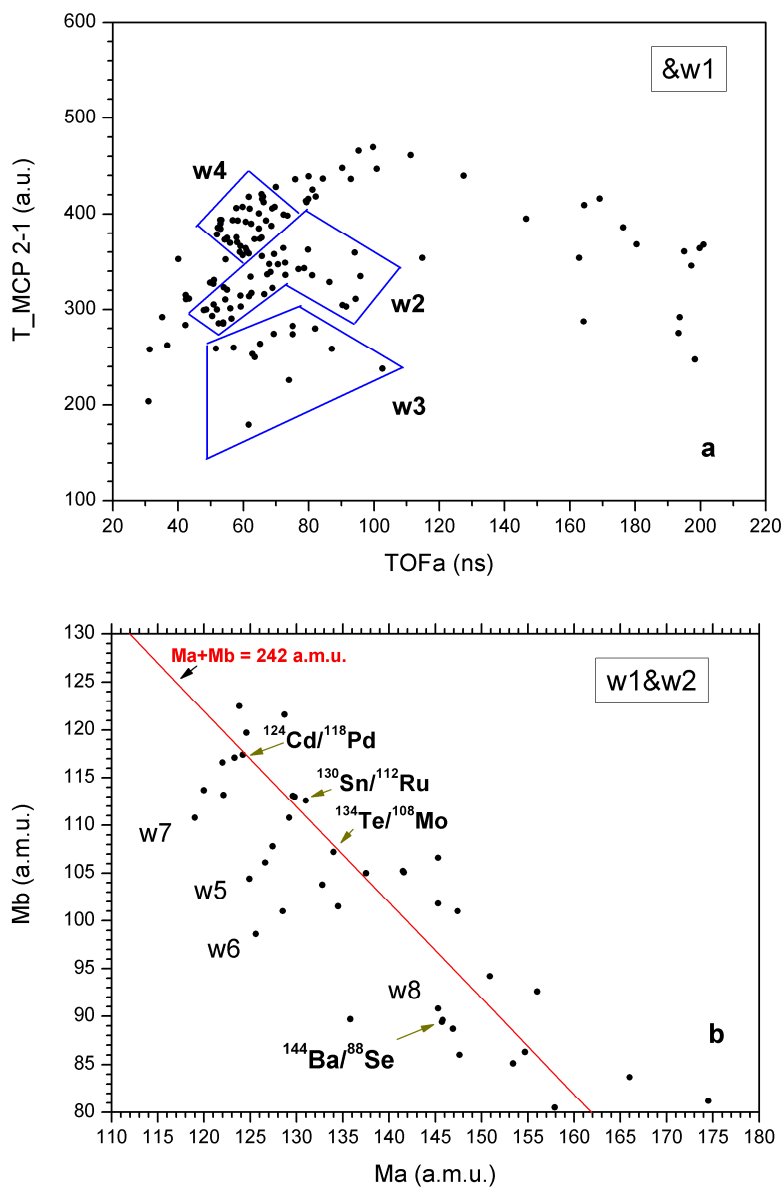


Figure 4.17 a) Time-of-flight versus time between “start” signals for the events gated by the window w1 (Figure 4.15a). b) Mass-mass distribution for the events selected using condition w1&w2.

The grouping of the points at Figure 4.17 attracts our attention. Corresponding groups are marked in the figure by contours w2-w4. The set of events w2 for instance, looks like some distinct families of points (marked as w5-w8 in Figure 4.17b) on Ma-Mb plane. The pair of magic fragments whose total mass is equal to the mass of compound nucleus (242 a.m.u.) “starts” each family. We have analyzed them event by event. The corresponding results are presented in Tables 4.4÷4.9 below.

Table 4.4 Information which was taken into account at derivation of the decay scheme for each triple event analyzed (example for an event from the family w5 in Figure 4.17b).

point №	parameter	parameter value				decay scheme
		common	fragment			
			A	B	C	
4	PIN number		205	111	208	
	M, a.m.u.		127.4	107.8	10.8	⁶ He
	V, cm/ns		0.867	1.22	2	
	E _{fr} , MeV		49.9	83.5	22.6	
	P _{arm1} , a.u.	131.6				
	P _{arm2} , a.u.	132.3				
	M _{sum} , a.m.u.	246.1				
M _{A+B} , a.m.u.	235.2					

$^{128}\text{Sn} + ^{108}\text{Mo} + ^6\text{He}$
 \downarrow
 \downarrow missing
 \downarrow -----
 \downarrow ^{114}Ru
 ^{12}C from "start" detector

The following notations are used in Table 4.4 above. Each column A, B, C, D (in order of decreasing of fragment mass) involves parameters of specific fragment. PIN number lets one to know which PIN diode was hit and in which arm. M, V, E_{fr} are, respectively, FF mass, velocity and true energy deposited in PIN diode (pulse-height defect was taken into account). P_{arm1, 2} are the total momentum of the fragments detected in a corresponding arm. M_{sum} is the total mass of all fragments detected in this event. M_{A+B} is the total mass of two heaviest fragments. D_{cal} is the mass of third fragment calculated using mass conservation law under the condition that the reference mass of the decaying system has to be 242 a.m.u. (the number of pre-scission neutrons emitted in a specific event is unknown).

For the event under discussion the following arguments were taken into account in order to restore the most reasonable decay scheme that could provide the parameters observed in the experiment. For three fragments the conservation law of the momentum measured is met very well. At the same time the total mass M_{sum} is too large even when compared with the maximal possible mass of the decaying system (242 a.m.u.). One can assume that the fragment C could be a Carbon ion knocked from the MCP detector foil. It is known from the Table 4.4 that fragments A and C fly in the same direction (for both fragments the numbers of PINs start from "2"). Using the Rutherford formula for elastic scattering one obtains that the energy of C-ion scattered at zero angle with respect to the velocity vector of fragment A having energy E_{A'} = E_{fr,A} + E_{fr,C} should be 22.72 MeV. This agrees well with the experimental value 22.6 MeV from Table 4.4. Experimental values of masses of the fragments A and B are very close to the masses of known magic nuclei ¹²⁸Sn and ¹⁰⁸Mo respectively. It is believed that just these nuclides are the decay partners. Conservation of nuclear charge and mass requires that the third fragment, such as ⁶He, should exist by composition. It can be as well ⁴He and two neutrons or 2·³H and so on.

Table 4.5 Summary on Sn/Ru mode (gate w5 in Figure 4.17b).

Point number	Decay scheme
	$^{50}\text{Sn}_{82} (\beta_2 \sim 0, "G", "G") / ^{44}\text{Ru}_{\text{Nucd}=69.1} (\beta_2 \sim 0.55, "C")$
1	$^{129}\text{Sn} + ^{113}\text{Ru}$ - binary fission \downarrow ^9Be from "start" detector
2	$^{130}\text{Sn} + ^{112}\text{Ru}$ - binary fission \downarrow ^{12}C from "start" detector
3	$^{129}\text{Sn} + ^{113}\text{Ru}$ - binary fission \downarrow ^{19}F from "start" detector

4	$^{128}\text{Sn} + ^{108}\text{Mo} + ^6\text{He}$ ↓ missing ↓ ----- ^{114}Ru ↓ ^{12}C from "start" detector
5	$^{126}\text{In} + ^3\text{H} + \text{n} + ^{106}\text{Nb} + ^6\text{Li}$ missing ----- ^{130}Sn ^{112}Ru
6	$^{129}\text{Sn} + ^{103}\text{Zr}^{(2)} + ^6\text{He} + ^4\text{He}$ missing ----- ^{113}Ru
7	$^{124}\text{Cd} + ^6\text{He} + ^8\text{Be} + ^{104}\text{Zr}$ missing ----- ^{130}Sn ^{112}Ru

The upper line of Tables 4.5÷4.9 provides the information concerning deformations and nucleon compositions of the shells involved while capital letters in the brackets correspond to the shell minima loci in [Wil76]. Unchanged charge density (Z_{ucd}) hypothesis was used for calculation, for instance number of neutrons in the nucleus with magic number of protons ($^{44}\text{Ru}_{\text{Nucd}=69.1}$) and vice versa. The fragment whose mass was corrected according the formulae 2 or 3 from Table 4.2 is marked by the corresponding number (for instance, $^{103}\text{Zr}^{(2)}$). Bold symbols in the decay schemes correspond to really detected fragments.

Table 4.6 Summary on Cd/Pd mode (gate w6 in Figure 4.17b).

Point number	Decay scheme
$^{48}\text{Cd}_{\text{Nucd}=75.4}$ ($\beta_2 \sim 0.8$, "K'") / $^{46}\text{Pd}_{\text{Nucd}=72}$ ($\beta_2 \sim 0.8$, "K'")	
8	$^{124}\text{Cd} + ^{118}\text{Pd}$ - binary fission ↓ ^{12}C from "start" detector
9	$^{124}\text{Cd} + ^{118}\text{Pd}$ - binary fission ↓ ^9Be from "start" detector
10	$^{122}\text{Ag} + ^{122}\text{Ag}$ ↓ ^{19}F from "start" detector
11	$^{108}\text{Mo}^{(2)} + ^{14}\text{C} + 2\text{n} + ^{118}\text{Pd}$ missing ----- ^{124}Cd
12	$^{122}\text{Cd} + 2\text{n} + ^{118}\text{Pd}$ - binary fission ↓ missing ^{12}C from "start" detector
13	$^{122}\text{Cd} + ^6\text{He} + ^{113}\text{Ru} + \text{n}$ missing ----- ^{119}Pd
14	$^{120}\text{Ag} + ^2\text{H} + ^6\text{He} + ^{114}\text{Ru}$ ----- ↓ ----- ^{122}Cd ^{120}Pd ^8Li
15	$^{119}\text{Pd} + ^{111}\text{Tc} + ^{12}\text{B}^{(3)}$ ----- ^{123}Cd

Table 4.7 Summary on Te/Mo mode (gate w7 in Figure 4.17b).

${}_{Zucd=52}^{Te}_{82}$ ($\beta_2 \sim 0$, "G") / ${}_{Zucd=42}^{Mo}_{66}$ ($\beta_2 \sim 0.58$, "C")	
Point number	Decay scheme
16	${}^{134}Te + {}^{108}Mo$ - binary fission ↓ ${}^{12}C$ from "start" detector
17	${}^{132}Sn + 2p + 2n + {}^{98}Sr^{2+} + {}^8Be$ missing (4He) ----- ${}^{134}Te \quad \quad \quad {}^{108}Mo$
18	${}^{134}Te + {}^{102}Zr + {}^6He$ missing ↓ ↓ ----- ↓ ${}^{108}Mo$ ↓ ${}^{12}C$ from "start" detector
19	${}^{126}In + {}^8Li + {}^{10}Be + {}^{98}Sr$ missing ↓ ↓ ----- ↓ ${}^{134}Te \quad \quad \quad {}^{108}Mo$ ↓ ↓ ${}^{12}C$ from "start" detector
20	${}^{128}Sn + {}^6He + {}^{101}Y + {}^7Li$ missing ----- ${}^{134}Te \quad \quad \quad {}^{108}Mo$

Table 4.8 Summary on Ba/Sr mode (gate w8 in Figure 4.17b).

${}_{Zucd=56}^{Ba}_{88}$ ($\beta_2 \sim 0.65$, "H") / ${}_{38}^{Sr}_{Nucd=60}$ ($\beta_2 \sim 0.38$, "B'")	
Point number	Decay scheme
21	${}^{144}Ba + {}^{88}Se + {}^{10}Be$ missing ↓ ↓ ----- ↓ ${}^{98}Sr$ ↓ ${}^{12}C$ from "start" detector
22	${}^{144}Ba + {}^3H + {}^7Li^{3+} + {}^{88}Se$ ----- ${}^{98}Sr$ ${}^{147}La$
23	${}^{144}Ba + {}^9Be^{3+} + {}^{89}Se$ ----- ${}^{98}Sr$
24	${}^{144}Ba + {}^{88}Se + {}^{10}Be$ missing ↓ ↓ ----- ↓ ${}^{98}Sr$ ↓ ${}^{16}O$ from "start" detector

Table 4.9 Some comments to the tables 4.6 and 4.8.

all 3 fragments were detected in the events below		
Event number	Decay scheme	Comments
13	Molecule after scission ←----- ${}^{122}Cd + {}^6He + {}^{113}Ru$ → ----- ${}^{119}Pd$	There are no shifts in the FF's velocities, thus (see scheme 1 in Table 4.2) 6He was born at the MCP detector due to the decay of the molecule ${}^{122}Cd + {}^6He$ in inelastic scattering on the carbon foil.

14	$ \begin{array}{c} {}^{120}\text{Ag} + {}^2\text{H} + {}^6\text{He} + {}^{114}\text{Ru} \\ \leftarrow \text{-----} \rightarrow \\ \text{-----} \downarrow \text{-----} \\ {}^{122}\text{Cd} \quad {}^{120}\text{Pd} \\ {}^8\text{Li} \rightarrow \end{array} $	<p>There are no shifts in the FF's velocities, thus ${}^8\text{Li}$ was born at the MCP detector. Namely, in the scission point the decaying system consisted of two clusterized nuclei of Pd. After scission the ${}^{120}\text{Ag}$ nucleus and the molecule ${}^8\text{Li}+{}^{114}\text{Ru}$ fly apart. The latter decays due to inelastic interaction with the nucleus of the converting foil. The decay products continue to fly in the same direction.</p>
15	$ \begin{array}{c} {}^{119}\text{Pd} + {}^{111}\text{Te} + {}^{12}\text{B}^{(3)} \\ \text{-----} \\ {}^{123}\text{Cd} \end{array} $	<p>Scheme 3 from Table 4.2 was used in the reconstruction of the decay scheme; thus ${}^{12}\text{B}$ was born at the MCP detector in a two stage process:</p> <ol style="list-style-type: none"> 1. $\leftarrow {}^{119}\text{Pd} - {}^{123}\text{Cd} \rightarrow$ immediately after scission; \downarrow 2. $\leftarrow {}^{12}\text{B} - {}^{111}\text{Te} \rightarrow$ after inelastic scattering of ${}^{123}\text{Cd}$ on the carbon foil of MCP detector.
22	$ \begin{array}{c} {}^{144}\text{Ba} + {}^3\text{H} + {}^7\text{Li}^{(3)} + {}^{88}\text{Se} \\ \text{-----} \\ \text{-----} \quad {}^{98}\text{Sr} \\ {}^{147}\text{La} \end{array} $	<p>Also two stage process presumably took place:</p> <ol style="list-style-type: none"> 1. ${}^{144}\text{Ba} + {}^{98}\text{Sr}$ to be clusterized as ${}^3\text{H} + {}^7\text{Li} + {}^{88}\text{Se}$ in the scission point; ${}^{144}\text{Ba} + {}^3\text{H}$ form molecule to be equal by composition to ${}^{147}\text{La}$, which was really detected. ${}^7\text{Li} + {}^{88}\text{Se}$ form also molecule till the 2-nd stage; 2. inelastic scattering of the latter on the carbon foil: $\leftarrow {}^7\text{Li} - {}^{88}\text{Se} \rightarrow$ (partners fly apart)
23	$ \begin{array}{c} {}^{144}\text{Ba} + {}^9\text{Be}^{(3)} + {}^{89}\text{Se} \\ \text{-----} \\ {}^{98}\text{Sr} \end{array} $	<ol style="list-style-type: none"> 1. $\leftarrow {}^{144}\text{Ba} - {}^{98}\text{Sr} \rightarrow$ after scission; 2. $\leftarrow {}^9\text{Be} - {}^{89}\text{Se} \rightarrow$ after inelastic scattering of ${}^{98}\text{Sr}$ on the carbon foil of the MCP detector

We observe here some distinct “families” of events based on two magic clusters each: Sn/Ru, Cd/Pd, Te/Mo, Ba/Sr. Experimental values of masses of the detected clusters prove to be unshifted or in other words agree with calibration obtained at ${}^{252}\text{Cf}$ (sf) source i.e. without beam. At the same time the FF's masses for the conventional binary fission (evidently prompt) are a little bit shifted, likely due to the influence of the beam on the MCP based detectors. Such difference can be understood if the ternary events analyzed above originate from the decays of isomeric states of Pu isotopes [Pol70], the decays to be delayed by their nature thus appearing predominantly between the bunches.

Analyzing the decay schemes presented in the tables Table 4.5 ÷ Table 4.8 one can notice the following general rule. Each initial cluster clusterises during an elongation of the fissioning system (secondary clusterization) forming lighter magic cluster and at least one light particle. The mechanism seems to be close to this standing behind a well known Ikeda rule [Ike88]. A rupture of prepared in such a way the multi-component system can occur along any of several boundaries (the points of contacts of prefragments in the nuclear chain) of the nuclei involved (see, for instance, events 13, 22 from the Table 4.9). Some light clusters, remained from the secondary clusterization, may be captured into heavier nucleus (see event 14 from the Table 4.9).

After scission, the disintegration of such at least di-nuclear “molecule” can appear to occur via inelastic scattering on the target backing or carbon foil of the “start” detector. It should be stressed that we deal with long lived bounded states bearing in mind a typical time-of-flight (~ 5 ns) between the target and the “start” detector where the decay of a molecule has happened (see Table 4.9).

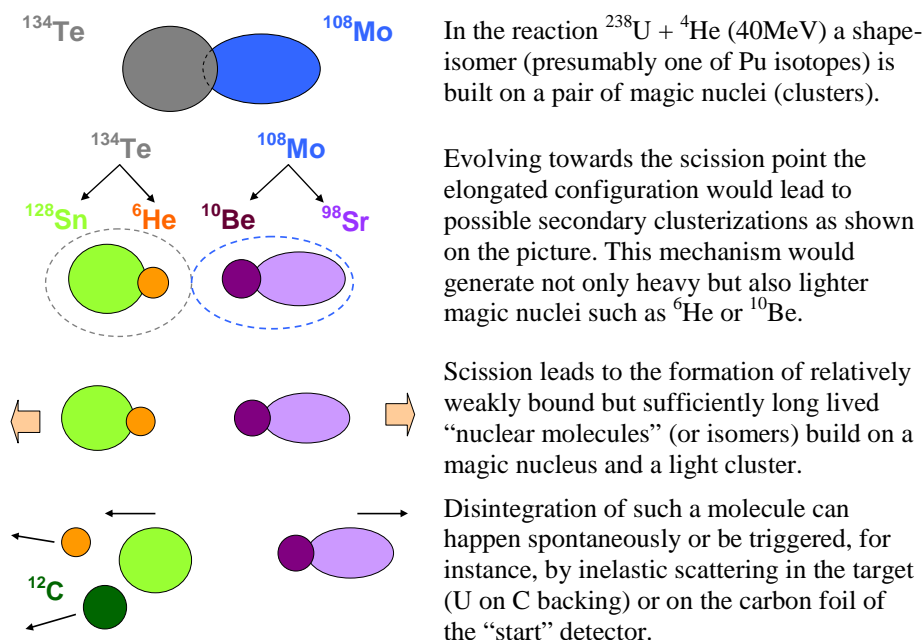
At the moment it must not be ruled out that the ternary decays observed are of the same nature as the known “polar emission” of α -particles and protons [Pia79].

4.6 Conclusions to in-beam experiment

The experiment described in this chapter is the best that we could do with our available equipment, know-how, and software tools for data analysis. A lot of care was taken on each step of this work: from the planning of the measurement to error analysis. For instance, a unified parametric procedure for simultaneous determination of the real fragment energy and M_{te} mass was worked out and several other dedicated computer programs were written.

The main goal of the experiment was to detect and properly identify all charged particles resulting from a possible multi-body decay from the heavy nucleus created in the reaction $^{238}\text{U} + ^4\text{He}$ (40MeV). From the total of 56289 events with multiplicity of 3 or higher, we have identified 35 events that are kinematically consistent with the proposed new hypothesis of a multi-fragmentation of the compound nucleus. Regrettably, with the current setup we were not able to exclude completely the possibility that some of the observed events originate from random coincidences or from other instrumental effects. In addition to a rigorous analysis, the strongest argument we have against a non-physical origin of the observed effect is the consistent grouping of the suspected multi-decay fragments around the magic number corresponding to known nuclear clusters.

Therefore, although the final proof for the existence of multi-partition of fissioning nuclei has eluded us, we would like to propose a possible scenario of such phenomenon that is fully consistent with our data and, to our knowledge, does not contradict the current theoretical understanding of nuclear matter. With those clarifications, the assumed evolution of the fissioning system could look like it is shown below:



Assuming the above scenario is correct, we have identified several distinct “families” of events each based on a pair of magic clusters: Sn/Ru, Cd/Pd, Te/Mo, Ba/Sr. To go much beyond that statement, that is to progress from the self-consistent hypothesis to the experimental certainty, an improved measurement must be performed.

As the starting point of the proposed decay model we require the formation of a shape isomer of Pu. Therefore, it would be highly desirable to incorporate to the next run the beam timing information that would allow measuring the timing of the event with the respect to the cyclotron Radio Frequency signal (RF). The cyclotron beam is not uniform in time but is bunched into short bursts with the width of 1-3 ns depending on the quality of the cyclotron tuning. The beam bursts are followed by a relatively long pause with no beam. In our case the length of the full beam cycle was 67 ns. If the lifetime of such a shape isomers is, as expected, at least several ns, the proposed decay will be visible also in the off-beam periods where the background due to the beam is significantly lower. The improved effect to background ratio for delayed decays will provide the missing proof for the correctness of our assumptions.

The second important improvement would be to increase the granularity of fragment detectors. The arrays of 3 by 3 cm silicon PIN diodes used in our measurement are not optimal for detection of two charged particles traveling on close trajectories. Smaller detectors would significantly enhance the total efficiency of the setup to register multi-fragment events of the type described above. Without these improvements the data collected in the present experiment is not sufficient for formulating and proving the complete physical model of the proposed exotic multi-body decay, but it provided us with sufficient information to propose a new hypothesis for the origin of such phenomenon.

Summary to Part 1

The first part of my thesis is devoted to the search and study of unusual multi-body decays in fission of actinides. The key-points of this research work are listed below.

- All in all five successive and independent experiments were performed and analyzed in two research laboratories, each time using different measurement techniques:
 - Experiment with $^{252}\text{Cf}(\text{sf})$ at the FOBOS setup at the Flerov Laboratory of Nuclear Reactions (JINR, Dubna, Russia).
 - Experiment with $^{252}\text{Cf}(\text{sf})$ with the modified FOBOS setup surrounded by an array of neutron detectors (JINR, Dubna, Russia).
 - The first JYFL experiment with $^{252}\text{Cf}(\text{sf})$ involving one MCP detector and two PIN diodes mounted in the Small Experimental Chamber.
 - The second $^{252}\text{Cf}(\text{sf})$ run at JYFL with 4 MCP detectors and 2 PIN diodes installed inside the Large Scattering Chamber.
 - In-beam experiment at JYFL using the reaction $^{238}\text{U} + ^4\text{He}$ (40MeV). The setup included 38 PIN diodes, 2 MCP detectors, and the longest TOF path possible inside of the LSC.
- One of the main reasons for including different experimental techniques was to minimize the possibility of systematic errors and instrumental artifacts that may be mistaken for real events.
- In parallel to the improvements in the detector setup and electronics, a lot of work went into perfection of the tools for data analysis. This work consisted in the writing of thousands of lines of dedicated computer codes in FORTRAN, C and C++. I have developed and implemented:
 - ✓ An improved procedure for the reconstruction of the M_{te} fragment mass in the case of high energy losses in the entrance window of ionization chamber of FOBOS module.
 - ✓ A unified parametric procedure for simultaneous determination of the M_{te} mass and of the real fragment energy with TOF + PIN detectors.
 - ✓ A time calibration procedure which accounts for the thickness of all absorbers and the corresponding energy losses.
 - ✓ Encoding and sorting of Gigabytes of raw data obtained with different data acquisition systems.
 - ✓ Checking the data stability by monitoring the mean value and the dispersion of all critical parameters in the spectra.
 - ✓ Hardware specific TOF and E calibrations making.
 - ✓ Extraction of the relevant physical parameters from the initial subset of the total data.
 - ✓ Resorting and the final analysis of the full data.
 - ✓ Monte Carlo simulations.

In all our experiments we have searched for almost collinear multi-body decays. After careful analysis following each experiment we were left with a small group of events that may be interpreted as registered products of a multi-fragmentation of the fissioning nuclei. The strongest argument in favor of such a bold interpretation is a

clear and strong correlation of the measured masses associated with these irregular events with the magic numbers expected from the clusterization of the fissioning nucleus. For the moment we are not ready to propose more or less detailed scenarios of the decays revealed.

In our experiments we have observed for the first time four different groups of the collinear cluster multi-body decays. They are realized with different probabilities but invariably linked with magic nuclei as the decay partners.

- The first and the most pronounced group was revealed in the two-dimensional bump lying below the locus of conventional binary fission on the fragment mass-mass distribution (Figure 3.10÷Figure 3.14). The events of this group were observed only in one of the spectrometer arm: the one from the side of the source (target) backing. This group was reproduced all in all in five experiments using both MCP based and gas filled detectors at very close level of yields: $\geq 4 \cdot 10^{-3}$ per binary fission. A strong argument in favor of physical nature (not methodical artifact) of the effect is that it is reproduced using neutron multiplicity gating and shows an increased neutron yield in comparison with binary fission (Figure 2.15). Moreover, the rectangular structures at masses 70 and 80 a.m.u. associated with the bump are also observed only in one spectrometer arm from the side of the source backing.
- The second group manifests itself via a regular and symmetric relative to the spectrometer arms structure (rectangle). This structure is lying on the diagonal of the mass-mass plot of coincident fragments far below the loci of binary fission events (Figure 2.18). The inferior limit of its yield is about 10^{-5} per binary fission. The registered fragments of this group meet momentum conservation law. The group is characterized by a little bit higher neutron multiplicity in comparison with conventional binary fission. This group was reproduced in three different experiments using gas filled detectors including recent experiment at the IBR-2 reactor (JINR, Dubna, Russia) dedicated to the reaction $^{235}\text{U}(n,f)$ [Kam07].
- The third group produces regular structures which look like tilted $M_1+M_2=\text{const}$ lines or $M=\text{const}$ lines (Figure 3.8 and Figure 3.9) in the fragment mass-mass plot. Both types of lines are linked with magic fragments actually detected or “missed”. The yield of these peculiar events is $\geq 10^{-4}$ per binary fission. It should be stressed the high reliability of the $M_1+M_2=\text{const}$ line structures against the hypothesis of their random nature: the masses involved were measured independently in two spectrometer arms but demonstrate strong correlation thus having clear physical sense.
- The fourth group was observed in the reaction $^{238}\text{U}+^4\text{He}$ (40MeV). Thanks to the high granularity of the detectors three partners of the decay were detected in this case. At least one of them was the magic nucleus; another one was the light ion. Analyzing the data we came to the conclusion that the initial nuclear molecule originated from fission and consisted in the magic cluster and the light ion is disintegrated in the inelastic interaction with the foil of the start detector (section 4.6). Experimental yield of the group is $\geq 10^{-6}$ per binary fission. Seemingly, this group corresponds to known polar emission of light particles.

The wide range of experimentally observed yields of collinear multi-body decays searched needs additional comment. We deal likely with the whole family of the multi-body decays, which are lying in the range from “polar emission” up to “true ternary fission” in known terms. All observed decay groups demonstrate almost collinear kinematics of the decay products but different yields. It is absolutely expected, reminding, for instance, the wide range of probabilities of emitting different light ions in conventional ternary fission.

The next comment concerns the repeatability of the observed structures. There are some gaps in this point. For instance, in the experiment dedicated to the $^{238}\text{U}+^4\text{He}$ reaction we observed only blurry and weak trace of group number one. The other example is that we have failed to reproduce the second group in the experiments where MCP based “start” detectors were used. For the moment we have not adequate scenario of the process (or processes) under study; that is why changes in experimental setup from experiment to experiment (geometry, thresholds of electronics, logic of data acquisition system) can be meaningful but uncontrolled. To get further in the understanding of the physical mechanism of the collinear cluster multi-body decay, more experiments and better theoretical understanding are needed.

In our experiment dedicated to the reaction $^{238}\text{U}+^4\text{He}$ (40MeV) an additional motivation for further study of collinear multi-body decays was found. One of the possible explanations of the origin for the ternary events observed is the hypothesis that we deal with multi-body decays of some shape-isomers of Pu isotopes. To be able to prove or refute the hypothesis about shape-isomers we need to perform a new, improved measurement. In the next experiment we could take advantage of the fact that the isomeric states of Pu isotopes have the half-lives permitting their detection between bunches of beam that is in conditions with substantially reduced background.

Conclusions to Part 1

Conclusions below sum up the results of the first part of the thesis:

- The five experiments described have revealed four persistent groups of events manifested themselves via different structures in fragment mass-mass distributions.
- Events in these groups can not be explained neither by experimental artifacts nor by traditional binary-like fission.
- Measured masses of fission fragments in registered events for all four groups have invariable link with magic numbers.
- These groups have reasonable interpretation as indication of the new effect of collinear cluster multi-body decays.
- The experimentally determined probabilities for observed groups lie in the range of $10^{-6} \div 4 \cdot 10^{-3}$ per binary fission depending on the group.
- Due to crucial changes in the experimental setups from experiment to experiment some real events were cut off by experimental conditions. Thus some structures associated with collinear cluster multi-body decays that were obtained in one experiment failed to be revealed in the other experiment.
- Additional efforts in both experiment and theory are needed for better understanding of the physical mechanism of collinear cluster multi-body decays.

The aim of the first part of my thesis was to study collinear multi-body decays of low excited nuclear systems with creation of massive third particle when at least one of the fragments is the magic nucleus. This new type of decays was explored in the thesis for the first time. An indication of existence of the effect via definite structures in mass-mass distributions of fission fragments was obtained as well for the first time. Nevertheless, formulation of the complete physical model of collinear cluster multi-body decays requires additional theoretical studies and carrying out new improved experiments.

Part 2

Energy distribution of ternary alpha particles

5 Measurement of the full energy distribution of ternary α -particles in $^{252}\text{Cf}(\text{sf})$

Alpha particles are the most abundant particles in ternary fission. The energy distribution of these particles from $^{252}\text{Cf}(\text{sf})$, the most often studied spontaneous fissioning nucleus, has been investigated by several groups. From the survey of literature it is clearly seen that this distribution has a deviation from the Gaussian shape at low-energy side. However, the experimental data are often truncated by the detection levels. We tried to realize dedicated experimental conditions to study the full energy distribution and especially to measure the low part of energy spectra for ternary α -particles from $^{252}\text{Cf}(\text{sf})$.

A new, significantly improved experiment has been performed at JYFL. We applied time-of-flight and coincidence techniques to fully separate α -particles from the background and from the neighbouring isotopes. For measuring the energy of ternary particles we used an array of silicon detectors. No protection foils were in front of the semiconductor detectors. Due to the placement of ternary particle detectors at right angle with respect to fission fragment direction the experimental setup register mainly so-called equatorial particles. Therefore, to be able to compare our results with data from other experiments we have applied a small correction (with the aid of the GEANT4 code from CERN) to the energy dependence of the angular distribution of ternary α -particles with respect to fission fragments. With our new experimental approach the energy distribution of α -particles from ternary decay of ^{252}Cf was, for the first time, measured down to 1 MeV. In the obtained spectrum of ^4He the excess in the yield as compared to a Gaussian shape is observed at energies below 9 MeV. This observation agrees with the recent measurement by Tishchenko [Tis02]. However, the earlier data published by Loveland [Lov74] exceed the low-energy yield of ternary α -particles by up to a factor of two. The energy spectrum of ^6He was also analysed, in spite of weak statistics, and the yield ratio $^6\text{He}/^4\text{He}$ was deduced.

5.1 Motivation

The ternary fission process was discovered in the '40s of the last century. Since that time there have been numerous experiments devoted to measurement of the energy distribution of the ternary particles, especially ternary α -particles. These particles have 16 MeV mean energy and exhaust $\approx 90\%$ of the total ternary fission yield [Wag91, Mut96 and Gön05]. The shape of the α -spectrum is compatible with a Gaussian distribution but there is some excess in yield at low energy [Wag04]. This low-energy tailing is significant and results in a deviation from Gaussian shape of about 6%. The ternary α -particles are assumed to be born in the last stage of the process near or right at scission during neck rupture [Gön05]. Thus they may provide important info about both the emission mechanism of ternary particles and the scission stage of the fission process. However, the decay of unstable ternary particles such as ^5He and ^7He ([Kop02]) may also contribute to low-energy part of ^4He and ^6He spectra respectively in sequential processes. It will lead to masking the true ternary particle emission. It is also common practice to determine the emission probabilities of the other ternary particles relative to that of ^4He . Without any doubts a good

knowledge of the full ternary α -particle energy distribution based on precise experimental data is very important. For instance, it is common practice to determine the emission probabilities of the other ternary particles relative to that of ^4He .

A survey of publications leads to the conclusion that most experiments performed up to now are not optimized for the detection of low energy α 's. Usually experimentalists used ΔE -E detector telescopes or ΔE -E detectors coupled to electromagnetic spectrometers for particles discrimination and for measuring the energy of α -particles. Thus in these experiments there were low-energy thresholds for α 's. Very often in order to stop 500 times more frequent fission fragments and the roughly 10 000 times more frequent 6.1 MeV α -particles from the radioactive decay protection foils are placed in front of the energy detectors. They increase the lower detection limit to 8 – 9 MeV. Moreover, uncertainty in absorber thicknesses and related energy losses give some uncertainty in the energy assignment for events close to the threshold. The mean value for the energy spectrum is 16 MeV and thus the 8 – 9 MeV threshold cuts away almost one fourth of the full distribution and, of course, the interesting low-energy part.

From the literature study only two articles [Lov74 and Tis02], which present results in the energy spectrum for the region < 9 MeV (see Figure 5.1), were found. Both experiments had no protection foils on the source or detectors, but in [Lov74] the ΔE -E telescope was used for particle separation. Thus the only measurement with unshielded energy detectors is the recent work by Tishchenko [Tis02]. The 4π Berlin Silicon Ball (BSiB) with 160 detectors was facing a weak ^{252}Cf sample (30 fissions/s), and particle separation was performed by simultaneous time-of-flight registration of ternary particles and fission fragments. The author reported the detection threshold of 2.0–2.5 MeV. Unfortunately, the short flight paths inside the ball (10 cm) provided weak separation of α -particles, tritons and so on and did not allow the separation of ^6He from ^4He .

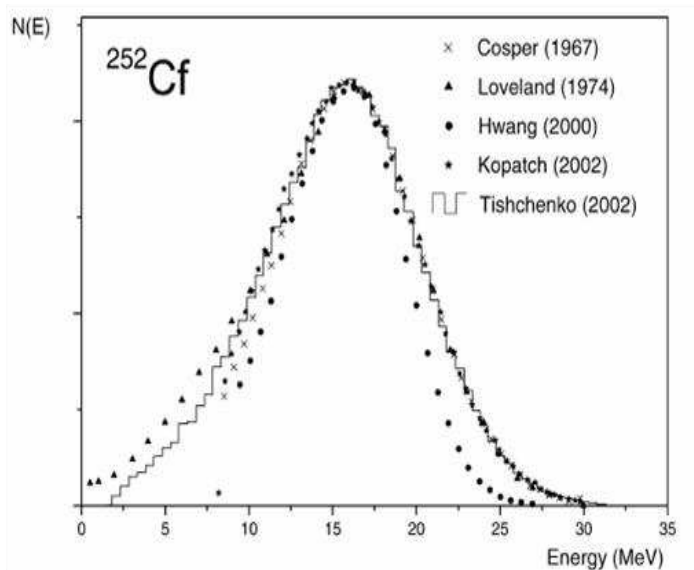


Figure 5.1 Comparison of the (renormalized) energy distributions for the $^{252}\text{Cf}(\text{sf})$ ternary α 's reported in literature. Figure from [Wag04].

In Figure 5.1 the main results of energy distribution of ternary α 's studies are presented. Here the old data of Loveland [Lov74] and Cospér [Cos67] are compared with recent results of Hwang [Hwa00], Kopatch [Kop02] and Tishchenko [Tis02]. All data except the data of Hwang [Hwa00] are in good agreement. For the region < 9 MeV the deviation from a Gaussian distribution observed by Tishchenko [Tis02] is less pronounced than the one reported by Loveland [Lov74]. The data of Hwang [Hwa00] are completely discrepant. According to comments given by Wagemans in [Wag04] it becomes clear that the method used by Hwang for the energy calibration of a detector covered with mylar is wrong, since it does not take into account the non-linearity of energy loss with increasing energy of the particle. Also the thickness of the E detector used is at the limit for a correct detection of the highest energy particles.

One of the main characteristic of the ternary fission process observed for the first time with nuclear emulsion was the almost perpendicular emission of ternary particles with respect to the fission axis (the so-called *equatorial* emission). Piasecki in [Pia70] reported about the existence of the so-called *polar* emission, when ternary charged particles are moving almost along the fission axis with a much higher energy than the equatorial ones. A detailed information about the dependence of the emission angle as function of energy for ternary α -particles from ^{252}Cf is given in Figure 5.2. The data were obtained by Heeg et al. with the gas chamber system DIOGENES [Hee90].

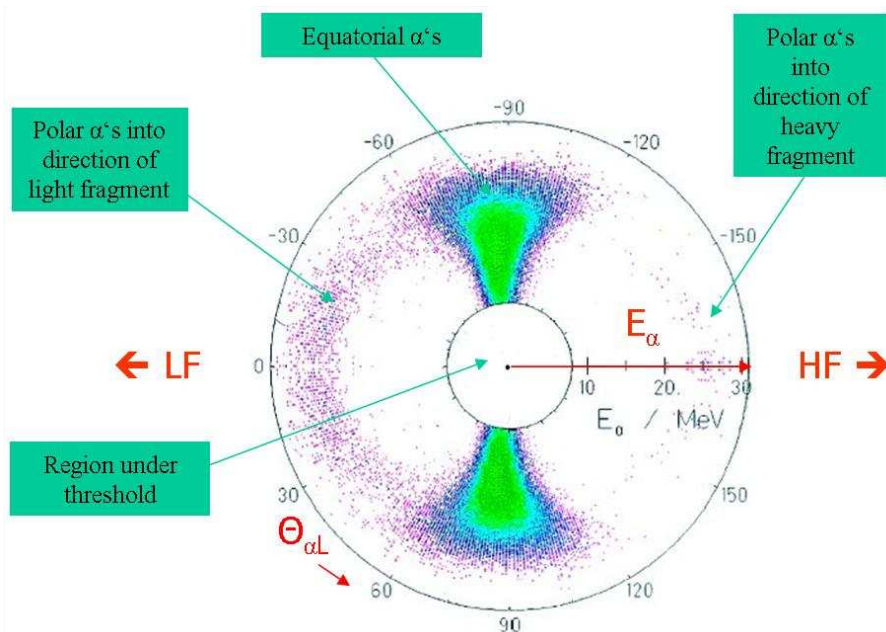


Figure 5.2 Scatter plot of ternary α -particle emission from $^{252}\text{Cf}(sf)$. Data from [Hee90].

In the polar diagram each point corresponds to an α -particle event. The distance of the point from the centre characterizes the kinetic energy and the polar angle Θ indicates the angle between the α -particle and the lighter of the two fragments. The lighter fragment flies in the figure at the polar angle $\Theta = 0^\circ$ to the left and the heavy fragment to the right ($\Theta = 180^\circ$). Evidently the α -particles have a broad energy distribution with energies up to 30 MeV. As to the angular distributions, the majority

of α -particles come off roughly at right angles to the fission fragments. It is obvious from Figure 5.2 that the angular distribution is not perfectly symmetric relative to the polar angle 90° . Instead, the distribution is shifted towards polar angles smaller than 90° , i.e. in direction of the lighter fragment due to the asymmetry of mass and charge split.

Besides the dominant equatorial α -particles in Figure 5.2 it is seen a small fraction of predominantly higher energy polar particles. At intermediate angles particles of polar origin mix with the much more abundant equatorial ones. This fact leads to difficulty in determination of polar-to-equatorial ratio, but without doubt the emission probability of the polar α -particles is very small. Alpha particles can be considered as purely polar in the angle intervals from 0° to about 25° and from about 155° to 180° , as it was chosen by the group of E. Piasecki in [Now82] to separate the polar and equatorial regimes. According to this agreement the ratio of polar-to-equatorial for ^{252}Cf was determined to be 0.53% and 0.79% in articles [Now82] and [Hee88], respectively. Other important observation made from Figure 5.2 is that the polar α -particles are preferentially emitted from the light fragment. As it will be shown in the next section it is quite possible that for ternary particles a minor part of the yield at higher energy may be cut out by a too narrow angular window covered by our experimental setup. The resulting slightly weaker slope at high energy will then be mirrored to the low-energy side in case the analysis is made in terms of Gaussian fits. So we need to correct the spectra for the unregistered polar α 's and also for the equatorial ones in the wings of the energy distribution at high energy.

5.2 Experimental details

A sketch of experimental setup with detectors actually included in data analysis is shown in Figure 5.3.

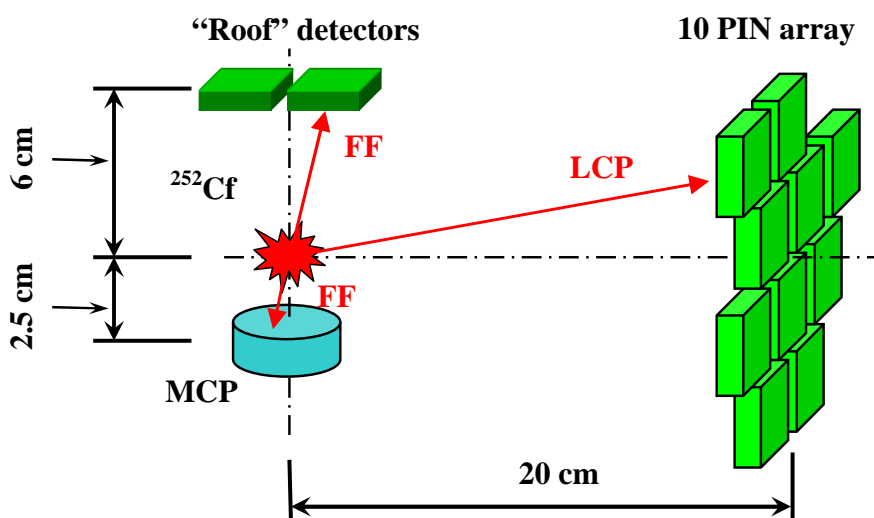


Figure 5.3 A sketch of experimental setup for measuring ternary α -particle energy spectrum from ^{252}Cf fission.

The ^{252}Cf sample, produced at the Radium Institute at St. Petersburg, had an activity of about 500 fissions/s. It was prepared by self-transfer method of ^{252}Cf from a mother source, purified by ion exchange from any stable and long-lived radioactive impurities. The transfer was limited to a 0.1 cm^2 area on the support backing. The backing of the source consisted of the $22.2\pm 3.4\text{ }\mu\text{g/cm}^2$ aluminium oxide (Al_2O_3) film with $10\text{ }\mu\text{g/cm}^2$ layer of gold evaporated. Typical energy loss of fission fragments emerging perpendicularly through the backing material was $\leq 1.5\text{ MeV}$. The fragment energy loss in the deposit layer, i.e. when emitted from the front surface of the source, was estimated to be less than 60 keV. The californium deposit (Cf_2O_3) is estimated to be $3.5\text{ }\mu\text{g/cm}^2$ thick.

For measuring ternary particles an array of 10 silicon PIN diodes ($380\text{ }\mu\text{m}$ thickness, and $30\times 30\text{ mm}^2$ area) was placed at a distance of $\approx 20\text{ cm}$ from the source. With dedicated preamplifiers and low-noise timing filter amplifiers in the timing channels the energy threshold could safely be reduced to $\approx 0.5\text{ MeV}$. This is the lowest cut-off value ever achieved in experiment. As the start signals, fission fragments emitted from the source were registered in a 30 mm diameter MCP detector placed at right angle to the particle detectors, at 2.5 cm distance to the source. Discrimination of fission fragment start signals from the 30 times more frequent 6 MeV alphas was achieved by coincident registration of the complementary fragments in 2 silicon PIN diodes of $20\times 20\text{ mm}^2$ area ("roof" detectors) mounted at a distance of 6 cm to the sample, opposite to the MCP. It has to be noted that having the particle detectors at right angles to the direction of emission of the fission fragments does bias the experiment to detect equatorial particles. The detector geometry covers an angular range between about 75° to 109° (FWHM of 33° around 92°) for the mutual angle Θ_{aL} between the ternary particle and the light-mass group of fission fragments thus even not measuring all equatorial particles especially at the higher energies (see below).

The target holder with the ^{252}Cf source was tilted at 45° to a plane of the PIN array. The backing side of the ^{252}Cf sample was faced to the MCP detector, so the detectors in the PIN array were viewing to the front surface of the source. The experiment was setup in the large scattering chamber LSC (Figure 5.4) at the Jyväskylä Accelerator Laboratory, Finland, and data were collected over a period of about 6 weeks.

The experimental setup had 10 "roof" detectors installed, but in data analysis only the 2 central ones were used, the rest were not optimized for measurements. The outermost 2 pairs had no correlation with the MCP detector and almost did not give any counts. The 4 detectors next to central ones also do not improve statistics significantly, because they provided only 20% of total counts of all roof detectors due to the reason that these detectors had only partial correlation with MCP. The ternary particle side detector triplets (4 boxes with 3 coupled detectors each inside) shown in Figure 5.4 close to PIN plate had not been included in the data analysis as well. Some of them had bad characteristics or had drastically changed in characteristics during the experiment. Moreover, we could not align all triplets properly. As a consequence we had a noticeably wider time distribution for side detectors in comparison with detectors from PIN plate due to difference in time of flight lengths to each detector in triplet. Thus to provide good results we decided to exclude data obtained with the side detectors from the total data array. Finally, the scheme of the experimental setup with detectors in actual use is shown in Figure 5.3.

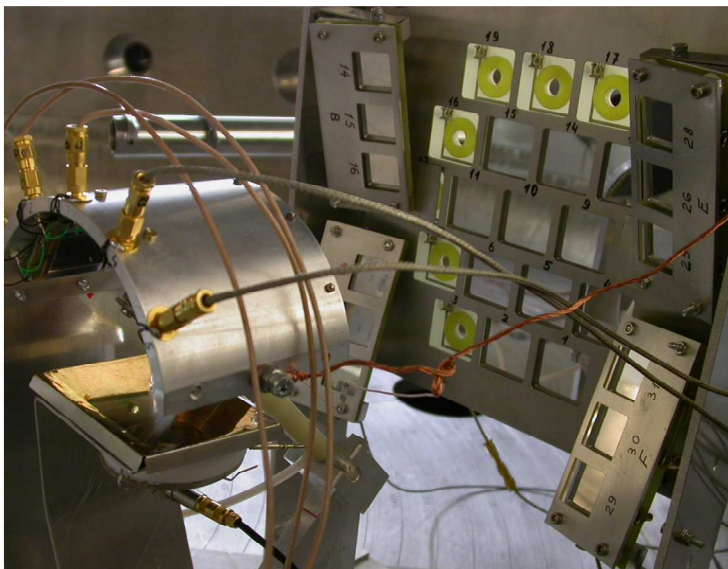


Figure 5.4 View of experimental setup installed inside of the large scattering chamber. Data from the sideward located detectors triplets have not been included in the analysis.

Due to the large total area of the silicon detectors the dose per unit area was rather low, so that radiation damage was not essential. Radiation damage in the roof detectors was more serious, but had no direct influence on the energy and time registration for the ternary particles. The edges of all detectors were shielded by proper diaphragms for minimizing scattering of fission fragments with an energy degradation to promote background pulses in the energy region of the ternary particles. Energy calibration of the silicon detectors was performed with alpha lines from a spectroscopic thin ^{226}Ra source and a BNC PB5 precision pulser.

5.3 Simulation of detector efficiency

Simulation calculations of the angular dependent coincidence efficiency of the present detector geometry were done with GEANT4 code [Ago03]. GEANT4 is a powerful software toolkit for the simulation of the passage of particles through matter, developed at CERN in the ninetieths of last century. It includes a complete range of functionality including tracking, geometry, physics models and hits. In our simulations of detector efficiency we used only a part of the GEANT4 resources mentioned above, mainly, geometry description of experimental setup.

The basic building blocks for setting up a GEANT4 simulation are:

- definition of the detector geometry and specification of materials in detectors;
- description of the primary particle and their initial states;
- definition of the physics processes and their particles to be used for simulations.

To be able to analyze the dynamics of simulation the next procedures should be defined:

- generation of primary particles

- tracking of primary particles
- extraction of simulation data during tracking

The detector geometry for the simulation of the angular dependent coincidence efficiency according to the real experimental setup consists of a MCP detector, two “roof” PIN detectors and an array of 10 PIN diodes. All distances and dimensions were set to those given in Section 5.2. As an approximation in simulations the ^{252}Cf source was described by point source, the silicon detectors were represented by thin squares and the MCP detector as a cylinder properly oriented in space. For each detector it was defined a virtual “*sensitive detector*” for the purpose of getting out its response, so if there was a passage of particle through the detector volume we have a signal “hit” and take all the information about detector and particle for further analysis.

In our simulation we need to obtain just the geometrical efficiency of the experimental setup to register α -particles in coincidence with fission fragments. We do not need to describe any interactions of any particles with the material of detectors. Obviously, we should count the number of hits into detectors. For such purposes there is a special particle called “*geantino*”. It is the virtual particle for simulation which does not interact with materials and undertake transportation processes only. Both fission fragments and α -particle were approximated by *geantino*-particle.

During simulations the direction of flight for light fragment (LF) in space was generated based on isotropic distribution. The angle of emission for α -particle $\Theta_{\alpha\text{LF}}$ with respect to the direction of LF was randomly generated in the range $0\text{--}180^\circ$. The azimuthal angle for α was also generated randomly in $0\text{--}360^\circ$. In ternary fission due to momentum conservation law the strict collinearity of two fission fragments is lost, therefore, the opening angle between LF and heavy fragment (HF) is more than 180° , and in our simulations it was set to 184° . Flight directions for all three particles are started in one point, where the point source of ^{252}Cf was set, and are laid in one plane.

We used also the visualization system in our simulations for setting up the correct geometry of the experimental setup, for seeing trajectories of particles and their interactions with detectors (hits) and for supervising and having flexible control in simulations. Figure 5.5 shows examples of two generated events drawn by visualization system.

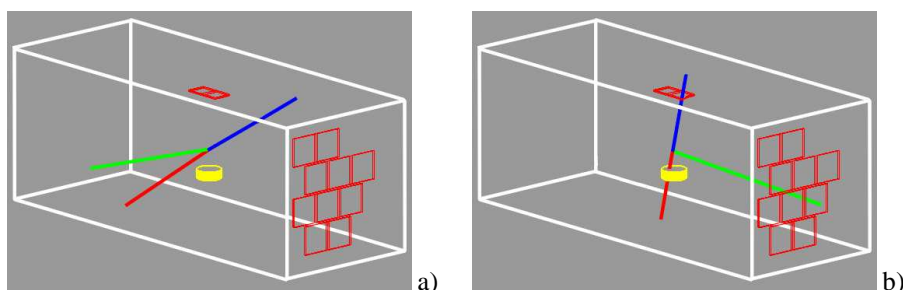


Figure 5.5 View of two events in simulation: a) the event is not registered in the experimental setup; b) registered event: LF hits the roof detector, HF gives a signal in MCP and the α -particle hits PIN detector number 5. See text for details.

The traces of heavy fragment, light fragment and α -particle in Figure 5.5 are marked by red, blue and green colors respectively. The big white box represents the so called “world volume”, which includes the experimental setup and where simulations take place. Outside the “world volume” all simulations are stopped. For

simplicity and visualization purposes the “world volume” was chosen to be of rectangular shape, with the source of particles emission being placed in its geometrical center, and the array of PIN detectors being placed parallel to the shortest side of the box. Figure 5.5a shows an event type that will not be registered in the experimental setup: all three particles did not hit any detector. The right-hand site panel of Figure 5.5 presents an event in which the LF hits one of the roof detectors, the HF produces a signal in the MCP and the α -particle touches the PIN detector number 5 in the array. Such event should be registered in our experimental setup and we take it for further analysis of efficiency registration for detector geometry. In general, a trigger for writing out the event from the simulation program consists of three coincidences: the α -particle touches any detector from the PIN array and, in the same time, the LF is registered in the MCP and the HF hits one of the roof detectors or vice versa for LF and HF.

Figure 5.6 presents results of simulations. The histogram gives the probability of event registration in the experimental setup as function of the emission angle $\Theta_{\alpha\text{L}}$ for the α -particle; the binning is 3 degrees. The histogram is normalized to unity at the peak maximum.

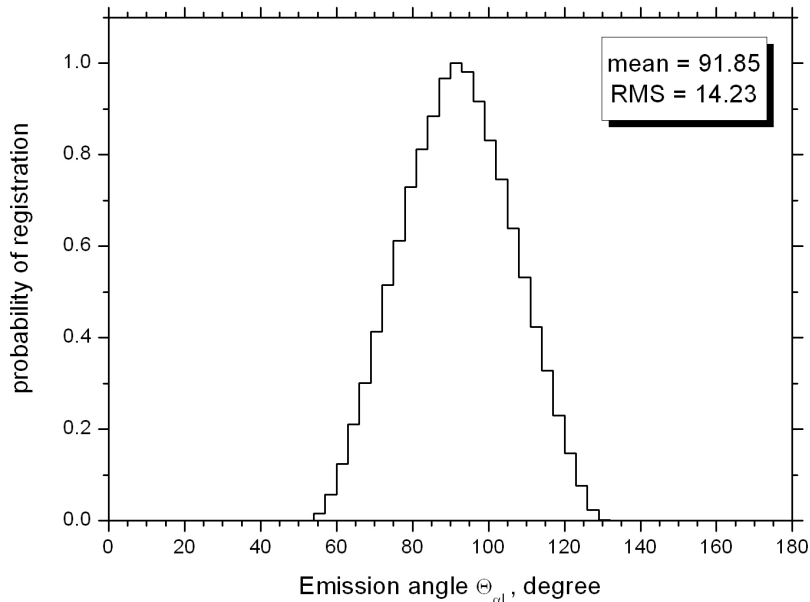


Figure 5.6 The efficiency of event registration in the experimental setup as function of the emission angle $\Theta_{\alpha\text{L}}$ for the α -particle. The binning is 3 degrees. The histogram is normalized to maximum counts in peak.

As it is seen from the histogram the detector geometry can register α -particles with the minimal mutual angle $\Theta_{\alpha\text{L}}$ between the ternary particle and the light fission fragment of about 55° and with the maxim angle of about 130° . The distribution has a full width at half maximum of 33° around 91.85° . The small shift of the mean value for the emission angle $\Theta_{\alpha\text{L}}$ to a range higher than 90° is due to coexistence of the geometry of detectors placement and the fact that the opening angle between the light and heavy fragments is more then 180° (in our simulations the opening angle was set to 184°). It has to be noted that we had the ternary particle detectors placed at right angle to the direction of emission of the fission fragments. Registration of ternary

particles in coincidence with both fission fragments results in the detection of mainly equatorial α -particles and in the loss of polar ones.

Applying the dependence of the event registration efficiency in the experimental setup as function of emission angle $\Theta_{\alpha L}$ for α -particles (Figure 5.6) to data from the work of P. Heeg (Figure 5.3 at page 66 in [Hee90]) we obtained the registration efficiency in our setup versus the energy of ternary α -particles (Figure 5.7). Corrections to the measured spectrum were made both for the wider than detected angular interval of equatorial particles ($50^\circ \leq \Theta_{\alpha L} \leq 130^\circ$) and for the full range of angles measured in experiments without fragment coincidences [Wag04, Tis02]. The emission angle was found to affect mainly the width of the energy distribution, by up to 1 MeV.

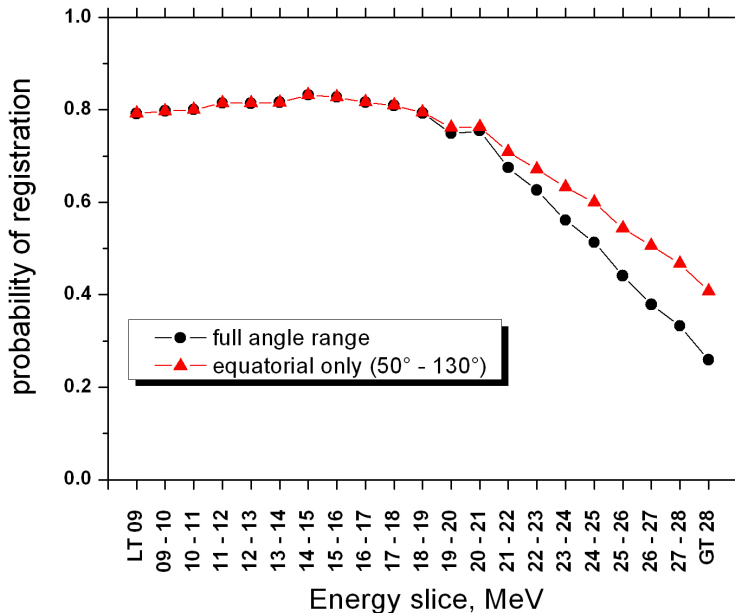


Figure 5.7 Registration efficiency for energy of ternary α -particles.

Later on this dependence was applied in a small correction for the energy dependence of the angular distribution of ternary α -particles with respect to fission fragments. Heeg's data are energy slices of 1 MeV from the polar diagram in Figure 5.2 and cover the energy range from approximately 8 MeV to about 30 MeV. Data below 9 MeV and above 28 MeV were grouped into bins "less then 9 MeV" (LT 09) and "greater then 28" (GT 28) respectively. With our new experimental approach the energy distribution of ternary α -particles was measured down to 1 MeV. In the measured spectrum at energies below 9 MeV the correction was done according to the assumption that the dependence in Figure 5.7 in the lower range (below 9 MeV) has the same behavior as in the region 9 – 16 MeV, i.e. a linear extrapolation holds. The Figure 5.7 indicates that we definitively have a constraint on the $\Theta_{\alpha L}$ angle in our measurement. This constraint will change the energy distribution a bit, mainly at the high energy side as it is shown in Figure 5.8, where the comparison of measured and corrected energy spectra for ^4He is presented. The behaviour of the ^6He spectrum to the same corrections is similar.

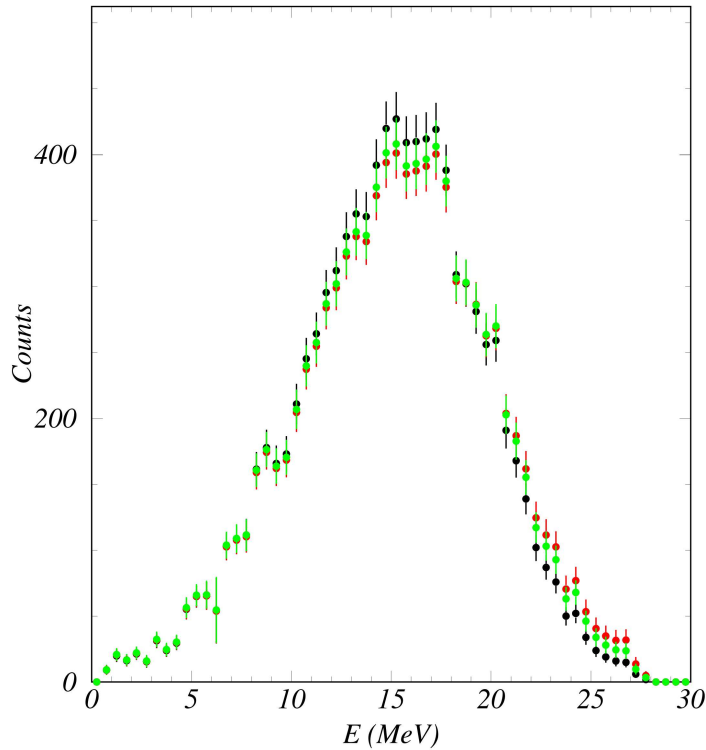


Figure 5.8 Comparison of measured and corrected energy spectra for ^4He . Black dots are measured experimental data, red dots correspond to data corrected for the full angle range and green dots represent data corrected only for angular interval of equatorial particles. Spectra for all three variants are normalized to the same number of counts.

5.4 Data analysis

As it was mentioned above our data analysis has been limited to the spectra measured with 10 silicon detectors from PIN array. Also, only events in coincidence with fission fragments registered in both, the MCP and the central roof detectors, have been analyzed.

Stability of the data was checked for each detector based on the stability of the position of the 6.1 MeV alpha line from ^{252}Cf radioactive decay. Particles from this decay are 10^4 times more frequent than ternary particles and could be used as a natural reference signal in the procedure for stability checks. We performed a gauss fit to raw energy spectrum for each 1000 registered events. The position of the center of the peak should be stable for the whole data array. In addition we determined the maximum of the same peak. Typical graphs for stability checks of the energy channel of one of detectors are presented in Figure 5.9. As it can be seen the data are stable in a range of 1-2 channels; this corresponds to ≈ 38 -77 keV. The situation is similar for all other detectors and it was concluded that all our data are stable and do not need any corrections.

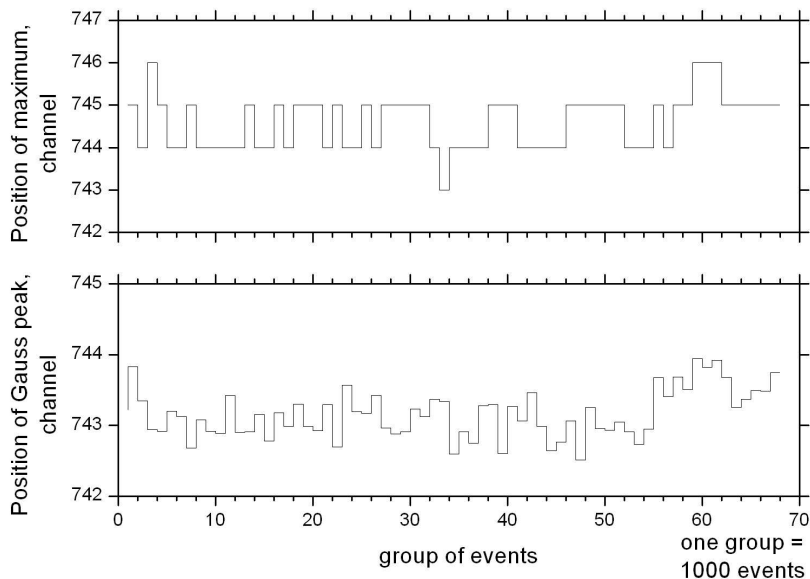


Figure 5.9 Typical plots for stability checks of the data.

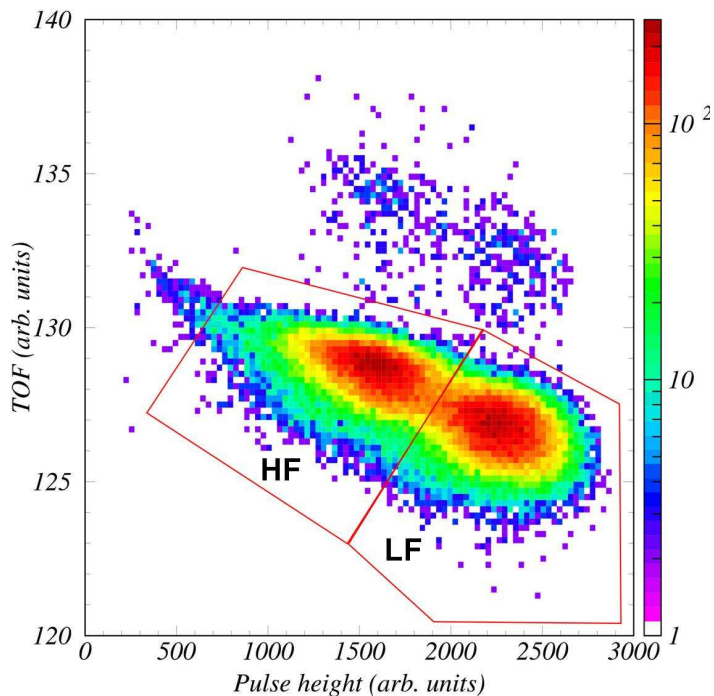


Figure 5.10 Fragment flight time difference $\Delta\text{TOF}_{\text{ff}}$ between roof detector and MCP versus fragment energy E_{ff} registered in the roof detector (arbitrary units).

Figure 5.10 shows the measured difference in fragment flight times $\Delta\text{TOF}_{\text{ff}}$ to the roof detector and MCP respectively, versus the fission fragment energy E_{ff} registered in the roof detector. The window “LF” designates events in which the light fragment hits one of the roof detectors and the heavy fragment is registered in MCP.

Events in the window “HF” correspond to the opposite situation. A linear interpolation of the gravity centers of spectra in vertical slices was done for events in windows “LF” and “HF” and then this information was used to correct the measured TOF spectra of ternary particles for the difference in the flight time between heavy and light fission fragment masses from the source to the MCP.

Figure 5.11 shows a scatter plot of TOF versus E of ternary particles summed over the 10 silicon PIN diodes. The intense bunch in the centre corresponds to ternary alphas, and the weaker bunches of the neighboring isotopes ^3H and ^6He , below and above the α -particle distribution, are nicely separated from it. The three bunches in the upper left corner are identified as ^{27}Al , ^{16}O and ^{12}C scattered off from the source backing or the roof detector surface by fission fragments. Between these groups and the ternary ^6He a few events from heavier ternary particles, mainly ^8He and ^{10}Be , are visible. It has to be noted that the TOF-E pattern in Figure 5.11 is particularly clean from fragment background, which is expected to be true also for the low-energy region of our major interest, below 9 MeV. The vertical line at 6.1 MeV indicates random coincidences with the α -particles from ^{252}Cf radioactive decay which are 10^4 times more frequent and of low enough probability to be safely subtracted in the time window of the ternary α -particle distribution.

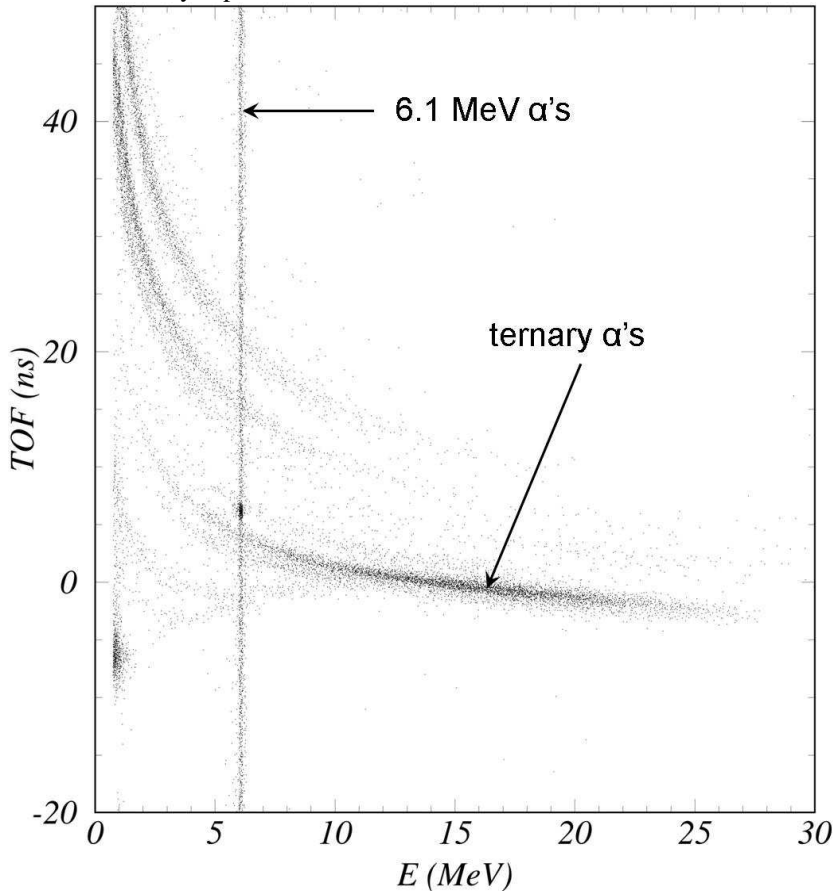


Figure 5.11 Scatter plot TOF vs. E of ternary particles in $^{252}\text{Cf}(\text{sf})$. Time is in ns with respect to the flight time of 16 MeV α -particles; energy E is in MeV.

It is interesting to see also a small 6.1 MeV peak about 2 ns above the pattern for the ternary α 's which is attributed to start signals from x-rays or conversion electrons in the MCP when the ^{252}Cf radioactive decay proceeds through the excited state of ^{248}Cm . This peak falls accidentally into the TOF-E pattern of ternary ^6He ruling out an analysis of the ^6He spectrum in a small energy gap around 6 MeV. At the high-energy side the ternary α -particles spectrum is cut off at 27.5 MeV due to the limited detector thickness of 380 μm . Since the cut-off takes place at a yield level of $\approx 3\%$ relative to the maximum yield at 16 MeV there is only a minor influence of it on the high-energy half of the spectrum. For ternary ^3H , the TOF-E pattern reaches its highest energy value already at 11.5 MeV due to the detector thickness; it bends back at higher ^3H energies and interferes with the TOF-E pattern for protons.

In order to extract the energy distributions of ternary ^4He and ^6He particles from the measured TOF versus E patterns the calculated time-of-flight curves for ^1H , ^3H , ^4He and ^6He were fitted to the data, as it is illustrated in Figure 5.12a. The TOF versus E data were converted into a mass A versus E relation. Finally, the clean separation of ternary α particles from tritons below 11.5 MeV was undertaken with evaluating the energy gated mass spectra from the data shown in Figure 5.12b, and by determining the $^3\text{H}/\alpha$ ratios, for narrow energy intervals of 0.5 MeV, with the aid of Gaussian fits.

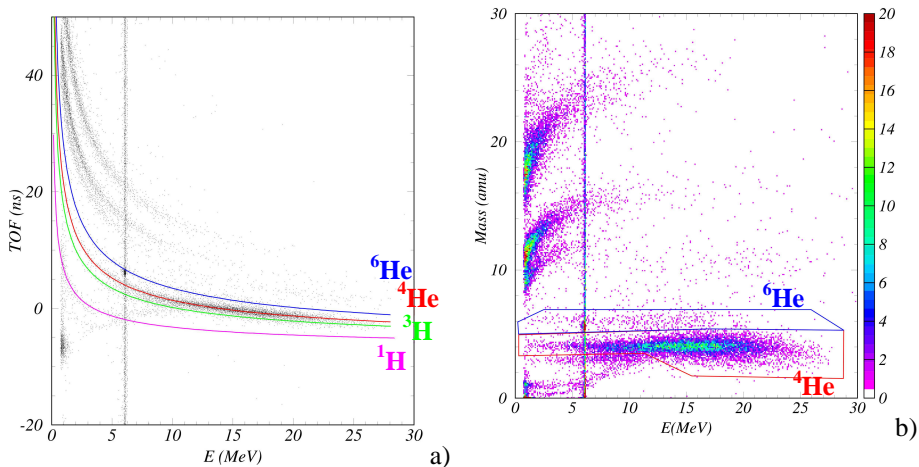


Figure 5.12 Extraction of energy distributions of ternary ^4He and ^6He particles from measured TOF versus E matrix. a) Fit of calculated time-of-flight curves for ^1H , ^3H , ^4He and ^6He to the data. b) Conversion of TOF vs E data into Mass vs. E. Solid contours are the analysis windows chosen for ^4He and ^6He .

5.5 Results of the experiment

Figure 5.13a is our experimental energy distribution of equatorial ternary α -particles, which covers the wide energy range from 1 to 27.5 MeV. Above about 9 MeV our data are in fair agreement with most of the previously measured spectra [Wag04, Kop02, Tis02, Lov74].

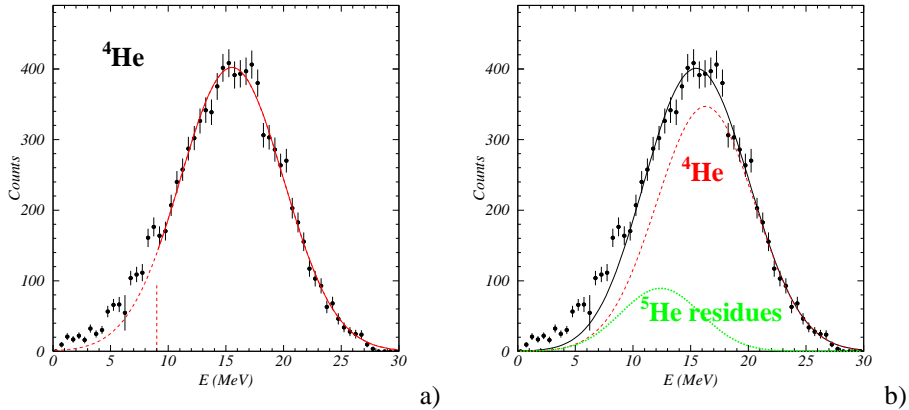


Figure 5.13 a) Energy distribution of equatorial ternary α -particles from $^{252}\text{Cf}(\text{sf})$. The solid line represents the Gaussian curve fitted to the data above 9 MeV. b) Two-Gaussian curves fitted to the data above 9 MeV, taking residual α -particles from ^3He decay into account, according to the results of Kopatch [Kop02].

The total number of events in the spectrum of ^4He amounts to 10654 events collected over 6 weeks period. This corresponds to a count rate of ≈ 250 events per day. Figure 5.13b shows two Gaussian curves which result from a fit to the present data above 9 MeV and take into account besides true ternary α -particles (the dominant Gaussian) also about 17% contribution of residual α -particles from the decay of ternary ^3He according to recent measurements by Kopatch [Kop02]. It is obvious from the data presented in Figure 5.13, that the ternary α spectrum shows more low-energy α -particles than would be predicted by the Gaussian shapes. Apparently, the spectral shape measured previously at energies $E > 9$ MeV [Wag04, Kop02] can not be extrapolated meaningfully to low energies. Of particular interest is the fact that there are ternary α -particles emitted from ^{252}Cf fission with energies as low as 1 MeV, with the energy distributions indicating a flat shelf or shoulder at energies below 5 MeV. We would like to note that in the present experiment there is not any material between the ^{252}Cf source and the surface of the detectors that could slow down the ternary particles even at low energy. All ion-implanted silicon detectors in use have aluminum front windows of nominally 140 nm thickness. The corresponding effective dead-layer was determined with angular dependent α spectroscopy to be 369 ± 11 nm of silicon equivalent thickness [Spi92], which results in an energy correction of 110 keV for 1 MeV α -particles, and 30 keV at 10 MeV.

Within experimental errors, the present spectrum of ^4He is in good agreement with the low-energy data obtained recently by Tishchenko [Tis02] between 2.5 and 9 MeV (Figure 5.14a). However, the ternary α -particles spectrum reported in the latter work contains about 4 % admixture of ^6He with a maximum yield around 12.3 MeV which may slightly change the spectral slope at the low-energy side. On the other hand, the data reported as early as 1974 by Loveland [Lov74] exceed the real low-energy yield of ternary α -particles by up to a factor of two (Figure 5.14b).

We have not been able to clarify the discrepancy of both recent works with Loveland's early result which has for a long time been the only ^{252}Cf data on low-energy ternary α 's available in literature. It also remains unclear to us how the method of ΔE -E applied in [Lov74] could provide precise data in the energy region below the threshold energy of the ΔE silicon detector used. The present experiment, and that of

[Tis02], show a smaller low-energy tailing as suggested from the data in [Lov74], being now comparable in magnitude with the tailing known from $^{235}\text{U}(n_{\text{th}},f)$ [Wag04].

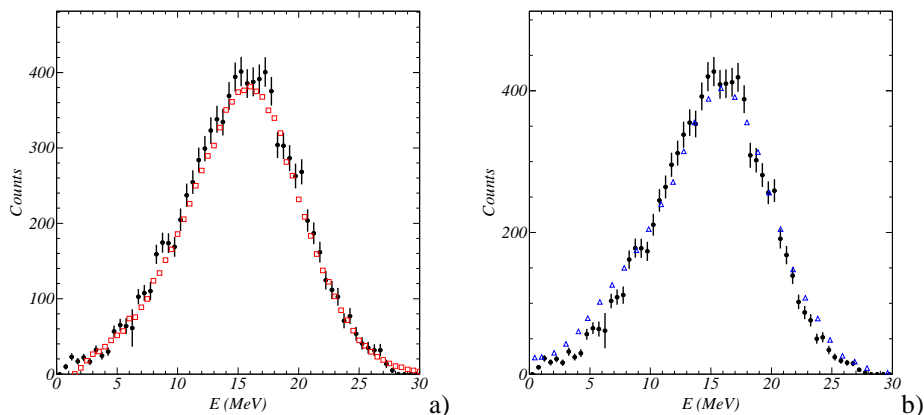


Figure 5.14 a) Comparison of the energy distribution for ^4He (black dots) with data by Tishchenko [Tis02] (full range of angles Θ_{aL}); b) Comparison of energy distribution for equatorial ^4He (black dots) with data by Loveland [Lov74].

We have finally extracted also the energy spectrum of ternary ^6He from our data shown in Figure 5.11, leaving out the energy region around 6 MeV. Our energy distribution of the ternary ^6He is plotted in Figure 5.15a.

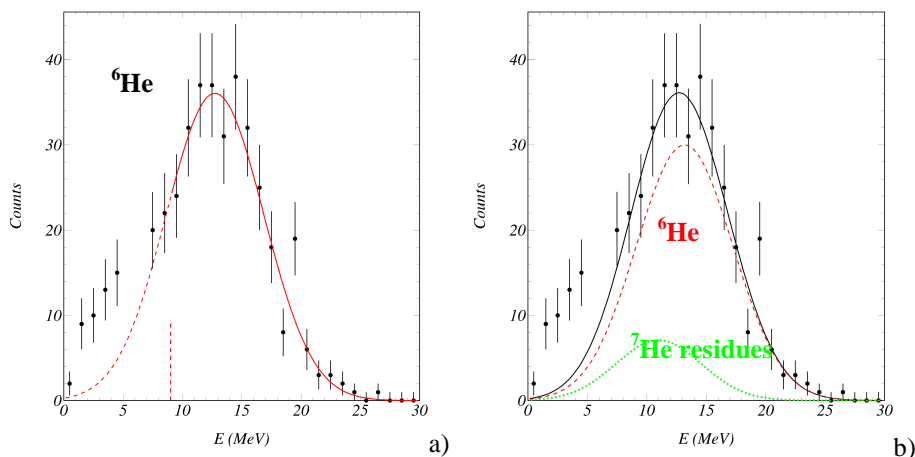


Figure 5.15 a) Energy distribution of ternary ^6He particles. The solid line represents the Gaussian curve fitted to the data above 9 MeV. b) Two-Gaussian curves fitted to the data above 9 MeV, taking residual α -particles from ^7He decay into account, according to the results of Kopatch [Kop02].

In the 6 weeks period of the measurement the total number of collected events of the ternary ^6He is 441. This gives a rate of about 10 events per day. To our knowledge it is the first time that ternary ^6He particles from $^{252}\text{Cf}(sf)$ were measured over their full energy range. The spectrum turns out to be asymmetric as well as the ^4He spectrum. Figure 5.15b shows the result of two Gaussians fit to the present data of

^6He above 9 MeV. Besides true ternary ^6He particles (the dominant Gaussian) also residual particles from the decay of ternary ^7He were considered here. Unfortunately, the low-energy component of the experimental spectrum can not be explained by the ^7He decay. However, the crucial point for the reliability of these low-rate data is the question regarding a possible interference with some background in the analysis window. Summing up, the spectrum shown in Figure 5.15, by interpolating the missing values around 6 MeV and by relating it to the sum of α -particles shown in Figure 5.13, has yielded for the ratio $^6\text{He}/^4\text{He}$ a value of 0.0466 ± 27 . Fitting the spectrum, for energies above 9 MeV, with a single Gaussian curve and taking the area under the Gaussian as the estimate for the ^6He yield gives for the $^6\text{He}/^4\text{He}$ ratio a value of 0.0414 ± 39 , which is in line with most values deduced earlier from experiments with a similar threshold energy (e.g., [Gra88, Rai68]). This is indicating that a background contribution to the present spectrum, which is difficult to determine precisely, is not essential. Furthermore, the analysis of the spectrum from the rare ^6He particles gives us confidence that an essential interference of fragment background with the about 25 times more intense ternary α spectrum, shown in Figure 5.13 and Figure 5.15, can safely be neglected.

Finally we want to compare the parameters of the present ternary ^4He particle spectrum with recent literature data. For the comparison with the other results our spectrum has been fitted two times with a single Gaussian curve for energies above 9 MeV and 12.5 MeV as it is shown as an example in Figure 5.13a. Resulting values of mean energy and width of the Gaussian together with the range limits of the Gaussian fit for our and literature data are listed in Table 5.1. For the ^6He data the corresponding comparison is given in Table 5.2.

Table 5.1 Energy parameters of ternary ^4He particles in $^{252}\text{Cf}(\text{sf})$ obtained in present work in comparison with recent literature data.

Mean energy, MeV	FWHM, MeV	Gaussian fit range, MeV	Angular range for $\theta_{\alpha\text{L}}$	Method	Reference
15.4 \pm 0.1	10.0 \pm 0.1	9–27	experiment ^{a)}	TOF-E (MCP-silicon)	present work
15.5 \pm 0.1	10.5 \pm 0.1	9–27	equatorial ^{b)}		
15.6 \pm 0.1	10.9 \pm 0.2	9–27	full		
15.7 \pm 0.1	10.6 \pm 0.2	12.5–27	full		
15.7 \pm 0.2	10.4 \pm 0.2	\geq 12.5	full	$\Delta\text{E-E}$ (silicon-silicon)	[Wag04]
15.7 \pm 0.2	10.9 \pm 0.2	8–28	full	$\Delta\text{E-E}$ (gas-silicon)	[Kop02]
15.7 \pm 0.1	10.6	\geq 10	full	TOF-E (silicon ball)	[Tis02]

^{a)} for the current experimental setup

^{b)} particularly defined as $50^\circ \leq \theta_{\alpha\text{L}} \leq 130^\circ$

Table 5.2 Energy parameters of ternary ${}^6\text{He}$ particles in ${}^{252}\text{Cf}(\text{sf})$ obtained in present work in comparison with literature data.

Mean energy, MeV	FWHM, MeV	Gaussian fit range, MeV	Method	Reference
12.7±0.5	9.7±0.9	9–28	TOF-E (MCP-silicon)	present work
12.3±0.5	9.0±0.5	≥ 10	ΔE-E (gas-silicon)	[Kop02]
11.0±0.9	9.6±0.5	5–12	recoil mass separator	[Obe05] ^{*)}

^{*)} Energy distribution for fission of ${}^{252}\text{Cf}^*$ obtained via reaction ${}^{251}\text{Cf}(n_{\text{th}},f)$ at the LOHENGRIN recoil mass-separator at the ILL, Grenoble.

As it is seen from Table 5.1 and Table 5.2, we have a good agreement with other results for the mean energy and FWHM for ${}^4\text{He}$ ternary particles in ${}^{252}\text{Cf}(\text{sf})$, when we artificially apply similar low-energy cut-off for the fit. For ${}^6\text{He}$, on the contrary, the situation is not so good, but for ternary ${}^6\text{He}$ we had quite weak statistics and having the threshold for fitting at 9 MeV we cut out almost a third of all counts and thus introduce an additional uncertainty to the determination of mean energy as centre of gravity of the Gaussian curve.

Summary and conclusions to Part 2

The new experiment to measure the ternary α -particle energy spectrum from ^{252}Cf spontaneous fission was presented in the second part of this thesis. The successful measurement was done with an array of unshielded silicon detectors and MCP timing detector. Unambiguous discrimination of α -particles from the neighboring isotopes was achieved with a time-of-flight technique using the fission fragments as the start.

The main results obtained in the study of the ternary α -particle energy spectrum from $^{252}\text{Cf}(\text{sf})$ are the following:

- For the first time the measurement of the full energy spectra of ^4He and ^6He have been performed using the TOF-E method for LCP identification.
- The energy distribution of ternary α -particles was measured down to 1 MeV. This is a substantial improvement over the previous experiments where the typical detection threshold is between 6 and 9 MeV.
- The constraint of our experimental setup for the detection angle was determined by using GEANT4. These data were applied to the energy dependent angular distribution of the α -particles obtained by Heeg [Hee90] for creation of the correction curve.
- Corrections to the measured spectrum were made for wider than detected angular interval of equatorial particles ($50^\circ \leq \Theta_{\alpha L} \leq 130^\circ$), as well as for the full interval of angles measured in experiments without fragment coincidences.
- For both, ^4He and ^6He spectra, at energies below 9 MeV an excess in the yield as compared to a Gaussian shape was observed. The magnitude of the excess for ^4He is in close agreement with the data presented by Tishchenko [Tis02] but is below the low-energy data published by Loveland [Lov74].
- We show that the low energy asymmetry in the energy distribution of ^4He and ^6He can not be explained by the residues of neutron-unstable ternary ^5He and ^7He particles.
- In spite of the relatively weak statistics for ^6He , the yield ratio $^6\text{He}/^4\text{He}$ was calculated. The value is equal to 0.0414 ± 39 .

The progress achieved with the present TOF-E measurement on the ternary α spectrum has stimulated us to plan the next experiment. We are going to use a 10 times stronger ^{252}Cf source on a thin Ni backing and an improved fragment trigger, which uses the sample as the conversion foil of a micro channel plate (MCP) start detector. This will improve the time resolution, the statistical accuracy in the low-energy regime, and will allow us to study the dependence of the energy distribution on the particle emission angle. We also want to scrutinize whether a combination of TOF with pulse-shape discrimination techniques in suitable reverse-mounted silicon surface barrier (SB) detectors [Sil06] can be applied for the discrimination of ternary particles according to both their mass and nuclear charge. This would permit to register ternary particle spectra up to carbon isotopes down to very low energy.

Low-energy α -particles may provide important insight into both the emission mechanism of ternary particles and the scission stage of the fission process. I hope that our precise experimental data of the full energy distribution for ternary particles

will be useful for other scientists and will contribute to untangling the mysteries of nuclear processes. Many of the results obtained in this work raise new questions and attract attention. New experiments and further studies are needed to fully understand the processes lying behind the subject of interest. Many of the fundamental questions about the ternary fission presented since its discovery still remain unanswered. I hope that the studies of this thesis will contribute a tiny portion to the sea of knowledge bringing the answers a little bit closer.

References

- [Ale00] Alexandrov A. A. et al., "Heavy Ion Physics" FLNR JINR scientific report 1999-2000, Dubna, 2001, Edited by A.G. Popeko, E7-2001-173, p.159.
- [Ago03] Agostinelli S., et al., "GEANT4: A simulation toolkit," Nucl. Instr. Meth. A. **506** N3 (2003) 250-303
- [Bud88] Budtz-Jorgensen K., Knitter H. H., Nucl. Phys. A **490** (1988) 307.
- [Col61] Colby L.J. et al., Phys. Rev. **121** (1961) 1415.
- [Cos67] Cospers S., Cerny J., Gatti R., Phys. Rev. **154** (1967) 1193.
- [Cse04] Cseh J. et al., Phys. Rev. C. **70** (2004) 034311.
- [Deb81] Debeauvais M., Tripier J., Jokic S., Todorovic Z., Antanasijevic R., Fission of U, Th, Bi, Pb, and Au induced by 200 and 300 GeV protons, Phys. Rev. C. **23** (1981) 1624.
- [Die73] Diehl H., Greiner W. Ternary fission in the liquid drop model, Phys. Lett. B. **45** (1973) 35.
- [Die74] Diehl H., Greiner W., Theory of ternary fission in the liquid drop model, Nucl. Phys. A. **229** (1974) 29.
- [Glä83] Glässel P. et al., Z. Phys. A – Atoms and Nuclei **310** (1983) 189.
- [Gön05] Gönnerwein F., Mutterer M. and Kopatch Yu., Ternary and quaternary fission, Europhysics News **36**, No. 1 (2005) 11.
- [Gön93] Gönnerwein F., Börsig B., Nast-Linke U., Mutterer M., Theobald J.P., Faust und H., Geltenbort P., Emission of Clusters in Nuclear Fission, Proc. 6th International Conference on Nuclei far from Stability and 9th International Conference on Atomic Masses and Fundamental Constants, Bernkastel-Kues, 19.-24. July 1992; IOP Publ. Ltd, London, 1993, p. 453.
- [Gra88] Grachev V., Gusev Y, Seliverstov D., Sov. J. Nucl. Phys. **47** (1988) 622.
- [Gru82] Grun C.R. et al., Nucl. Instr. and Meth. **196** (1982) 33.
- [Hal71] Halpern I., Three fragment fission, Annu. Rev. Nucl. Sci. **21** (1971) 245.
- [Ham97] Namsch F.-J., Oberstedt S., Nuclear Physics A **617** (1997) 347.
- [Hee90] Heeg P., Ph.D. Thesis, TH Darmstadt (1990) unpublished.
- [Her02] Herbach C.-M. et al., Nuclear Physics A **712** (2002) 207.
- [Hud69] Hudis J., Katcoff S., High-energy-proton fission cross sections of U, Bi, Au, and Ag measured with mica track detectors, Phys. Rev. **180** (1969) 1122.

- [Hud76] Hudis J., Katcoff S., Interaction of 0.6-300 GeV protons with U, Bi, Au, and Ag; mica track detector study, *Phys. Rev. C* **13** (1976) 1961.
- [Hus71] Husain L., Katcoff S., Antiproton- and pion-induced fission at 2.5 GeV/c, *Phys. Rev. C* **4** (1971) 263.
- [Hwa00] Hwang J., et al., *Phys. Rev. C* **61** (2000) 047601.
- [Ike88] Ikeda K., Proc. 5th Int. Conf. on Clustering Aspects in Nuclear and Subnuclear Systems, Kyoto, 277 (Contributed papers, 1988).
- [Iye66] Iyer R. H., Cobble J. W., Evidence of ternary fission at lower energies, *Phys. Rev. Lett.* **17** (1966) 541.
- [Iye68] Iyer R. H., Cobble J. W., Ternary fission of ²³⁸U induced by intermediate-energy helium ions, *Phys. Rev.* **172** (1968) 1186.
- [Kam07] Kamanin D., Kopach Yu., Pyatkov Yu., Tjukavkin A., Lavrova J., Study of the multi-cluster decays in the neutron induced fission of ²³⁵U. Presented at the 15th International Seminar on Interaction of Neutrons with Nuclei, Dubna, Russia, 16-19 May 2007. In press.
- [Kar63] Karamian S.A., Kuznetsov I.V., Oganessian Yu. Ts. and Penionzhkevich Yu. E., *Yadernaya fizika* **5** (1963) 959.
- [Kat72] Katcoff S., Hudis J., Fission of U, Bi, Au, and Ag induced by 29-GeV ¹⁴N ions, *Phys. Rev. Lett.* **28** (1972) 1066.
- [Kat76] Katcoff S., Hudis J., Interaction of 2.0-, 3.9-, and 29-GeV ¹⁴N ions with U, Bi, Au, and Ag: Track detector study, *Phys. Rev. C* **14** (1976) 628.
- [Kau74] Kaufman S.B., Steinberg E.P., Wilkins B.D., Unik J., Gorsky A.J., Fluss M.J., *NIM* **115** (1974) 47.
- [Kha84] Khan H. A., Khan N. A., Fission and spallation induced by 7-GeV protons on U, Bi, Pb, Au, W, Ho, and Ag, *Phys. Rev. C* **29** (1984) 2199.
- [Kie92] Kiesewetter J. et al., Precise determination of mean velocities of fragments from spontaneous fission of ²⁵²Cf, *NIM A* **314** (1992) 125.
- [Kon] Kondratiev N.A., the Flerov Laboratory of Nuclear Reactions (FLNR) of the Joint Institute for Nuclear Research (JINR) in Dubna, Russia. Private communications.
- [Kop02] Kopatch Yu., Mutterer M., Schwalm D., Thierolf P., Gönnerwein F., *Phys. Rev. C* **65** (2002) 044614.
- [Kor85] Kordyasz A.J. et al., Angular distributions of light charged particles from ²⁵²Cf fission in the range 0-46° and 134-180°, *Nucl. Phys. A* **439** (1985) 28.
- [Kra99] Kravtsov A. V. and Solyakin G. E., *Phys. Rev. C* **60**, (1999) 017601.
- [Kug71] Kugler G., Clarke W. B., Mass-spectrometric search for neon and argon isotopes in ternary fission of ²³⁵U, *Phys. Rev. C* **3** (1971) 849.

- [Kug72] Kugler G. and Clarke W.B., Phys. Rev. C **5** (1972) 551.
- [Lov74] Loveland W., Phys. Rev. C **9** (1974) 395.
- [Mar67] Mariscotti M. A., Nucl. Instr. Meth. **50** (1967) 309.
- [Mey71] Meyer L., Phys. Stat. Sol. (b) **44** (1971) 253.
- [Min] MINUIT, Function Minimization and Error Analysis,
<http://wwwasdoc.web.cern.ch/wwwasdoc/minuit/minmain.html>
- [Mug63] Muga M.L., Ternary fission of ^{235}U induced by thermal neutrons, Phys. Rev. Lett. **11** (1963) 129.
- [Mug67a] Muga M.L., Rice C.R., Sedlacek W.A., Ternary fission of heavy nuclei, Phys. Rev. Lett. **18** (1967) 404.
- [Mug67b] Muga M. L., Rice C. R., Sedlacek W. A., Ternary fission of Uranium-236* and -234*, Phys. Rev. **161** (1967) 1266.
- [Mug69] Muga M.L., Rice C.R., Ternary fission of ^{240}Pu and ^{242}Pu , Proc. of 2nd IAEA Symp. on the Physics and Chemistry of Fission, Vienna, 28 July - 1 August 1969 (IAEA-SM-122/99), 1969, p. 107.
- [Mul97] Mulgin S. et al., NIM A **388** (1997) 254-259.
- [Mut96] Mutterer M. and Theobald J, in Nuclear Decay Modes, editor D.N. Poenaru, IOP, Bristol, UK, 1996, chapter 12.
- [Nel] Nelder-Mead method,
<http://math.fullerton.edu/mathews/n2003/NelderMeadMod.html>.
- [Now82] Nowicki L. et al., Investigation of polar emission in ^{252}Cf and $^{235}\text{U}+n_{\text{th}}$ fission, Nucl. Phys. A **375** (1982) 187.
- [Obe05] Oberstedt S., Oberstedt A., Rochman D., Gönnewein F., Tsekhanovich I., Becker J., Sartz A., Bax H., Hamsch F.-J. and Raman S., Nucl. Phys. A **761** (2005) 173.
- [Ogi86] Ogihara M., Nagashima Y., Galster W., Mikumo T., NIM A **251** (1986) 313.
- [Ogl01] Ogloblin A. A., Pik-Pichak G. A. and Tretyakova S. P., Cluster radioactivity, Proceedings of the International Workshop "Fission Dynamics of Atomic Clusters and Nuclei", Luso, Portugal 15 - 19 May 2000, Published in World Scientific (2001) 143.
- [Ort89] Ortlepp H.-G., Romaquera A., Nucl. Instr. and Meth. A **267** (1989) 500.
- [Ort98] Ortlepp H.-G. et al., Nucl. Instr. and Meth. A **403** (1998) 65.
- [Pas71] Pashkevich V. V., Nucl. Phys. A **169** (1971) 275.
- [Pia70] Piasecki E., Dakowski M., Krogulski T., Tys J. and Chwaszczewska J., Evidence of the polar emission of alpha-particles in the thermal neutron fission of ^{235}U , Physics Letters B **33** (1970) 568.

- [Pia79] Piasecki E., Nowicki L., Polar emission in fission, IAEA, Vienna.: Proc. of an int. symp. Phys. and Chem. of Fission (1979) 193
- [Poe99] Poenaru D.N. et al., Multicluster accompanied fission, Phys. Rev. C **59** (1999) 3457.
- [Pol70] Polikanov S. M. and Sletten G., Nucl. Phys. A **151** (1970) 656.
- [Pre41] Present R.D., Possibility of ternary fission, Phys. Rev. **59** (1941) 466.
- [Pri89] Price P. B., Heavy-particle radioactivity ($A > 4$), Annu. Rev. Nucl. Part. Sci. **39** (1989) 19
- [Pya00] Pyatkov Yu.V. et al., Proc. Int. Conf. on Nuclear Spectroscopy "Nuclear shells-50 Years", Dubna, 1999, edited by Yu.Ts. Oganessian and R.Kolpakchieva, Published by: World Scientific Publishing Co. Pte. Ltd., Singapore (2000) p.144.
- [Pya02] Pyatkov Yu. V. et al., Nucl. Instr. Meth. A. **488** (2002) 381.
- [Pya03] Pyatkov Yu. V. Kamanin D. V., Alexandrov A.A., Alexandrova I. A., Khlebnikov S.V., Mitrofanov S. V., Pashkevich V. V., Penionzhkevich Yu. E., Ryabov Yu.V., Sokol E. A., Tishchenko V. G., Tjukavkin A. N., Unzhakova A. V. and Yamaletdinov S. R., Physics of Atomic Nuclei, **66** (2003) 1631.
- [Pya04] Pyatkov Yu. V. et al., Phys. Atom. Nucl. **67** (2004) 1726.
- [Pya06a] Pyatkov Yu., Trzaska W., Mutterer M., Yamaletdinov S., Bolgov D., Kamanin D., Khlebnikov S., Kopach Yu., Kuznetsova E., Lavrova J., Lyapin V., Sillanpää M., Tishchenko V., Tjukavkin A., Tyurin G., Peculiarities of data processing in experiment aimed at searching for rare decays of Pu* isotopes, Proc. 14th International Seminar On Interaction Of Neutrons With Nuclei: «Fundamental Interactions & Neutrons, Nuclear Structure, Ultracold Neutrons, Related Topics» May 24-27, 2006, Dubna, Russia. Dubna (2007) 134.
- [Pya06b] Pyatkov Yu. for HENDES and FOBOS collaborations, Preliminary Results Of Experiment Aimed At Searching For Collinear Cluster Tripartition of $^{242}\text{Pu}^*$, Proc. 6th International Conference "Dynamical Aspects of Nuclear Fission", October 2 - 6, 2006, Smolenice Castle, Slovak Republic (in press)
- [Pya07] Pyatkov Yu., Trzaska W., Mutterer M., Yamaletdinov S., Bolgov D., Kamanin D., Khlebnikov S., Kopach Yu., Kuznetsova E., Lavrova J., Lyapin V., Sillanpää M., Tishchenko V., Tjukavkin A., Tyurin G., Searching for Rare Decay Modes in the Reaction $^{238}\text{U} + ^4\text{He}$ (40 MeV), Proc. International Symposium on Exotic Nuclei (EXON-2006), July 17-24, 2006, Khanty-Mansiysk, Russia, AIP Conference Proceedings, Melville, New York, Volume **912** (2007) 144.
- [Pya97] Pyatkov Yu. V. et al., Nucl. Phys. A **624** (1997) 140.
- [Rah73] Rahimi F., Gheysari D., Remy G., Tripier J., Ralarosy J., Stein R., Debeauvais M., Fission of U, Th, Bi, Pb, and Au induced by 2.1-GeV ^2H ions, Phys. Rev. C. **8** (1973) 1500.

- [Rai68] Raisbeck G.M. and Thomas T.D., Phys. Rev. **172** (1968) 1272.
- [Roc04] Rochman D. et al., Nucl. Phys. A. **735** (2004) 3.
- [Ros50] Rosen Louis and Hudson Alvin M., Symmetrical tripartition of ^{235}U by thermal neutrons, Phys. Rev. **78** (1950), N 5, 533.
- [Roy61] Roy J. C., Can. J. Phys. v.**39** (1961) 315.
- [Rub01] Rubchenja V.A. et al., Nucl. Instr. Meth. in Phys. Res. A **463** (2001) 653.
- [Sch65] Schmitt H.W. et al., Phys.Rev. **137** (1965) B837.
- [Sch83] Schmidt R. and Henkel H., Nucl. Phys. A **395** (1983) 15.
- [Sch87] Schall P., Heeg P., Mutterer M., Theobald J.P., On symmetric tripartition in the spontaneous fission of ^{252}Cf , Phys. Lett. B. **191** (1987) 339.
- [Sei88] Seidel W., Ortlepp, H.-G., Stary F., Sodan H., Nucl. Instr. and Meth. A **273** (1988) 536.
- [Sil06] Sillanpää M., Khlebnikov S., Kopatch Y., Mutterer M., Trzaska W. H., Tyurin G. and Lyapin V., Proceedings of the XL Annual conference of the Finnish Physical Society, March 9-11 2006, Tampere, Finland (2006) 261.
- [Sok97] Sokol E.A. et al., Nucl. Instr. and Meth. A **400** (1997) 96.
- [Sol96] Solyakin G. E. and Kravtsov A. V., Phys. Rev. C **54**, (1996) 1798.
- [Spi92] Spieler A., Diploma Thesis, TU Darmstadt, 1992, unpublished.
- [Ste70] Steinberg E. P., Wilkins B. D., Kaufman S. B., Fluss M. J., Alternative evaluation of ternary-fission data, Phys. Rev. C **1** (1970) 2046.
- [Sto66] Stoenner R. W., Hillman M., Search for radiochemical evidence for ternary fission of ^{235}U by thermal neutrons, Phys. Rev. **142** N3 (1966) 716.
- [Str63] Strutinsky V. M., Lyashchenko N. Ya., Popov N. A. Symmetrical shapes of equilibrium for a liquid drop model, Nucl. Phys. **46** (1963) 639.
- [Swi58] Swiatecki W. J., Proc. of Second UN Intern. Conf. on the Peaceful Uses of Atomic Energy, Pergamon, New York, 1960, 15, P/651, Genf 1958. p. 248.
- [Ter97] Ter-Akopian G.M. et al., Phys. Rev. C **55** (1997) 1146.
- [Tis02] Tishchenko V., Jahnke U., Herbach C.-M., Hilscher D., Report HMI-B 588, Nov. 2002.
or Tishchenko V., Ph.D. Thesis, Dubna, (2002).
- [Trz02] Trzaska W.H. et al., Proc. Symposium on "Nuclear clusters: from light exotic to superheavy nuclei", Rauschholzhausen, Germany, 2002, p. 237.

- [Tsi47] Tsien San-Tsiang, Ho Zah-Wei, R. Chastel and L. Vigneron, Phys. Rev. **71** (1947) 382.
- [Van00] Vannucci L. et al., Eur. Phys. J. A **7** (2000) 65.
- [Wag04] Wagemans C., Heyse J., Jansen P., Serot O., Geltenbort P., Nucl. Phys. A **742** (2004) 291.
- [Wag91] Wagemans C., The Nuclear Fission Process, editor C.Wagemans, CRC Press, Boca Raton, Florida USA, 1991, chapter 12.
- [Wah88] Wahl C., Atomic data and nuclear data tables, **39** (1988) 60-61.
- [Whe63] Whetstone S. L., Coincident time-of-flight measurements of the velocities of ^{252}Cf fission fragments, Phys. Rev. **131** (1963) 1232.
- [Wil76] Wilkins B. D. et al., Phys. Rev. C. **14** N5 (1976) 1832.